Strength anisotropy of rock: a theoretical and experimental study

Sandford, M. R.

STRENGTH ANISOTROPY OF ROCK:
A THEORETICAL AND EXPERIMENTAL STUDY

being

A Thesis submitted for the Degree of

Doctor of Philosophy

in the

University of Durham

by

M. R. SANDFORD

September 1974

Acknowledgments

The author wishes to thank Dr. P. B. Attewell (Supervisor) and Mr. J. P. Woodman (Co-worker) for help, encouragement and theoretical and practical assistance during the project.

The work was financed by a Research Grant to P. B. Attewell and Research Studentship to M. R. Sandford from the Natural Environment Research Council.

Abstract

The use of X-ray texture analysis techniques enables a simplified picture of the microstructure of a rock to be built up. In this thesis it is shown that, in spite of a wealth of evidence on pre-failure rock behaviour, a simple application of Griffith theory to the assumed microstructure can provide an adequate description of the failure characteristics of an anisotropic rock. It is suggested that the crystallite structure within the rock controls the pre-failure activity in such a way as eventually to produce the crack formation initially deduced from that crystallite structure. These conclusions are drawn from work done on two rocks of different character, Penrhyn Slate and Lumley Mudstone.

Contents

Appendices

Figures

1. Representation of sample in the texture goniometer, showing principal directions.
2. Locus of projection, onto xy plane of rock specimen, of the normals to the sampled crystal planes, showing the spiral scan.
3. Diagram of X-ray reflection from a small volume in a sample. This diagram is used to show the independence of reflected intensity on the sample elevation angle, ζ
4. Diagram showing how three orthogonal samples for the X-ray texture study are related.
5. Chart record with peak at $2\theta = 9^{\circ}$ and showing a background interpolation under the peak.
6. Intermediate computer printout of pole figure for Penrhyn Slate, illite (001). Sample section A.
7. Intermediate computer printout of pole figure for Penrhyn Slate, illite (001). Sample section B.
8. Intermediate computer printout of pole figure for Penrhyn Slate, illite (001). Sample section C.
9. Final computer printout of smoothed pole figure for Penrhyn Slate, illite (001), showing locus of average intensity. I_R.
10. Intermediate computer printout of pole figure for Penrhyn Slate, chlorite (001). Sample section A.
11. Intermediate computer printout of pole figure for Penrhyn Slate, chlorite (001). Sample section B.
12. Intermediate computer printout of pole figure for Penrhyn Slate, chlorite (001). Sample section C.
13. Final computer printout of smoothed pole figure for Penrhyn Slate, chlorite (001), showing locus of average intensity, I_R.

14. Pole figure printout of Penrhyn Slate illite (001) data fitted by a series of associated Legendre polynomials.

15. a. Generalised stress-strain curves for rock in compression. (after Bieniawski, 1967).

    b. Generalised resistivity and microfracturing curves for rock in compression. (after Brace et al., 1968).

16. Strength data for Penrhyn Slate, for various values of confining pressure, shown as a function of cleavage inclination.

17. Data from Penrhyn Slate compared with the modified form of Donath's equation:

$$\sigma_1 = a + b\,\mathrm{Cos}\,2(\alpha + \beta) \ .$$

18. Plot of function $\omega(\xi,\gamma)n(\xi,\gamma)$ used in the Weibols and Cook integration showing its generally parabolic shape.

19. Plot of Weibols and Cook strain energy against σ_1 for various values of β .

20. Family of curves of τ_{eff} for various σ_1.
    $\sigma_2 = 2.10^3$ lbs/in^2, $\mu = 0.5$.

21. Showing graphical solution of $\tau_{eff} = B/\sqrt{c}$.
    The two curves are moved relative to each other until they just touch. The displacements α and β represent the orientation of σ_1 to the failing crack and the cleavage plane respectively.

22. Plot of $B/\sqrt{c}$, in arbitrary units, against angle of crack, length c, with respect to the cleavage plane. The crack length distribution is taken directly from X-ray data shown elsewhere.

23. Theoretical curves obtained by the application of Griffith theory to X-ray derived crack distribution. Penrhyn Slate data is shown for $\sigma_2 = 0$.

24. Comparison of theory and experiment for Penrhyn Slate at $\beta = 30^\circ$.

25. Comparison of theory and experiment for Penrhyn Slate at $\beta = 15^\circ$.

26. Comparison of theory and experiment for Penrhyn Slate at $\beta = 75^{\circ}$.

27. Comparison of theory and experiment for Penrhyn Slate at $\beta = 45^{\circ}$.

28. a. Experimental relationship between orientation of failure plane, α, and orientation of cleavage, β, for Penrhyn Slate. The bars mark one standard deviation either side of the mean.

b. Theoretical relationship between α and β used in the final version of the theory.

29. Solution of $\tau_{eff} = B/\sqrt{C}$ under the conditions $\alpha = \beta$ (see fig.21)

30. Plot of σ_T versus β for a confining pressure of zero. The full line gives the theoretical plot as modified by shear plane entrainment.

31. Plot of $(\sigma_1 - \sigma_2)$ versus σ_2 at $\beta = 15^{\circ}$ given by the theory modified for shear plane entrainment.

32. Showing how a failed crack may become entrained in the cleavage plane for angles $\beta < 30^{\circ}$.

33. Experimental strength data for Lumley Mudstone.

34. X-ray texture for Lumley Mudstone used in the application of the theory.

35. Plot of $B/\sqrt{C}$ as a function of orientation for Lumley Mudstone taking $B = 3$.

36. Strength variation with sample orientation from theory applied to the distribution for Lumley Mudstone with $B = 3$ and $\mu = 0.6$.

37. Comparison of theory and experiment for Lumley Mudstone for various sample orientations.

38. Theoretical and experimental relationship between failure plane angle and orientation of sample for Lumley Mudstone.

39. Comparison of two τ_{eff} curves showing effect of σ_2 on radius of curvature. $\mu = 0.6$ for both curves.

1. Introduction

The technique of using X-rays in texture analysis, the determination of crystallite orientation density distribution, is now well established (Barrett and Massalski, 1966) and is used in many disciplines (Nightingale and Lewis, 1971; Dunn and Walter, 1959). The geometry used in present commercial texture goniometers is due to Shulz (1949) and this forms the most common way of determining textures, in metals at least. (Starkey, 1964, has developed a geometry based on photographic film rather than a moving counter but his method seems little used at present.)

Shulz' geometry has in fact been the subject of close analysis by a number of authors (von Gehlen 1960; Chernock and Beck, 1952) and subsequent workers have made use of and expanded this work to produce accurate pole figures from X-ray data (Baker, Wenk and Christie, 1969; Fayad, 1967). Despite all this, however, the data has only been used in a qualitative way in rock mechanics (Attewell 1970; Attewell and Taylor 1969; Brace 1965). The purpose of this thesis is to examine one particular anisotropic property of a rock, that of strengh anisotropy, and to try to relate this in a quantitiative way to the X-ray texture.

The process of failure in rock has been studied extensively (see reviews by Murrell, 1969 and Brace, 1969) and these studies have given the impression that the failure of rock is gradual and the final shear plane is but the last manifestation of a very complex process. The data obtained (for example, Brace, Paulding, and Scholz, 1966) shows that there is indeed great activity within a rock some time before it fails, and that this activity is related to the final failure. This has been taken to show that simple theories, for example, those based solely on the theory of Griffith (1921) are not applicable to rock.

The previous studies of rock failure have only rarely included any work on anisotropic failure (Donath 1961; Jaeger, 1960, and there have been no attempts, to the author's knowledge, to describe anisotropic failure by any other than the simplest exposé of Griffith theory (Walsh and Brace, 1964; Hoek, 1964). The effect of the pre-failure behaviour of rock on anisotropic failure theories seems to have been ignored.

There are two related cooperative failure theories in existence (Weibols and Cook 1968; Brady, 1969) and both of these can be made to deal with anisotropic material by inserting a non-uniform crack distribution of some sort. This thesis describes an attempt to do this and to relate the crack orientation distribution to important fabric elements determined by the X-ray texture method.

2. Texture Analysis

In studying the anisotropy of a given rock it is reasonable to suppose that such anisotropy is due at least in part to some property of the minerals in the rocks.

Thus it is interesting to look at the orientation distribution of the mineral crystals within the material.

The way to do this is to define some identifiable direction within the crystal morphology, for example an optic axis, a pole to a twin plane or a pole to an X-ray diffraction plane, and to count the density of these poles per unit solid angle. When such a density distribution is plotted on the surface of a sphere the resulting pattern is called a pole figure.

If two or more such directions can be defined and their orientation density distributions measured, then a more complete description of the texture may be obtained. The adequacy of this description being related to the crystallographic symmetry and the (hkil) multiplicity. In particular, if, for samples with an axial symmetry, instead of plotting the distribution of a crystallographic axis with respect to the sample axes, the distribution of the sample axis with respect to crystallographic axis is plotted, then an inverse pole figure is obtained. This type of plot is much used in studies of metals and plastics.

For samples with less than axial symmetry the crystallite distribution function of Roe (1965) may be required. This function expresses the inverse pole figure as a series of generalized spherical harmonics and enables the pole figure for any given plane in the particular crystal to be obtained. However, there are practical problems,

particularly in the case of polymineralic aggregates, of peak overlap and low resolution.

There are two basic groups of techniques for obtaining data for pole figures: optical and X-ray. The optical techniques differ in their methods of defining the directions, within the crystal, to be counted but they all require that the sample be placed on a Universal Stage under a microscope so that the distribution may be obtained by direct observation. There are therefore limits on the smallest size and the largest number of crystals that can be counted by this system.

The use of X-rays is based on the selective reflection properties of crystal planes, as described by Bragg's law. The apparatus is characterised by the fact that the source and detector always subtend the same angle at the sample, this angle being related to the Bragg angle for the crystal planes of interest, and that the detector or the sample or both are moved such that the resultant variation in intensity bears a known relation to the pole figure.

X-ray methods differ in detail, particularly in the detector used, which may be photographic film (for example, Starkey, 1964) or a counter of some sort, and a review of some of these methods has been published by Barrett and Massalski. (op cit). A counter method is to be described here.

The instrument used is a Philips X-ray texture goniometer* making use of a geometry due to Schulz (1949). That is, the source, counter and the centre of the sample surface are kept fixed, the angle

* Texture attachment, PW1050; Goniometer, PW 1078/10; Diffractometer, PW 1310; using Ni filtered $Cu_{k\alpha}$ radiation.

between them being chosen to select the diffraction line required, and the sample is rotated about two axes through its centre point. The first axis, line A A' in fig. 1, is the line of intersection between the plane of the sample surface and the plane containing the incident and reflected beams. The second axis, B B' in fig. 1 is the normal to the sample surface.

These two rotations bring successive sets of the planes at different orientations into position so that the detector may receive X-rays reflected from them. The detector output is thus a continuously varying analogue of the X-ray intensity corresponding to the volume of crystal reflectors in the orientations singled out by the motion. *

If the selected orientations are plotted on a suitable projection with respect to a defined set of axes in the sample, taking the sample normal as the axis normal to the plot, then an outward directed spiral scan is produced (fig. 2). The parameters of this scan, that is the time for one rotation of 2π in the angle γ and the change in angle ζ for each such rotation, can be set to a number of standard values on the Philips equipment and so the output from the detector may easily be correlated with the position in the scan.

To increase the volume of crystals irradiated and thereby to increase the statistical reliability of the count, the sample is oscillated from side to side in its own plane and within the plane of the latitude (ζ) ring so that the beam sweeps across its surface. The rotation about B B' is effected by a pawl and ratchet mechanism which operates once every oscillation, ensuring that the same part of the surface is always sampled.

* The quantity measured by this method is an integral quantity and therefore takes account of crystal size. It differs in this respect from the optical method which counts points irrespective of the size of crystals producing those points.

As the sample rotates through χ the effective scattering volume increases as does the attenuating volume. According to the analysis of Schulz (1949) these two effects cancel each other out, making the diffracted intensity independent of χ . (See appendix A)

This analysis depends on the assumption that the X-ray beam does not leave the surface of the specimen and that all reflected rays are counted by the detector. (Von Gehlen 1960).

Since the X-ray illuminated area on the specimen becomes wider for increasing χ the edges of the spot will eventually fall outside the specimen area and a loss of intensity results. For samples of other than circular shape this fall of intensity will also vary with γ , although a sufficiently small counter input slit should reduce this effect. In addition to the spot size effect there is a defocusing effect which occurs simply because the specimen surface is not normal to the plane of the X-ray beams and the reflecting volume ceases to lie near the Bragg-Brentano focusing circle (Chernock and Beck, 1952). These two effects combine to cause a fall off in intensity after $\chi \approx 70°$ though this angle is dependent on slit widths and two theta values (Baker, Went & Christie 1969), as well as specimen size (Von Gehlen, 1960). One scan is therefore insufficient to complete a pole figure for a particular specimen.

The method adopted in this study for completion of the pole figure was to use three mutually orthogonal samples cut from a single specimen and to combine the scans from these to satisfy the empty annulus on the projected pole figure. This requires that the texture of the sample does not vary significantly over the volume from which the three samples were taken.

Although a chart record was made of each scan for visual inspection, the data from the counter were collected automatically at known sampling intervals on paper tape. The information was thus in a suitable form for immediate use by the specially written computer program. (See Appendix B).

The program accepts data on the settings of the goniometer scan rates and applies them to the intensity data to produce either an equal angle or equal area projection of the spiral scan. The data from two scans of a set of three is rotated into the same system of axes as the third and overlayed with it, the average intensity being taken whenever the value at any particular point is multiply specified. The resulting raw projection can then be smoothed (Baker, Wenk and Christie, 1969) and any empty points filled in to produce a complete pole figure. For ease of printout the data is normalized to the maximum recorded intensity, Imax, and plotted by a line printer to a modulus 10 (rounded up or down between increments) so that 10% contours can easily be drawn. An integration may be performed under the pole figure and a value corresponding to the intensity that would be produced by the same sample if it showed no preferred orientation may be produced. This is the random intensity

$$I_R = \tfrac{1}{2\pi} \int_{\gamma=0}^{2\pi} \int_{\zeta=0}^{\pi/2} I(\gamma,\zeta) \sin\zeta \, d\zeta \, d\gamma .$$

A contour of I_R is plotted out. *

* This contour may, for conditions of simple mechanical rotation, be shown to be a contour defining the intersection of the surface of zero finite longitudinal strain with the plane of projection. However this condition is too limiting to be of use.

The ratio of Ir to Imax is called here the anisotropic index and may be used to indicate degree of anisotropy, though it takes no account of the shape of the distribution.

The sequence of overlayed pole figures to obtain the complete pole figure is shown in Figs. 6 to 9. These show how the data from three scans is combined and smoothed to fill in all the empty points on the mesh. The final printout is shown with the random intensity contour marked by '+' characters, serving to pick out the overall form of the texture.

The scans have been identified by letters A, B, & C in the figures and these correspond to the letters identifying the samples shown in Fig.4. This shows the spatial relationship between the three samples and it can be seen that this relationship is upheld by the plotting program.

The plot shown in Fig. 9 is of the illite basal reflection for Penrhyn Slate, corresponding to a 2θ of 9 degrees ($Cu_{k\alpha}$ radiation), and this clearly shown a maximum concentration normal to the cleavage plane; that is the flat plate-like crystallites have tended to align with each other. Attewell and Taylor (1969) have shown that the principal axes of this texture conform to the principal directions of the tectonic stresses which developed the slaty cleavage at the point in the rock from which the sample was taken.

The plot shown in Fig.13 is of the basal chlorite reflection from the same samples of Penrhyn slate, with a 2θ of 12.5 degrees ($Cu_{k\alpha}$ radiation). This plot has the same characteristics of the illite plot, which is to be expected since the two crystals have a very similar morphology and it is the morphology of the crystals which determine the texture, with the major difference being that the chlorite texture appears less drawn out in the y direction.

There are two difficulties which affect the accuracy of the final texture representation. These are the determination of the background radiation pickup and the allowance for 'fall off' in the received signal as the sample tilts.

The fall off effect and the reasons for its occurrence have already been mentioned and the use of three orthogonal samples is supposed to allow for this effect by enabling a scan to be stopped before the signal becomes noticeably degraded. However, even with the high accuracy of the Philips texture-goniometer used to obtain these textures it is usually possible to observe some fall-off for quite small angles of tilt. The fall off is exaggerated by the rounding in the printout and a variation of 1 to 0 may only be due to a variation of 0.51 to 0.49.

Fall off variations of one unit may be seen in both the illite and chlorite textures shown (Fig.9 and 13). These variations appear as unexpected maxima at points on the circumfrence of the plot corresponding to the centres of the two scans used to fill in the periphery. The width and clarity of these maxima is due largely to the smoothing procedure used to fill in unspecified points on the net which forms the plot, and examination of the intermediate stages shown in Figs. 11 and 12 shows that the variation is quite small and probably not much greater than the general noise level in the signal. For this reason the degree of fall off may be taken as sufficiently small so long as it is accepted that the printed pole figure overestimates this variation.

The estimation of the amount of background radiation contributing to the signal is of some importance as any error has a direct effect on the apparent variation of X-ray intensity with angle. This

coupling is directly due to the use of the recorded maximum as a normalizing factor. Any additive error in the final value of X-ray intensity used may be catered for in any quantitative system using the intensity in a linear fashion but some non-linear function, e.g. square-root (Section 9), may be required in which case compensation becomes more difficult.

The background radiation is made up of X-rays scattered within the cavity of the goniometer and, for small 2θ, X-rays from the source, which in general has a non parallel beam, directly entering the counter, which itself has a non parallel entrance corridor. A representation of a 2θ scan for a peak at $2\theta = 9^{\circ}$ is shown in Fig. 5. As can be seen, the background consists mostly of the direct component. The background for the angle of interest is obtained by interpolating the intensity plot under the peak and reading off at the required point. This interpolation is complicated by the fact that the ends of the peak are not well defined and considerable variation is possible. Further inaccuracy arises because of the rapid variation of the background over the region. Thus a good reading can be spoilt by subsequent mis-setting of the 2θ angle for the scan. Though every effort was made to avoid this, there is bound to be an error from this source of a few percent in all the measurements.

It has been mentioned that it is possible to describe the orientation distribution of a crystal type within a sample more completely by specifying the orientation distribution of the sample within the crystal axes. This inverse pole figure has been described in terms of spherical harmonic functions by Roe (1965) and Baker, Wenk and Christie (1969) and the essence of the description is given in Appendix C. Those authors also describe the procedure required for obtaining an inverse pole figure from a family of pole figures but the procedure is not immediately useful for anything more complex than quartz as any rock contains many minerals whose X-ray 2θ peaks tend

to overlap, thus making it difficult to obtain pole figures for all but a few crystal planes. In particular, those pole figures given for Penrhyn slate are sensibly the only ones obtainable for the minerals concerned. As these pole figures were all that were required for the present study no attempt was made to isolate any others.

Baker, Wenk and Christie, in their work on inverse pole figures use a particular spherical function, the Associated Legendre Polynomial, to describe the pole figures from which they worked and it was found convenient to use the same technique in this study when using the pole figures for quantitative work on a digital computer. Accordingly the intensity data, corrected for background, was fitted by a least squares criterion by a function

$$I(\zeta,\gamma) = \sum_{l=0}^{\infty} \sum_{m=-l}^{l} \left(P_l^m(\zeta) \sin(m\gamma) A_{lm} + P_l^m(\zeta) \cos(m\gamma) B_{lm} \right)$$

(see Appendix C) where ζ and γ are defined in Figs. 1 & 2 and the function P_l^m is a Legendre polynomial with quantum numbers l and m.

The above function was fitted to the data for the illite basal reflection in Penrhyn Slate with a value for the limit l of 8. This gave some 45 coefficients, providing a not unreasonable load for a fast digital computer. The result of the fit was printed out in the form of a pole figure for comparison and this is shown in Fig.14. This plot, in conjunction with Fig.9 shows that the fit is not perfect but that sufficient of the form of the original is present to warrant acceptance of the method and the coefficients obtained were used in all subsequent computer analyses of this texture.

3. General properties of Stress - Strain Behaviour

Any attempt to quantify the process of rock failure on a theoretical basis must recognise the basic mechanism of that process, a mechanism that will be determined by the internal structure of the rock material. Information about this structure and its properties may be obtained directly, by observation under the microscope, by optical data processing methods (Pincus and Dobrin, 1966; Gardner & Pincus, 1968) or by X-ray fabric analysis (see section 2), or indirectly by measurement of elastic properties, permeability or other physical properties (Brace, 1969).

Direct observation reveals grains or small crystals of rock minerals, joined in places by some form of intergranular cement but otherwise separated by cavities. These cavities appear to be more or less interconnected and the fact that rocks possess some primary or "intrinsic" permeability confirms this. From the mechanical point of view this means that rock is highly inhomogenous, on an inter-crystalline basis, and clearly it would be difficult to model at this level, though attempts have been made (Te'eni & Staples, 1969; Brace, 1965; Ko & Hass 1971; Hsiao and Moghe, 1969). However, most laboratory experiments are on such a scale that the rock may be considered to be homogenous and rock data are used on an even larger scale in civil engineering practice so it may still be worthwhile to begin by studying gross properties.

That intact rocks have highly non-linear stress-strain behaviour is now well known (Brace, 1969; Bieniawski, 1967; Cook & Hodgson, 1965: Morgenstern & Tamuly Phukan, 1969) and a study of such behaviour

(Brace, Paulding & Scholz, 1966) coupled with information on the variation of resistivity (Brace & Orange, 1968) and microseismic acticity (Scholz, 1968 ; Barron 1971; Knill, Franklin & Malone, 1968) with applied stress lends insight into the bulk properties of rock and its failure mechanism. Figure 15 shows a set of generalized curves for these quantities. Such a set of curves may be the result of a compression experiment on a cylinder of rock under confining pressure in a standard triaxial testing machine. (The machine is a "soft" one because strength failure is almost coincident with rupture (Rummel & Fairhurst 1970). Failure is clearly brittle.

These curves may conveniently be divided into four regions (Bieniawski, 1967) and each of these regions will now be discussed.

Region 1: Characterized by the non-linear toe of the axial strain line. The lateral strain line is almost straight.

Walsh and Brace (1966), working on rocks under hydrostatic pressure found that the volumetric strain versus pressure curve became linear after 2 to 3 kb pressure. They proposed a model which assumed that a rock was composed on a linearly elastic matrix containing more or less equant cavities, called pores, and rather long and thin cavities, called cracks. The cracks were supposed to close under pressure, the thinner cracks closing first. A closed crack could no longer contribute to the volume compressibility and so the compressibility varied with pressure. Simmons & Brace (1965) confirmed this picture by experiments on wave velocity in materials under various confining pressures. They found that apparently crackless materials (fused quartz, steel, aluminium and fine-grained sandstone) did not show this low pressure effect. This model may also be applied to the case of non-hydrostatic compression. The axial pressure closes cracks whose normals are sub-parallel to the applied load, while the lateral pressure, which

remains constant, has no further effect on the cracks, lateral strain being a function of the Poisson ratio of the matrix and its contained pores (Walsh, 1965c). Scholz (1968a) observed that the toe of the stress-strain curve disappeared under high confining pressure. Scholz also observed some microseismic activity in this region, an effect which he explains as the collapsing of some weaker pores to form closed cracks.

Region 2: Here, behaviour is linear. Unloading shows some hysteresis but there is little or no permanent axial strain. Resistivity is increasing.

Cook & Hodgson (1965), McClintock and Walsh (1962) and Hurrell (1964) have shown that closed cracks may slide, and in doing so affect the apparent elastic properties of the rock concerned. Cook & Hodgson also showed that the cracks which have distorted by sliding do not immediately relax on relief of pressure, thus some apparently permanent strain is introduced, producing hysteresis. This permanent strain may be removed by removing any confining pressure. Calculations by Walsh (1965 a and b) show that the effect of sliding cracks on the elastic constants of the rock is linear, the pores and virgin material together behaving as a linear elastic solid with its own modified elastic constants.

The observed increase in resistivity is explained as being due to the partial closure of the pores as they distort under pressure (Brace and Orange, 1968).

Region 3: This is the onset of failure (failure initiation). The lateral strain curve begins to deviate from a straight line while the axial stress line remains linear. Permanent lateral strains may be observed, though the axial strains are still purely elastic

(Brace, Paulding & Scholz, 1966). Scholz (1968a) and Barron (1971) have observed that microseismic activity begins to increase at this point and Scholz remarks that the total activity is proportional to the inelastic volumetric strain. Wawersik (1968) has taken samples into this region and sectioned them and reports "minor signs of intragranular fracturing, loosening of grain boundaries, intergranular sliding and some crushing of corners of isolated grains".

The results of Wawersik and Scholz indicate that some sort of material breakdown has begun to occur and that this breakdown corresponds to an increase in volume of the specimen. Unless the mineral grains themselves are increasing in size this result means that cavities must be expanding, and according to Brace, Paulding and Scholz (1966), only expanding laterally. Such an increase in pore volume would produce the decrease of resistivity observed in this region.

According to theoretical work by Brady (1969), in a material containing open and closed cracks of roughly uniform size and having all orientations, at failure initiation the closed cracks will be in the correct orientation to fail first. However, experimental work by Brace and Bombolakis (1963) and Hoek & Bieniawski (1965) as well as theoretical work by Murrell and Digby (1970), indicates that such closed cracks will extend and curve so that the extension becomes parallel to the applied compression.

Such a mechanism has been invoked by Brace, Paulding and Scholz (1966) to explain the generation of cavities that can open in a lateral direction, while the model is consistent with the elastic model proposed for regions 1 and 2.

Region 4: At the start of this region, the axial strain curve becomes non-linear and the volumetric strain curve reverses

direction. These two points do not always coincide exactly (Morlier, 1971) but they are sufficiently close to define the upper region together. Unloading in this region shows permanent axial strain and a decrease in Young's modulus.

The identification of this region is due to Bieniawski (1967) who, using Irwin's (1958) critical energy release rate theory, suggests that in region 3 cracks are driven by the applied stress whereas in region 4 the critical energy release rate has been attained and cracks propagate spontaneously, the necessary surface energy being acquired at the expense of the elastic strain energy available in the rock, without any further input stress. Morlier (1971) points out that this is consistent with the instability implied by an apparent Poissons ratio of greater than 0.5. However, Morlier also proposes a different mechanism. He states that, in region 3, "easy" cracks along planes of cleavage and grain boundaries propagate until stopped by a whole grain, but, in region 4, the grains themselves then fail, and, being stronger, once failing, continue to do so unimpeded. The latter explanation is perhaps more in line with a geological conception of a rock while the former lends itself more to quantitative analysis. Brace, Paulding and Scholz (1966) do not distinguish region 4.

In summary, then, the following main points about the stress-strain behaviour and internal structure of rock may be put forward.

a) Rock is non-linear elastic and shows a form of hysteresis. Both the non-linearity and the hysteresis may be adequately explained by postulating that the cavities in the rock are in the form of pores and cracks.

b) Failure is controlled by these cavities, in particular the cracks, and fracture initiation occurs at stresses below the ultimate

bearing (failure) stress (some 0.3 - 0.6 of the failure stress). This effect has also been observed in rocks under tension (Wawersik, 1968).

c) Before failure, dilation occurs, the increase in volume being mainly due to an increase in lateral strain.

Any theoretical discussion of rock properties should include these points either as a basis or as a prediction.

4. Fracture Theories and Criteria

It is interesting to compare existing theories and criteria for failure with the picture of rock behaviour just presented and with observed dependence of rock strength on experimental conditions. These criteria vary widely in appearance and it is difficult to divide them into empirical and theoretical types since they all contain, of necessity, a degree of empiricism. They will be presented, therefore, in order of depth of treatment.

The maximum shear stress theory is perhaps the most obvious. This states simply that, at failure, $(\sigma_1 - \sigma_2)$ = const. However, it predicts a failure plane angle of 45° and that the uniaxial tensile strength will equal the uniaxial compressive strength. The theory describes the behaviour of some ductile metals but is inapplicable to rocks.

Next, the Coulomb - Navier criterion proposes that the effective shear stress across the eventual failure plane should be a maximum. Thus, if τ_n and σ_n are the shear and normal stresses respectively. across a plane and μ is a coefficient of internal friction then $|\tau_n| - \mu\sigma_n = \tau_o$ = the cohesion of the material. This approach works better and fits the data for a significant number of rocks whose Mohr envelopes happen to be straight lines. τ_o and μ have no physical significance however.

More generally, the failure envelope for a rock will not be a straight line and Franklin (1968) found that he could fit the expression

$$\tau_{max} = \tfrac{1}{2}\left(2.\sigma_{max}\right)^{B}$$

to most data, where B varied between 0.6 and 0.8.

A more systematic approach to the whole subject of brittle failure was made possible by Griffith (1920) when he proposed that a solid might contain flaws, envisaged as flat elliptical cracks, whose action would be as stress raisers, thereby locally enhancing the applied stress. By applying an energy balance principle to an extending crack, Griffith obtained the relation

$$\sigma_c = \sqrt{\left(\frac{2S E_o}{\pi c}\right)}$$

where E_o is the Young's modulus of the material, S is the crack surface energy, c the crack half-length, and σ_c the stress required to propogate the crack.

In a biaxial stress field such that $\sigma_3 \geq -\sigma_1/3$, Griffith's formula becomes

$$(\sigma_1 - \sigma_3)^2 + 8T_o(\sigma_1 + \sigma_3) = 0$$

or when $\sigma_3 < -\sigma_1/3$

$$\sigma_3 - T_o = 0$$

McClintock and Walsh (1962) and Murrell (1964) modified this theory to include closed cracks, sliding, with a coefficient of friction μ . Their formula is

$$-\mu(\sigma_1 + \sigma_3) + (\sigma_1 - \sigma_3)\sqrt{1+\mu^2} = 4T_o$$

which may be rewritten in the form

$$\sigma_1 = \frac{4T_o}{\sqrt{1+\mu^2} - \mu} + \frac{\sqrt{1+\mu^2} + \mu}{\sqrt{1+\mu^2} - \mu}\,\sigma_3$$

This is a straight line, like the Coulomb-Navier expression, and has had a similar degree of success in describing the results of rock experiments. McClintock and Walsh found for their data that μ was in the range 0.8 - 1 while Hoek and Bieniawski (1965) found a wider range of 0.5 - 1.5 for various rock types.

Griffith's original theory took no account of the effect of

the intermediate principal stress and a number of workers have assumed that a variation of σ_2 would have only a small, and therefore negligible effect. Experiments by Murrell (1965) and Mogi (1971, 1967) have shown that such an assumption is invalid and that the strength of rock observed when $\sigma_1 > \sigma_2 > \sigma_3$ is a function of both σ_2 and σ_3. This has also been shown in theoretical work on large discontinuities done by Attewell and Woodman, 1971.

Murrell (1964) generalized the Griffith formula by analogy replacing $(\sigma_1 - \sigma_3)$ by $\sqrt{\{(\sigma_1-\sigma_3)^2+(\sigma_1-\sigma_2)^2+(\sigma_2-\sigma_3)^2\}}$ and $(\sigma_1 + \sigma_3)$ by $\sigma_1+\sigma_2+\sigma_3$ Thus the Griffith formula for closed cracks becomes

$$\tfrac{2}{3}(\sigma_1+\sigma_2+\sigma_3) + \alpha\sqrt{\{\tfrac{2}{3}[(\sigma_1-\sigma_3)^2+(\sigma_1-\sigma_2)^2+(\sigma_2-\sigma_3)^2]\}} = \beta$$

where α and β are functions of the crack friction and the stress required to close the crack.

Mogi (1971), on the other hand, estimated a failure curve based on a Von Mises failure criterion, which states that the distortional strain energy, proportional to the octahedral shear stress, τ_{oct}, is related to the volumetric strain energy, or

$$\tau_{oct} = f(\sigma_{oct})$$

Mogi's criterion takes the form

$$\tau_{oct} = f(\sigma_1 + \alpha\sigma_2 + \sigma_3)$$

where α is a parameter to be determined.

Looking back, it can be seen that all these formulae may be written in the form

$$\tau = f(\sigma)$$

Moreover, in most cases

$$f(\sigma) \propto \sigma^{\beta}$$

where β varies between $\frac{1}{2}$ and 1. Such a similarity between results is, however, a measure of the form of real rock data and not of the success of the theoretical predictions. That the Griffith theory,

for instance, appears to be ameans to an end and not a description of rock fracture may be seen from the experimental data on rock before failure. Some form of failure initiation begins before fracture, in both compression and tension, and Griffith suggests that failure initiation should be coincident with fracture; also, failure initiation should lead, in compression, to a distribution of S-shaped cracks far removed from the simple ellipsoids treated by previous workers. Thus, it would seem that Griffith's theory is only valid as a theory for failure initiation and its applicability to fracture can only be coincidence.

Barron (1971) has observed that the coefficients of friction required to satisfy the modified Griffith theory are greater than the coefficients of friction for the same rocks, measured directly (Jaeger, 1959) and he has used this fact, coupled with the fact that the form of the Griffith theory is correct for failure to postulate an imaginary effective crack, whose parameters are found from experiment, to describe fracture, leaving the actual crack model, with parameters measured directly, to describe failure initiation. By this method he is able to relate the occurrence of failure initiation and fracture to the applied stress field, though his results, being so dependent on experimental data, are still little more predictive than, say, the Coulomb - Navier expression.

Clearly, any work based on a single detail, as Griffith's work was based on a single crack, is of limited application in the field of rock mechanics where the material to be dealt with is so complex and interaction effects so difficult to study, either experimentally or theoretically. In order to tackle such complexity, statistical approaches have been taken by a number of workers.

In the field of pure statistics Weibull's (1929) weakest

link theory was perhaps the earliest. He modelled a general solid by a distribution of strengths within the solid and worked out the probability that the solid would fail under a given stress. The main result to come out of the theory was the prediction of a size effect, diminishing as the sample volume became very much bigger than the flaw volume, that is, as the number of discrete flaws became large. In intact rocks with no visible flaws, there is no observable size effect in normal laboratory samples, implying that the flaws governing failure are very small (Brown E.T. 1971; Bordia F.K., 1971). The disadvantage of Weibull's theory is that there is no physical basis for the assumption of the form of the distribution.

Weibols and Cook (1968) have suggested that the process of failure may be controlled by the total amount of strain energy stored by the deformed cracks within the rock and in particular that fracture occurs when this strain energy reaches a maximum. Their procedure for calculating the strain energy of the crack system takes full account of the effect of the stress system on a closed crack's ability to slide and the theory predicts correctly the form of the strength dependence on the magnitude of the intermediate principal stress. The difficulties with the theory are that the coefficient of crack interfacial friction required to fit the data does not seem to match with directly-determined values and that the crack distribution upon which the calculation is based is not necessarily the distribution obtaining at fracture. The physical principles of the theory appear to relate more to failure initiation, or to the initiation of unstable crack growth, than to fracture.

The concept of a rock as a mass of, perhaps, interacting cracks has also been used as the basis of an approach by Brady (1969).

Brady used the stress field applied to his model rock to determine the density of open cracks, the density of closed and sliding cracks, and, by Griffith's theory, the density of cracks that are in the process of failing. He then used the results on dilatancy reported by Brace Paulding and Scholz (1966) to form a semi-empirical stress-strain relationship for the model. This stress-strain relationship is related to fracture, he claims, by a critical volumetric strain criterion; that is, the material fails when a maximum value of volumetric strain is attained within the rock. The strain criterion is equivalent to one in which the total density of deformable, and Griffith-extendable, cracks reaches a critical value, representative of the number of micro-cracks needed to join to form a failure plane. His argument thus leadshim to an integration involving a crack distribution. He assumes that the final distribution is proportional to the initial distribution and is thus able to reduce his integral to 'known' functions. For a random distribution function this theory shows an apparently linear relationship between σ_1 and σ_3 with no dependence on σ_2 when σ_3 is compressive. Brady also shows that a curved relation between σ_1 and σ_3 of the correct form, may be produced by assuming that the rock contains a number of different phases and therefore cracks with a range of values for interfacial friction. Such a material may be approximated by a homogenous material with an equivalent coefficient of friction which varies with applied pressure. Presumably the form of pressure variation may be 'bent' to accommodate any experimental data.

Brady's theory is empirical in its approach and the results are not conclusive but it remains as a major attempt so far to relate cracking to stress-strain behaviour and stress-strain behaviour to failure. The theories of both Brady and Weibols and Cook are able to

relate rock properties to something that is, at least in principle, measurable by other means than strength tests; that "something" is the crack distribution and may be considered as a step towards a fuller theoretical description of rock behaviour.

5. Intrinsic Rock Anisotropy

Many rocks are banded or possess marked foliation as a result of the geological conditions under which they were formed. Such visual evidence of a defined directionality within the rock is usually accompanied by a preferred orientation of the constituent mineral crystals, a preferred orientation that can be determined by either optical or X-ray methods. For fine-grained rocks, such X-ray evidence may be the only sensible indication of any sort of anisotropy.

The presence of banding or foliation and its accompanying crystallite texture indicates that the bulk physical properties of the intact rock may show some anisotropy, either due to crystal anisotropy or a non-random crack distribution (for those properties that are affected by the cavities of the material), and in most cases that is so. Brace (1965) related variations in intrinsic (no cracks) elasticity to fabric in quartzite, where the crystals have an equant morphology, and Attewell (1970) showed a concordance between fabric and elastic properties for slate, whose crystals are platy in form. Pinto (1970) and Rodrigues (1970) have obtained experimental data on the variation of Young's modulus with direction in particular rocks.

Anisotropy may also be induced by applied stresses. Tocher (1957) observed a wave velocity anisotropy in a rock under a non-hydrostatic stress field and Nur (1971), reporting a similar effect, suggests that the stress field may preferentially close cracks, creating a non-random crack distribution which will then account for the observed anisotropy. Nur was able to predict velocity anisotropy from a given distribution function but found that the inverse problem, that of determining a unique crack field given a distribution of velocities, could not be solved.

Observations by Nishihara (1954) and Brace (1964) of a variation of Young's modulus with direction under a non-hydrostatic stress were explained by Brace in a similar way.

A variation of strength with the direction of application of the maximum principle stress may well also be expected, especially in the case of slate with a well defined plane of weakness, or cleavage plane. Such a variation is indeed observed, though for some rocks it is not large enough to warrant separate study and is considered merely as a factor affecting the scatter of experimental results (Bieniawski, 1967; Bernaix, 1969). Casagrande and Carrillo (1944) were perhaps the first to study the effect quantitively and Jaeger (1960) considered a rock where the shear strength varied according to the formula

$$S = S_1 + S_2 \cos 2(\alpha - \beta)$$

where S is the shear strength at an angle α (usually defining a shear failure plane) when the cleavage plane or bedding is inclined at an angle β to the maximum principle stress.

Donath (1961) expanded Jaeger's results and obtained a failure criterion of the form

$$\sigma_1 = a - b\cos 2(30 - \beta)$$

This relationship was shown to fit reasonably well to his experimental data on Martinsburg slate.

Rodrigues (1970) showed that variations in strength could be observed within the cleavage plane itself, and suggested the following empirical relationship

$$\sigma_1^4\left[\frac{\cos^2\alpha}{d^4} + \sin^2\alpha\right]\cos^2\phi\sin^2\phi + \sigma_1^2\left[\left(\frac{\cos^2\alpha}{a^2} + \frac{\sin^2\alpha}{b^2} - \frac{1}{c^2}\right)\cos^2\phi + \frac{1}{c^2}\right] = 1$$

Walsh and Brace (1964) and Hoek (1964) independently produced

a suggested mechanism for rock strength anisotropy. Their theory was an expansion of Griffith theory and used a non-random distribution of crack lengths. Walsh and Brace applied the theory to a distribution of long cracks the planes of which were all parallel to each other, and obtained a good fit to Donath's (1961) results. Hoek had similar success with his data.

For a crack system of particular length inclined at an angle β to σ_1, Walsh and Brace have suggested the equation:

$$C = \frac{C_0[(1+\mu^2)^{\frac{1}{2}} - \mu] + 2\mu' p}{2\sin\beta\cos\beta(1-\mu\tan\beta)}$$

for the strength of that system, where C_0 is the strength of the equivalent random array of the cracks. The theory has the same data fitting power as any Griffith theory and, by allowing C_0 to become a function of angle (that is, by saying that cracks become, usually, shorter as their orientation departs from bedding or cleavage) then almost any form of strength anisotropy may be accounted for. Barron (1971), for instance, has applied a multiple crack system to a sandstone with some success.

A proper test for such a theory would consist of a comparison between the crack distribution suggested by fitting to strength data and a distribution measured by some independent means. Such a comparison has not been done, and although Walsh and Brace suggest that their slate results are qualitatively correct and the theory is consistent with the long cracks of Morlier, it seems doubtful if, were it possible to measure a distribution, the result would be positive owing to the known rapid changes in crack formation undergone by a failing rock.

Two other theories, those of Brady and of Weibols and Cook, may be applied to the anisotropic strength behaviour of rock. Both

these theories require a crack distribution known beforehand, and the introduction of a non-random distribution should produce a variation in strength with direction. The next section compares the results of these two theories when applied to Penrhyn Slate, a rock whose anisotropic characteristics, in intact form, can be specified in some detail.

6. Analysis of Penrhyn Slate

Penrhyn Slate was formed, during the Caledonian orogeny, by dynamic metamorphism and its structural character presents the summetry of the constraints that acted in its formation (Attewell and Taylor, 1969). It is a fine grained rock, with a well-defined cleavage and a wide variation in mineralogy and colour, the particular form with which this study is concerned being the "hard blue" form.

Strength analysis of this material was performed by Linney (1969) and his data are shown in fig.16. It is clear from the diagram that there is a great variation in strength with direction with a minimum near $\beta = 30^{\circ}$. This minimum may be expected at the point where the maximum shear stress coincides with the minimum shear strength direction within the rock, that is, the cleavage direction.

Donath's cosine formula for such curves may be generalised to include any minimum angle and is then written

$$\sigma_1 - \sigma_3 = a + b \cos 2(\alpha - \beta)$$

Fig.17 shows the fit of this formula to the data for two values of confining pressure. It would appear from this that the data is rather less symmetrical about the minimum than is Donath's surve although it is worth noting that all the fitted curves had minima at angles somewhere between $\beta = 47^{\circ}$ and $\beta = 48^{\circ}$.

Each point in Fig.16 represents but a single sample and it is therefore difficult to draw any quantitative conclusions from the data. However, from the consistency found in the fitting of the Donath formula and from the general appearance and self-consistency of Linney's results, it would seem justifiable to use this data in a general study of the properties of the rock failure theories.

It is clear that Penrhyn Slate is structurally anisotropic but, in order to relate its apparent anisotropy to the strength data, a detailed specification of the structural anisotrophy is needed. The best information available for this purpose is the X-ray texture diagram defining the sub-fabric (0001) illite, such a diagram for Penrhyn Slate being shown in Fig. 9. The plane of the diagram is the plane of the rock cleavage and the main feature is that there is a maximum of reflected intensity normal to this cleavage, that is, there is a maximum volume of X-ray reflectors lying in the cleavage plane. This relationship and the finer relationship between X-ray texture and crystal fabric are discussed in the section of this thesis dealing with textural analysis.

The X-ray data only provide information on the volume of crystal planes comprising the crystal fabric, but provide no information on how these crystal planes are spatially distributed. In particular there is no information on the sizes of the rock crystals or on the sizes of the grains within those crystals. What is more disturbing, and this is most important where failure theories are to be considered, there is no information on the cavities between the crystals. This means that any attempt to form an idea of a distribution of cracks for the material must be based on interpreting the X-ray texture in the light of some additional fact or idea. In this case the facts must be the supplied strength data and the idea must be the failure theories to be tested. It must then be assumed that a combination of interpretation and theory which fits the data must be close to the true situation. Such an assumption is open to criticism but, in the absence of any proven method of obtaining a crack distribution, it will stand as a basis for this thesis.

There is one assumption which will aid the interpretation of the X-ray data and which can be made independently of any failure

theory and that is that the anisotropy is sufficiently described by the X-ray texture due to illite (001). This assumes that the structure of the rock is controlled by the crystals (illite, chlorite) having a plate-like morphology and ignores the contribution of the more equant crystals within the rock. There is essentially no difference between the c-axis sub-fabrics due to illite and chlorite and either could in fact be used. Any further assumptions concerning the interpretation of the texture diagram will be mentioned in their appropriate section.

7. Weibols and Cook's Failure Theory

If one considers only explosive or catastrophic failure of rock then one is considering a system in which there is a rapid release of energy. This being so, it may be reasonable to suppose that the energy concerned was stored within the material by the distortion of the contained microcracks under stress, and this is the basis of the Weibols and Cook concept.

In particular, if, under compressive stress, σ_n is the normal stress across a crack and τ_c is the shear stress associated with it and if the crack is closed and has a coefficient of friction of μ then that crack will slide when

$$|\tau_c| > \mu\sigma_n$$

and there will be an effective shear stress, for movement across the crack, of

$$\tau_{eff} = |\tau_c| - \mu\sigma_n$$

Under these conditions, the crack will store recoverable energy ω, where

$$\omega = k(\tau_{eff})^2$$

k being a constant, the value of which depends on the elastic constants of the surrounding material.

The total energy of distortion of the cracks will be the sum of all the ω's over all the cracks which are sliding and for a very large number of cracks this may be written as

$$W = k\int \omega(\zeta,\gamma)\, N(\zeta,\gamma)\, d\zeta\, d\gamma$$

where $N(\zeta,\gamma)$ is the number of cracks whose normals lie in the direction (ζ,γ) and the integral is taken over those values of ζ and γ for which $\tau_{eff} > 0$. The constant k is assumed to be independent of direction, though for an anisotropic matrix this will not be true.

The postulate is that the rock will fail when W reaches some materially defined limit, W_{max}, and the problem becomes one of finding, for a specified principle stress system and known μ and W_{max}, the amplitude of the stress difference at failure. This, in effect, requires the solution of the equation.

$$W = W_{max}$$

and can only be achieved if $N(\zeta, \gamma)$ is known.

The solution of the failure equation does not require W or W_{max} to be known absolutely and it is possible, therefore, to use values of k and N which are only proportional to the real values. Accordingly, in the numerical solution of this problem, k has been taken as unity and N has been taken as the normalized distribution function obtained directly from the Penrhyn Slate X-ray analysis, with no modification.

The use of the above orientation distribution function assumes that the cracks in the material vary in number but not length. The assumptions leading to this are as follows: a) that the crystallites in the rock do not vary in size; b) that the crystallites are spatially independent; c) that cracks are the voids at the flat faces of the plate-like crystallites; d) that the cracks are spatially independent. These assumptions allow the X-ray data to specify the number of crystallites directly and hence to specify the number of cracks directly and justification, or otherwise, for their use will be found in the quality of the results.

The form of the function

$$f = \omega(\zeta, \gamma) N(\zeta, \gamma)$$

is shown in Fig. 18 and, being smooth and quasi-parabolic, lends itself to a simple Simpson's rule integration procedure. Two such procedures, one for ζ and one for γ, were interleaved to perform

the double integration. Each integration was done repeatedly, with decreasing step length, until a convergence criterion had been satisfied. Execution time for the program was markedly dependent on the required accuracy and as a suitable compromise between the two factors, the convergence criteria were set such that the overall accuracy of the result was 1% or better.

Values of W were obtained for various values of the variables β, μ, σ_1 and σ_2 and these values were plotted against σ_1 to produce a family of curves, an example of which is shown in Fig. 19.

Such a set of curves can be used to produce a solution for W_{max} by choosing values of W until the values of σ_1, given by the curves correspond with the values of σ_1, given by experiment. However, by observation it will be seen that such a fit would be impossible with the given set of curves. These curves predict that the material strength will decrease for $\beta=0^\circ$, 30°, 45°, 60°, in that order and this is in complete contrast to the experimental order which has the minimum strength at $\beta = 30^\circ$. An explanation for this result has been sought both in terms of human error in incorrectly specified angles and in terms of the properties of the theory itself, but no sensible conclusion has been reached and the result must stand on its own merit.

It would seem, therefore, that the Weibols and Cook theory is not applicable when used with this particular crack distribution but in the light of information yet to be discussed this would appear to be a property of the distribution rather than the theory.

A point to note about the curves of Fig.19 is that they show a reduced dispersion in σ_1, for reducing W, thus, for small W,

there will be no variation in strength with angle. This is precisely the result that the Griffith theory would produce when applied to a crack distribution where the crack length was constant. As must be expected, this limiting value is lower than the minimum strength value of experiment. The limit increases with increasing μ and approaches the $\beta = 30^0$ strength value when μ approaches 0.8. but, as this limiting σ_1 value is the value at which τ_{eff} just becomes positive the usefulness of this result for strength predictions must only be to provide an upper limit for the possible values of μ .

8. Brady's Failure Theory

This theory is a mixture of analysis and empiricisms based on some aspects of pre-failure stress-strain behaviour of rock. The work is based on a prediction of the permanent strains produced by cracks undergoing failure and a failure criterion using the predicted strains. Numerical predictions rely heavily on experimentally determined strain and failure measurements.

Though the theory is quite capable of handling very general stress systems it will be necessary only to consider compressive systems in which $\sigma_2 = \sigma_3$ in order to make comparison with the data. This will allow only closed microcracks to be considered (but see Murrell and Digby, 1970, for a discussion of failure due to closed or open cracks).

As a rock is strained, a value of stress is reached at which microcracking begins and permanent lateral strain becomes just noticeable, although axial stress remains elastic. This leads to two assumptions: first, that permanent lateral strain is due to the extension of microcracks and, second, that microcracking does not contribute to permanent axial strain. Thus, if the change in strain e_i for a single microfracturing event is (de_i), Brady writes:

$$(de_1) \simeq 0$$
$$(de_2) \simeq (de_3)$$

The last expression will be valid only if the crack distribution is independent of the azimuthal angle γ.

These permanent strains will be functions of both crack orientation (and possibly length, although Brady does not suggest this) and stress, and, for a general crack distrib ution. where (λ, η) are the polar coordinates of the crack normal with respect to σ_1 Brady's formula becomes

$$(de_2) = \tfrac{1}{2} B\, g(\lambda, \eta) \frac{d\sigma_1}{(\sigma_1^f - \sigma_1)^m}$$

where B and m are constants, σ_1^f is the macroscopic failure strength of the material and $g(\lambda,\eta)$ is an unknown function of the orientation of the crack.

In general, the formula states that strains become larger for increasing σ_1, but, in particular that the strains become infinite when the rock fails. This form is not unreasonable for strains and stresses close to failure, but the existence of a finite post-failure strength in a number of rocks studied in stiff testing machines (Bieniawski, 1967; Rummel & Fairhurst, 1970; Wawerski & Brace, 1971) suggests either that Brady's proposed form is incorrect or that the formation of a failure plane immediately prior to failure allows the operation of a mechanism other than differential crack extension. However, as the failure plane does not begin to form until some 98% of the failure stress has been applied (Scholz, 1968b) its presence may conveniently be ignored for the moment and Brady's results taken as they stand.

From the incremental strain of each crack, the average microcracking strain may be given as:

$$\langle de_1 \rangle = 1/2\, A \rho \frac{d\sigma_1}{(\sigma_1^f - \sigma_1)^m}$$

where $$A = B \int_{\eta_1}^{\eta_2} \int_0^{2\pi} g(\lambda,\eta)\, P(\lambda,\eta,c)\, d\lambda\, d\eta$$

and $$\rho = \rho_e \int_{c_1}^{c_2} \int_{\eta_1}^{\eta_2} \int_0^{2\pi} P(\lambda,\eta,c)\, d\lambda\, d\eta\, dc$$

$P(\lambda,\eta,c)$ being the crack distribution probability, ρ being the density of microcracks able to extend, and ρ_e being the density of flaws within the specimen. Thus η_1 and η_2 and c_1 and c_2 are the limits defined by the Griffith criterion $|\tau| - \mu\sigma_n > 2\left(\frac{K}{c}\right)^{1/2}$ with K a constant.

Since $\langle de_i \rangle \simeq 0$ the total average volumetric microcrack strain is given by:

$$-(de) = A \rho \frac{d\sigma_1}{(\sigma_1^f - \sigma_1)^m}$$

Now, Paulding's work on dilatancy (Brace, Paulding, and Sholz, 1968) suggests to Brady that a critical volumetric strain criterion may be operative. Accordingly, he takes the total volumetric work done over the microcrack strains:

$$W_v = V \int \sigma_{ii} \, |de_{ii}|$$

where V is the volume of the specimen, and he states a criterion such that $W = W_{max}$. This is equivalent to the Weibols and Cook theory.

The total volumetric strain is given by:

$$|de_i| = \int_{\sigma_i^{min}}^{\sigma_i^{f}} A \rho \frac{d\sigma_i}{(\sigma_i^{f} - \sigma_i)^m}$$

the limits being those over which microcracking may take place.

At this stage Brady states, without proof, that the above work criterion is equivalent to the density criterion

$$\rho = C$$

C being a material constant. Either form of this criterion, he states, expresses the assumption that total failure takes place when there is a sufficient number of microcracks available so that the probability of their joining up to form a macroscopic fracture surface is large.

The constant crack density form of the criterion requires for its operation the evaluation of the integral

$$\rho = \rho_c \int_{c_1}^{c_2} \int_{\eta_1}^{\eta_2} \int_{0}^{2\pi} P(\lambda, \eta, c) \, d\lambda \, d\eta \, dc$$

where ρ_c is the density of flaws within the specimen. For $P(\lambda, \eta, c) = P(\lambda, \eta)$ the same distribution function as used for the Weibolls and Cook theory evaluation may be used.

Using the same distribution function as that used in the Weibols and Cook evaluation, that is, one in which the crack length is assumed constant and the number of cracks is taken to vary, produces much the same shaped plot when applied to crack densities with much the same negative results as for the previous evaluation. The same comments apply here as for the Weibols and Cook case. The apparent

failure of these two related theories must, for the moment, be assumed to be due to the crack distribution used. The following section will deal with an approach which, hopefully, will resolve this problem.

9. Modified Approach to Failure Theories

It has been shown in the previous chapter that an approach to rock strength anisotropy based on a crack distribution, where all the crack lengths are assumed to be the same, does not fit with the volume interaction theories independently given by Brady and by Weibols and Cook. The source of the discrepancy between theory and experiment may lie with the theories or with the distribution, and, since the formulation of the distribution function may be said to be based on weaker assumptions than those used in the two theories, it would seem reasonable to look for an alternative distribution function.

The work of Walsh and Brace (1964) and Hoek (1964) provides the starting point for the formulation of a new crack distribution function. These workers used crack distributions such that all cracks had the same length and were all aligned parallel to the bedding or cleavage plane of their material and they used their results to postulate that a good fit with experiment could be obtained over a wide range of the angle β by applying Griffith theory to a system of cracks the length of which grew shorter as their orientation departed from the plane of the bedding. The implication was that a crack length distribution could be derived from the experimental data and Barron (1971) performed just such a derivation for a sandstone.

The problem in the present work is the inverse of this however in that it is required to relate the strength variation to a known property of the rock, in this case the X-ray texture. The problem is simplified in the sense that it is known from the previous work that a variation in crack length is required such that the longest cracks lie parallel to the bedding and the form of the experimental data suggests that this variation should be smooth with the shortest cracks lying perpendicular to the

bedding. A function of this shape is, of course, supplied by the X-ray texture function itself.

In the previous attempt at formulating a crack distribution it was assumed that crystallites, and hence cracks, could be considered to be spatially independent. This assumption was the weakest of the assumptions used but was nevertheless the most important in that it formed a direct bridge between the assumptions of crystallite size and the final assumed form of the crack distribution. In work on wave attenuation in rocks, Walsh (1966) observed that his results suggested the existence of one crack for every grain. For the type of cracks Walsh considered, that is, those which were just closed under very small pressures, he thought that a crack to grain ratio of almost unity was unlikely. The work of Brace, Orange and Maddon (1965) on electrical resistivity of rock suggests the presence of a large volume of contiguous pores within (most) rock and Walsh suggests that a rock should have a looser structure than his own model with the attenuation caused by larger displacements on fewer cracks. This immediately implies, though Walsh does not say so explicitly, that the cracks must be larger than his model suggests and each crack must therefore encompass more than one grain. This means that it is no longer possible to assume that each grain contributes one crack. It must now be allowed that individual grains may join together in some fashion to form larger cracks and if this effect has some dependence on orientation then crack lengths may vary with orientation.

In any rock, the grains or crystallites may take any orientation, though the number of grains in any one orientation may be a function of that orientation, and clearly cavities of many shapes will form. In particular, crack shaped cavities can only form between grains which are subparallel to each other although it is possible to imagine a series of crack shaped cavities of many orientations all joining to produce a large crack which may be far from flat. However, while

acknowledging the internal complexities of such natural polymineralic aggregates it is both necessary and reasonable to use a model of reduced complexity.

Brace, Paulding, and Scholz (1966) have suggested that all cracks which are going to close will have closed under a reasonably low stress and Brady (1969) has said that it will be the closed cracks which will be in the correct orientation to fail first. The first point suggests that only cracks which are almost closed will close, the second point shows that it is only necessary to look at closed cracks of one orientation at a time and these two together mean that the discussion may be limited to grains which are subparallel, that is, in interpreting the X-ray texture as a means to formulating a crack length distribution the data in each orientation may be considered in isolation from the data for all other orientations. Berg (1965) emphasises this point by suggesting that typical cracks in rock tend to be very fine with aspect ratios, thickness/length, of the order of 10^{-3} and this implies that crack faces are very closely parallel to each other.

Given this assumption it should be possible to relate the numbers of grains in a given orientation to the probability of forming clusters of a given size and thence to an estate of a crack distribution function. Mack (1949, 1953) has studied an appropriate two dimensional form of this problem and has produced a formula for the expected number of a k-aggregate in a "random" distribution of points, where a k-aggregate is defined as k points which may be covered by a window of known size.

A window is an area of fixed size which is moved over the surface to be examined and at each new position, an infinitesimal distance away from the previous position, the number of points in the distribution falling within the window area is counted. If the number of points so counted is "k" then a k-aggregate has been found. It is, of course,

possible for a new window position to include exactly those points which were counted in the previous position and Mack has allowed for this. In the present application the points to be counted are the centres of crystallites sufficiently close together to form a large crack face.

There are, however, a number of problems associated with the use of this method. For cracks considered to be associated with crystallite faces, it is possible to imagine two crystallites, say, sufficiently close as to be overlapping, thus producing a crack length of less than two unit crack lengths. A window which included all reasonable pairs of cracks would also include all overlapping cracks and it would be necessary to perform at least two calculations, with different window sizes, to take the overlap effect into account. Such a calculation would not of itself be excessively difficult but there is a further problem which may be difficult to overcome. There is no simple way of distinguishing a k-aggregate that is also part of a k+1 aggregate. In particular it may be seen that a 3-aggregate may contain 1, 2, or 3 off 2-aggregates depending on the sizes of the windows used to view the aggregates. For the case of clusters of two or three it should be possible to take account of this effect but the complexity of the problem increases with the size of the cluster being considered and rapidly becomes unmanageable.

These problems, coupled with the complexity of Mack's original expression, mean that it will not be possible to produce a complete crack distribution function even though Mack's approach is apparently suited to the problem.

For the purposes of Griffith's theory, it is not necessary to have the complete distribution. All that is required is a knowledge of the length of the longest crack cluster in any orientation. In theory, the longest crack is only limited by the size of sample and the total number of discrete unit cracks in the sample with that particular orientation but clearly these limits are rarely reached, especially when

samples tend to be chosen so that they appear to be homogenous, with no major flaws! A more practical limit should be obtained if it is assumed that the number of k-aggregates which are not part of (k+1)-aggregates reduces the population available for (k+1)-aggregates. However, this approach still requires the complete distribution function and, as has already been noted, this is not available.

All that this leaves, then, is the indication that the maximum length will be some function of the total number of unit cracks and for the rest of this discussion it will be assumed that this function is linear. This means that the assumed maximum crack length will be directly proportional to the (0001) distribution function as output by the texture-goniometer.

Having obtained some form of crack distribution, the Griffith theory can be applied and predicted strength curves obtained.

The Griffith failure criteria can be written (Walsh and Brace, 1964)

$$\tau_{eff} = |\tau| - \mu \sigma_n = 2\sqrt{\frac{K}{c}}$$

where c is the crack length and K is a constant. K and c are to be found. For the present work, c is taken from the unmodified, normalised, X-ray texture and the criterion becomes

$$|\tau| - \mu \sigma_n = B/\sqrt{I}$$

I being the normalised diffracted X-ray intensity value. The values of μ and B have to be determined by experiment.

The process of finding values for μ and B and using these values to predict strengths was carried out in two stages. The first stage involved the use of a direct application of the formula of

Walsh and Brace to the simple distribution of cracks, all having the same length and all being mutually parallel. The parameters for this formula (Co, the uniaxial compressive strength for a random array of the same cracks and μ, the coefficient of crack interfacial friction) were chosen such that the theory gave a least squares fit with the experimental data at $\beta = 30^{\circ}$. The value of μ was found to be 0.5. This value is determined largely by the position ($f(\beta)$) of the minimum strength value and can thus be very well determined as this minimum position is clearly defined. A number of curves of $\tau_{eff} = |\tau| - \mu\sigma_n$ as a function of angle were drawn for $\mu = 0.5$ and various values of σ_1 and σ_2 (Fig.20). These curves may be used with a plot of $B/\sqrt{c}$ against angle to determine strength values and conversely strength values may be used with the τ_{eff} curves to produce $B/\sqrt{c}$ values. For the simple crack distribution so far considered there is only one $B/\sqrt{c}$ value at zero angle and the Walsh and Brace distribution and results were used to find that for these conditions the value of $B/\sqrt{c}$ was 2.9 in the units used. This value must correspond to the minimum $B/\sqrt{c}$ value for any more general function that may be used to describe the strength data. As B is a constant the function must also satisfy the maximum value of c. In the more general function chosen c, the crack length, is the same as I, the normalised X-ray intensity and it is known that the largest value of I is 8. This gives a value of B = 8.2.

The second stage is actually to plot the values of $B/\sqrt{c} \equiv B/\sqrt{I}$ and to use the τ_{eff} curves to determine the angles for which failure will take place with a given stress system. This is done by superimposing the τ_{eff} curve on to the $B/\sqrt{c}$ curve such that, for a given σ_1, the two curves just touch. The angle through which the τ_{eff} curve must be displaced to produce this result is the angle at which σ_1 is the failure stress (see Fig.21). The $B/\sqrt{c}$ curve is shown in Fig.22 and a plot of strength against angle for four values of σ_2 is

shown in Fig.23. Experimental values for $\sigma_2=0$ are also shown in Fig.23 and it can be seen that the fit of theory with experimental data seems less marked for low values of β . This is because the theoretical values are almost symmetrical about the minimum when the data values clearly are not.

The fit of this theory with data is shown in Figs. 24 to 27 where $(\sigma_1 - \sigma_2)$ is plotted against σ_2 for various angles β . These diagrams show a reasonable fit for angles greater than $\beta = 30^{\circ}$ but a less than reasonable fit below that. It is to be noted that the theory shows a linear relationship between σ_1 and σ_2 and that the slope of this line does not vary significantly with β .

10. Discussion of Penrhyn Slate Results

The applied theory is a Griffith Theory and as such produces a straight line plot between σ_1 and σ_2 with the slope being dependent on the coefficient of crack interfacial friction, μ. There is however one less degree of freedom in fitting the Griffith Theory to anisotropic data in as much as the value of μ must also define the angle β_{min} at which the minimum strength is observed such that $\tan 2\beta_{min} = 1/\mu$, and for this reason it seems reasonable to suppose that the value of μ obtained, giving, as it does, such a good fit to both slope and minimum, will represent quite closely the average value of the real coefficient of friction actually in force in the rock. Walsh (1966) quotes values of μ obtained experimentally for both smooth and roughened crystal surfaces and the value of 0.5 fits into the range of various crystal surfaces roughened by sliding across each other. This must be reasonable as there will be sufficient displacement prior to failure across already rough surfaces (involving more than one grain) to grind those surfaces and roughen them and it must be these ground faces which control the final failure.

Finding the value of C_o appropriate to the experimental data has no theoretical significance unless it can be used to give some indication of crack size. However this needs some knowledge of the elastic constants of the intrinsic material of the rock and this data is not available.

The fact that the application of Griffith's theory to the simple crack length distribution provided produces an anisotropic strength distribution is not of itself remarkable but the result is, none the less, a useful one in that the strength distribution so obtained bears a close resemblance to that obtained by experiment. In particular there is quite a close fit between theory and experiment for angles $\beta \geq 30°$

and in this the crack distribution postulated from the evidence of clay mineral basal plane orientation distribution improves on the simplest distribution where all cracks are parallel. The crack length distribution obtained from the X-ray data is not necessarily, and indeed is unlikely to be, the true distribution, but the very fact that such a distribution, obtained independently of the data it was hoped to fit, does produce such results argues against simple coincidence.

The main difficulty in allowing the theory to describe the experimental data lies in the discrepancy between the two for $\beta < 30^{\circ}$. This arises because the theoretical curve is symmetrical about its minimum, a symmetry which is not shared by the experimental points. This symmetry is built in to the two components which go to make up the final curve. The crack distribution is naturally symmetrical; and an asymmetric distribution seems most unlikely. The τ_{ff} curve is almost symmetrical about its maximum but what asymmetry there is does not become obvious until some way below each peack and can have little effect.

The asymmetry of the experimental data is similar to that noted by Donath (1961) in his data on Martinsburg slate. Donath in fact only noticed a serious departure from his symmetrical curve in the data for $\beta = 0^{\circ}$ and in this instance claimed that the constraining effect of the sample end plates affected the result. This could well be so as Donath also reports that the inclination of the shear plane at failure followed closely the inclination of the cleavage plane for angles β up to 30° and a little beyond and under those conditions the failure plane would have interacted with the end plate of the compression apparatus. For a standard sample with a length to diameter ratio of 2/1 such interaction would be expected for shear plane angles of less than about 26°.

The interaction between the angle of the failure plane and

the orientation of the sample reported by Donath is also seen in Penrhyn Slate. The inclination, α, of the failure plane with respect to σ_1 is plotted against β, the sample orientation, in Fig. 28a. for all the samples of Penrhyn Slate at all angles and confining pressures. No distinction is made between data obtained at different confining pressures as no distinction was discernable. This plot shows a trend towards control of the failure plane angle by sample orientation and it seems significant that the data for $\beta = 15^\circ$ and $\beta = 30^\circ$ shows much less scatter than that for other angles. The relationship between α and β indicated by this data may be generalised to the assumption that $\alpha = \beta$ for $\beta \leq 30^\circ$ and with this assumption some new results may be obtained from the theory presented in the last section.

The expected form of interaction between the effective shear stress and the crack lengths is shown in Fig. 21. Where the τ_{eff} curve just touches the $B/\sqrt{c}$ curve defines the failure point and it would be expected that that point of contact would also define the angle, α, of the subsequent shear plane, as shown. Normally this angle α would lie quite close to the expected angle of 30° but, if it is known that has some other constraint on it then a different situation obtains. In particular, the case where $\alpha = \beta$ is shown in Fig. 29 and this clearly requires a higher value of σ_1 than would normally be predicted. A new set of values for σ_1 may be obtained using the assumption that for $\beta < 30^\circ$ then $\alpha = \beta$ and results for $\sigma_2 = 0$ are plotted in Fig. 30. As can be seen, the required upturn is obtained and a plot of $(\sigma_1 - \sigma_2)$ against σ_2 for $\beta = 15^\circ$ in Fig.31 may be compared to Fig.15 which shows the same plot obtained before this modification. The improvement is significant.

Fig.28b shows the relationship between α and β given by the above considerations and modified by the applied constraint. It can be seen that the predicted angles, α, above $\beta = 30^\circ$ are larger than the

data suggests but that the general form of the data is preserved.

Even so the answer is far from complete. For angles $\alpha = \beta$ close to zero the τ_{eff} curve vanishes and the theoretical strength of the rock becomes infinite. Thus the proposed modification still leaves an unknown gap.

A more obvious, though perhaps related, deficiency is expressed by the question: why should the shear plane be constrained to follow the cleavage plane for only that range of angles? There is nothing in the theories so far presented which suggests any reason for the region $\beta < 30^{\circ}$ being different from the region $\beta > 30^{\circ}$. It is, however, possible to imagine a mechanism and this is described here.

A number of workers (for example Brace and Bombolakis, 1963; Hoek and Bieniawski, 1966; Murrell and Digby, 1970) have shown that a crack will propagate in the S shape form shown in Fig. 32a such that the extensions tend to become parallel to σ_1. Now the initially propagating crack will be at approximately 30° to σ_1, but the new extensions will have the effect of producing a new effective crack at a smaller angle to σ_1. Thus the crack will seem to rotate either away from or towards the cleavage plane according to whether β is greater or less than 30°, as shown in Fig.32b. In this way the failing cracks may become entrained in the plane of weakness, the cleavage plane, and the orientation density distribution will become depleted for crack orientations away from the cleavage plane. This entrainment becomes less and less easy for β approaching zero and there must be some gradual modification into yet another failure mode, for example, the effective tensile stress mode of Brown and Trollope (1967).

Having obtained a theory which enables the anisotropic strength variations of a material to be predicted to a reasonable degree of accuracy, it is necessary to examine the success of that theory in

the light of the pre-failure behaviour of rock.

The fact that the proposed theory relies solely on a Griffith criterion immediately suggests that the pre-failure behaviour of the material has been ignored. This is not necessarily true. The examination of rock failure theories showed that only the Weibols and Cook and Brady theories made any attempt to take into account a cooperation of cracks in forming the failure but it is easily seen that these theories provide little or no improvement over the Griffith one. In particular, the constraints on the crack friction coefficient, μ , are the same in all theories. Examination of Fig.19 shows that the strain energy function, for constant crack length, produces the same slope for the σ_1 against σ_2 line independently of the total strain energy and there is no reason to suppose that the change in the form of the distribution would change that. Similarly the shape of the σ_1 against β variation would remain symmetrical as in the simple case though the detailed shape would depend on the exact form of the $B/\sqrt{c}$ curve used and, as has been shown, this is open to some manipulation. Thus the two cooperative theories would produce very much the same results as the simple Griffith theory.

Where the strain energy and strain volume criteria do depart from the Griffith theory is in their ability to predict the angle of the failure plane. Neither theory contains any mechanism whereby the expected failure plane angle may be derived and it would be very difficult to modify either theory to take into account the crack entrainment mechanism proposed for $\beta < 30^{\circ}$. Such a modification is not impossible and it may well be feasible to implement the appropriate integration over a dynamic crack population by use of a digital computer but, having done so, the answer would turn out to be a series of applications of Griffith's theory and the basis of the work, either strain energy or strain volume, would become lost in the detail. Indeed such theories become irrelevant when such a detailed model of the structure becomes available.

It would seem that, even for anisotropic data, the Griffith theory still holds good despite a large quantity of data on pre-failure rock behaviour which suggest that a more complex cooperative theory is required. The question is, if the Griffith theory is applicable to rock failure rather than failure initiation then what is happening to cause all the activity observed between failure initiation and failure? Murrell (1969) provides the clue.

Murrell points out (Murrell, 1969) that the microcrack events which occur prior to failure contribute to the formation of new crack distributions and that there must be a whole range of crack distributions formed during the pre-failure period. He also points out that any crack may propagate more than once as a stress distribution becomes modified by the surrounding activity. Morlier (1971) also provides part of the answer when he suggests that initial microcracking may be due to cracks in weaker material propagating until halted by, say, a harder grain, causing fracture hardening.

Neither of the above statements contravenes any of the observed pre-failure occurrences but, equally, neither necessarily implies cooperation in the sense of Weibols and Cook or Brady.. However, a form of cooperation is taking place in that the pre-failure activity is setting up the required conditions for failure.

It was remarked in an earlier section that cracks in rock were formed by associations of sub-parallel grains. It was also pointed out that cracks so formed may take all orientations and may join together to produce larger cracks which are not flat but bend and twist in space in an undefined manner. It is now possible to envisage such distorted cracks as having weak points, say, at crystallite edges, and that under stress these weaknesses will allow some form of microfracture. Such microfractures will propagate only to the surface of the crystallites concerned and any excess energy will appear as additional strain on the

whole crack and as microseismic activity. In other words, the surface of such a distorted crack will become ground and splintered until it tends to become flat and the orientation of the resulting flat crack will be just that orientation undergoing maximum shear stress. The overall texture of the rock will not be altered by this operation, only the crack distribution, and in fact it will be the crystallite structure of the rock which will control the formation of the new crack distribution. This modification of the crack distribution will only take place for those orientations for which the shear stress is large, but within that limitation the crystallite texture of the rock will define the final crack distribution and not the initial one. In this way catastrophic failure will not occur until a well-defined crack-like cavity, terminated by some stronger part of rock material, has formed, whereupon the Griffith criterion comes into play with all that that implies.

11. Application of Theory to Lumley Mudstone

Having obtained a theory which provides a reasonable fit to experimental data for one rock, Penrhyn Slate, it is appropriate to apply the same theory to a different rock and to examine the differences, if any, exposed in the process.

The rock chosen is a Coal Measures mudstone, from Lumley, County Durham.* This is a lightly lithified material, with a well defined cleavage, characterised by light and dark laminations derived as a result of cyclic sedimentological regimes. It suffers from rapid weathering on exposure.

Information on strength variation with cleavage inclination was obtained and the relationship between the two is shown in Fig.33 for three values of confining pressure. It can be seen that the material is not strong and is anisotropic with a strength minimum in the region of $\beta = 30^{\circ}$.

An X-ray texture diagram was obtained and is shown in Fig.34. As expected, there is a maximum intensity perpendicularto the plane of the cleavage but this runs off quite quickly to a wide plateau of constant intensity starting at about 40° away from the maximum. The case of Penrhyn slate showed that the texture is significant up to 50° away from the maximum and therefore this plateau can be expected to influence the predicted strength results.

The values of the two parameters of the theory, μ, the coefficient of friction and B, from $B/\sqrt{c}$, were chosen by eye as this enabled the effects of the theory to be evaluated. The values chosen were $\mu = 0.6$ and $B = 3$.

The plot of $B/\sqrt{c}$ is shown in Fig.35 and shows the plateau from the texture. Allowing for the rounding up of values printed on the texture diagram has little effect as this can only be assumed to

* The roof rock of the High Main coal seam

come into force towards the rim of the diagram, that is at an angle of 40° the intensity must be close to 3 as printed and can only fall to 2.5. which rounds up to 3, towards an angle of 90°. This has been shown in Fig.35.

The strengths predicted using the theory are plotted against cleavage inclination in Fig.36. for two of the values of confining pressure that were used to obtain the data shown in Fig.33. The plateau in intensity is now seen to produce a cut-off in strength for $\beta < 70^{\circ}$, a cut-off which is not reflected in the experimental data.

For angles $\beta < 70^{\circ}$ however the predicted values follow the usual pattern, and comparison of σ_1 vs. σ_2 for various angles β, shown in Fig.37. indicated that only minor modifications to B and μ would be required to make a good fit with experiment.

The results obtained with the theory here do not include the effects of failure plane entrainment and yet Fig.37 shows that the predicted strengths for $\beta = 15^{\circ}$ fall quite close to the experimental values. This is a major departure from the ideas put forward with Penrhyn Slate and requires a certain amount of detailed discussion.

As shown in Fig.21 it is possible to make use of the theory to predict the angle of the failure plane, α, with respect to σ_1. The variation of α with β for Lumley Mudstone is shown in Fig.38 for two different confining pressures. The averaged experimental results are included for comparison. It is clear from this figure that confining pressure does have a significant effect on failure plane angle and this may be explained by reference to Fig.39 where two τ_{eff} curves at two different confining pressures are compared. This comparison shows that the lower the confining pressure the flatter the τ_{eff} curve becomes, and a greater variation in contact point between τ_{eff} and B/C will occur for a flat τ_{eff} curve than for a less flat one. This variation was not so marked with Penrhyn Slate, and was small enough to be ignored

because the higher σ_1 values reduced the effect*. As in the case of Penrhyn Slate the predicted values of α are higher than the experimental ones.

The plateau in the texture diagram manifests itself in the α vs. β plot as a dip in α for $\beta > 65$, this dip being greater for low values of σ_2 . The experimental data shows a similar dip and it is tempting to use this fact as a confirmation of the plateau. This is, however, still inconsistent with the strength data and it is felt that further work is required before the conflict can be resolved.

The major difference between Penrhyn Slate and Lumley Mudstone, and in the application of the theory to them both, seems to be that Penrhyn Slate suffers a high degree of entrainment of α with β whereas Lumley Mudstone does not. The fact that α follows close to β for some values of $\beta < 30^{\circ}$ with Lumley Mudstone is not due to entrainment but merely a ramification of the simple theory. Since the theory otherwise works well for both rocks it becomes necessary to ask why one rock behaves in this fashion and another does not. It is, of course, virtually impossible to answer such a question on a study of only two rocks.

Given that cracks do propagate in order to cause bulk failure it is reasonable to assume that they would prefer to propagate along the plane of least strength, that is, the cleavage fissility plane of the rock. Given also that cracks propagate in the sigmoidal fashion described previously then, for $\beta < 30^{\circ}$, an extending crack should, at some time, have the correct orientation to be entrained by the cleavage fissility. This entrainment would seen to be the natural course of events. Why, then, does not Lumley Mudstone exhibit the effect?

* The radius of curvature of τ_{xy} at its maximum increases with both σ_1 , and σ_2 .

The first significant fact is that entrainment enhances the strength of the rock for those orientations at which it occurs. This suggests that a crack finds greater difficulty in propagating if it extends at small angles to the cleavage plane ($\beta < 30^{\circ}$) than if it extends almost perpendicularly across the cleavage plane ($\beta > 30^{\circ}$). That is, if a crack extends through the crystallites in its path, rather than between them, this must occur most easily if the local shear is at a high angle to the plane of the crystallite.

The second significant fact is that Penrhyn Slate has undergone dynamic metamorphism, whereas Lumley Mudstone has not. Thus the crystallites of any particular mineral are likely to show little variation in average size with orientation in Lumley Mudstone, but, because of preferential growth under stress, crystallites in Penrhyn Slate may well show a variation in linear dimensions with orientation. Such an effect will, of course, make little difference to the analysis of the X-ray texture as one large crystallite will appear the same as two crystallites, of half the size, close together, but, it may have a significant effect on the ability of a crack to propagate across the cleavage plane. In particular, it may be that a crack within Penrhyn Slate must extend by breaking through crystallites whereas a crack in Lumley Mudstone may extend by passing round such obstacles since the crystallites concerned are much smaller.

The presence of more equant crystallites within a rock will, of course, modify the effect of the platy ones and this modification is not yet quantifiable. The mechanism of the formation of a failure plane is also not fully understood and thus the above suggestion for the entrainment mechanism must be taken as a tentative one.

12. Conclusion

Previous work (see Chapter 3) has shown that the brittle failure of rock is a very complex process, made more complex by anisotropy of the rock structure. Because of this it was suggested that a simple theory, such as that of Griffith, was too simple to be of use. However, Walsh and Brace (1964) demonstrated that strength anisotropy could be included in the Griffith theory by allowing crack length to become a function of orientation, and it has been shown that, despite the complexity of the failure process, the simple Griffith theory may be applied to anisotropic rocks with some success, provided that the crack lengths used by the theory are taken as the crack lengths obtaining in the rock immediately prior to failure. For the case of Penrhyn Slate considered, the required orientation distribution of crack length appears to be given by the unmodified data from the X-ray texture diagram of illite basal(0001) planes and it would appear from this that the plate-like illite and chlorite crystals are a major factor in determining the way that large cracks will form in the material. It has also been shown that the lack of symmetry in the experimental strength data may be explained by allowing the failure plane to be entrained by the cleavage plane for sample orientations of $\beta < 30^{\circ}$. Such entrainment has been observed for Penrhyn Slate as well as for other anisotropic rocks.

The importance of these results is twofold. Firstly, they show that the use of anisotropic material can provide a greater insight into the mechanism of failure, as, in this instance, it has shown that the Griffith theory still describes rock behaviour rather better than any others, and, secondly, they show that it is possible to relate quantitively an independently measured property, in this case X-ray textures, to measured strength data and find reasonable agreement between them.

Examination of the data for Lumley Mudstone has emphasised the applicability of the overall concept described here but this has also shown that the angle, α, of the failure plane is a significant parameter in the description of the failure mechanism.

The predicted angles, α, for both materials used are only in general agreement with the experimental data and further study is needed to find where the discrepancy lies. However, there is a significant difference between the form of the two sets of results in that only Penrhyn Slate shows a proper entrainment effect. This has been interpreted as a reflection on the internal structure of the materials and it suggests that, for Penrhyn Slate, grain size (as well as crack size) may be a function of orientation.

It was the original purpose of this work to examine ways in which an X-ray texture, or pole figures, could be used in a quantitative fashion to describe properties of anisotropic material, with a view to defining the accuracy requirements of the process for obtaining the pole figures. In the present application the X-ray data are already more accurate than the strength data and it will have been observed that, for a rock with a smoothly decreasing orientation density distribution of the fabric feature being studied (the situation which applies to Penrhyn Slate), cracks with an orientation greater than approximately 50° away from the bedding plane can never take part in the failure process as described in this Thesis. This implies that, for strength anisotropy experiments, only one X-ray sample need be used. Moreover, the orientation of the sample need not be specified very closely as this will be given by the observed maximum. Thus, the fabric determination may be greatly simplified.

It has been assumed throughout this Thesis that failure has been due to closed cracks, and that these cracks have been controlled by one type of mineral phase only. Both assumptions are, to some extent, justified by the results.

The control of failure by the platy minerals within the rock is, perhaps, obvious. Rocks which contain small amounts of micaceous, allied platy, or other inequant minerals would not be expected to show significant intrinsic strength anisotropy and there is a clear relationship between such strength anisotropy and a preferred orientation of plate-like crystallites.

The assumption that failure is by closed crack follows from this in that the longest cracks within rocks of the type considered here are best formed by the adjacent faces of micaceous mineral crystallites. Such cracks are likely to have small aspect ratios (Berg, 1965) and would appear to close quite easily, this being shown by a linear stress-strain relationship after the initial curve (Fig.15). The presence of a positive, finite, value for crack interfacial friction completes the connection and, thus, for rocks of the type considered, open cracks appear to have very little effect.

In conclusion, strength anisotropy of rock has been associated with a textural anisotropy observable by X-ray techniques but it must be said that the structural anisotropy, in the form of a crack length orientation distribution, may only be a control on other, more complex, perhaps, failure devices and may not describe the complete failure mechanism.

The concepts presented here should allow the prediction of the complete brittle strength orientation relationship for an anisotropic rock from a single texture measurement and sufficient uniaxial strength measurements to define the minimum strength orientation. Further work on crack length orientation distributions and failure plane formation is, of course, required, and it is hoped that this Thesis has sufficiently emphasised the importance of such work.

Appendix A. Schulz' calculation to show independence of reflected intensity on sample elevation

The independence of diffracted intensity on the sample elevation angle ζ was given by Schulz (1949) as follows:

From Fig.3 an elemental volume at depth t is given by

$$dV = \frac{WS\ dt}{\sin\theta\ \cos\zeta}$$

where W = horizontal width of beam

S = vertical width of beam

The path length through the material for X-rays diffracted at the depth t is given by

$$l = \frac{2t}{\sin\theta\ \cos\zeta}$$

Now, if μ is the linear absorption coefficient for the material and D is the scattering efficiency at the angle θ then the total intensity diffracted is given by

$$I = I_0\ D \int \exp\left(-2\mu t / \sin\theta\ \cos\zeta\right)\ dV$$

where the integral extends over the entire volume of an infinitely thick sample

Substituting for dV gives

$$I = I \frac{D\ W\ S}{\sin\theta\ \cos\zeta} \exp\left(-2\mu t / \sin\theta\ \cos\zeta\right)\ dt$$

which becomes, after integration,

$$I = \frac{I\,D\,W\,S}{2}$$

showing that, for a sample of infinite thickness, or of sufficient thickness to produce sensibly complete absorption, the reflected intensity is independent of the angle.

Appendix B

The texture goniometer Data Reduction programme

The Philips texture goniometer, in common with other equipment of this type, scans along its observation spiral (Fig.2) at a constant rate and the mechanism is so designed that equal increments of time imply equal increments of ζ and γ (Figs. 1 & 2) and it is this fact which provides the basis for the program.

For ease of handling, the X-ray intensity data was sampled at known fixed intervals of time and punched on to paper tape by an Addo-X punch. Under some circumstances it was found convenient to reproduce the data on to cards (this was performed by a Computer Unit facility) but in any case the program will accept the data in any form and in any format provided that successive data items are in the correct sequence. The data for each scan are terminated by a zero.

The program must be provided with information on the rate of revolution (TIME) of γ, the rate of change of ζ with each full revolution of γ (TILT) and the sampling interval for the data (STIM). With this information the program can work out the change in γ ($\delta\gamma$) and ζ ($\delta\zeta$) for successive data items such that

$$\delta\gamma = 360 * \text{STIM} / (60 * \text{TIME})$$

$$\delta\zeta = \text{TILT} * \text{STIM} / (60 * \text{TIME})$$

The first data item is assumed to start with $\zeta = \gamma = 0$ and the angles are incremented approximately for each item.

As the angular position for each point is determined then it must be transformed from the sample coordinate system x_1, x_2, x_3 to the projection coordinate system X_1, X_2, X_3. In the simplest case the two will

be the same and no transformation will be required but in general a set of 3 Euler angles will be required, these are:

A, a rotation about the x_3 axis taking $x_1 \rightarrow x_1'$ and $x_2 \rightarrow x_2'$

B, a rotation about x_2' taking $x_3 \rightarrow X_3$

C, a rotation about X_3 taking $x_1' \rightarrow X_1$ and $x_2' \rightarrow X_2$

These angles are taken as positive if a right hand screw moves away from the origin and the coordinate transformation becomes:

$$X_i = L_{ij}\, x_j$$

where L_{ij} is

Cos(A).Cos(B).Cos(C) -Sin(A).Sin(C)	, Sin(A).Cos(B).Cos(C) +Cos(A).Sin(C)	,-Sin(B).Cos(C)
-Cos(A).Cos(B).Sin(C) -Sin(A).Cos(C)	,-Sin(A).Cos(B).Sin(C) +Cos(A).Cos(C)	, Sin(B).Sin(C)
Cos(A).Cos(B)	, Sin(A).Sin(B)	, Cos(B)

Having obtained the proper coordinates of the point the projection coordinates are then found as

$$x_{pi} = X_i\, r/(r + X_3) \qquad i = 1, 2$$

or

$$x_{pi} = X_i\, r/\sqrt{r^2 + rX_3} \qquad i = 1, 2$$

for equal angle or equal area projection respectively. The data may now be entered into the array at the appropriate (rounded) coordinate position.

It can happen, particularly near the centre of a spiral, that a number of data points will fall into the same square on the net. This possibility is catered for by keeping a total of the number of times each net square is accessed and averaging the data entered.

Some samples may contain crystals of much larger size than average for that sample and should such a crystal be in the correct orientation and fall under the X-ray beam then the signal may be enhanced by several hundred per cent, forming a spurious peak on the trace. When this is done then the data is examined over the six current values H(1) to H(6) and truncation occurs if

$$\text{MAX}\ (H(4), H(3)) - \text{MAX}\ (H(6), H(1)) > \text{PEAK}$$

That is to say, PEAK represents a height above the wanted data such that data values above this value will be truncated. In such a case, new values will be chosen for the points H(2) to H(5) such that they fall on a straight line between H(1) and H(6).

Before being entered onto the net all data values are corrected for background. The background value (BKG) is determined according to the method illustrated in Fig.5.

A scale factor must also be introduced and this is done through the parameter SCALE. This relates the millivolt reading of the counter to counts per second and must include any scaling factor introduced at the datalogger. Since the background value is normally taken from the chart record the value of BKG must also be adjusted to include the datalogger scaling.

The data is collected and the pole figure built up, one sample at a time, and it is possible to request a printout of the intermediate states of the pole figure. The plot so obtained is a plot of the average of (I - BKG) /BKG, where I is the data value appropriate to each point on the net, and this plot therefore only serves to provide an indication that samples have been correctly matched and little more.

When all the data have been entered the data are smoothed. This has the dual function of reducing the effect of noise on the signal and of filling unspecified points on the net with estimated values. The smoothing algorithm is exactly as used by Baker, Wenk and Christie (1969), that is each point takes the value of a weighted average of its previous value and the 8 surrounding values. In order to avoid distortion of the picture as the smoothing window is swept across the net the new values are kept separate from the old and only old values are used on each application of the algorithm. To ensure complete coverage the net is swept twice with different weights used in each pass.

In order to avoid edge effects when the collated data is smoothed, an annulus is defined on the net, inside the primitive circle of the projection, such that any points within this annulus are mirrored at the corresponding point outside the primitive circle. The width of this annulus is specified by BAND in terms of lines in the y direction of the paper. The dimensions of the storage array are calculated from this value according to the projection being used. A value of 6 is suggested for normal use, though if only the central part of the projection is being used a value of zero is more appropriate.

Finally, for ease of printout, the data is normalized to the value of the overall maximum found in the set. If required, a value for this maximum may be forced by the TOTMAX parameter.

Printout occurs with single characters, blank, 1 to 9, 0, in each print position, being the data value in that position to modulus 10. The centre of each character position the location for its particular value.

The printing devices normally used have a vertical scale of 6 lines to the inch down the page and 10 characters to inch along the page. This ratio is allowed for in calculating the x and y coordinates of the

projected points and is fixed in this program. The scaling of the coordinates must, of course, be taken into account when working back to angles from the printed diagram.

An integration may be performed on request to find the average value of the X-ray intensity. This integration is performed simply by summing the values in each square of the net and subsequently dividing by the total number of squares counted and is thus only valid for an equal area projection. The result of this integration is printed and points within a certain tolerance of the value are replaced on printout by a plus (+) character. Any number of printouts with this feature may be requested.

The program is also designed to deal with data from a transmission X-ray sample (Baker, Went & Christie, 1969) as well as the reflection data. It is important that data from the two types of scan be distinguished and space is provided for specifying "R" or "T" for relevant information. One or other of these characters must be included where appropriate as there is no default.

Data Input to PROJ 4

Card 1	Col 1 - 5	F(5)	SNO		Sample Number
Card 2 - 5	all columns		4 title cards		
Card 6	Col 1	F(2)	Q		No. of data sets
	Col 4	F(2)	RAD		"y" radius of output circle
	Col 7	F(2)	BAND		lines
	Col 10	B(1)	P		(1-equ.Ang. Proj (ø-equ. Area. Proj
	Col 12	F(4)	TOTMAX	*	
	Col 16	A(1)	PINT	*	R or T
	Col 17	A(1)	IP	*	I - int. printout
Card 7 & subs. cards for Q data sets					
	Col 1	A(1)			R or T
	Col 3	F(3)	TIME		minutes
	Col 7	F(3)	TILT		degree
	Col 11	F(2)	STIM		seconds
	Col 14	F(4)	NUM		
	Col 19	F(3)	BKG		mV
	Col 23	F(4)	SCALE		cps = mV + SCALE
	Col 28	F(4.ø)	SETPHI	*	trans only
	Col 33	F(3)	A	*	
	Col 37		B	*	rotation angles (degrees)
	Col 41		C	*	
	Col 45	F(3)	PEAK	*	mV
	Col 73	A(8)	IDENT	*	

Further list input

N1, N2, N3.....ad inf if Ni < 1

causes print out with randomization + uses window

Ni * 100% . Last Ni=Nj > 1 causes repeats of last printout.

Lastly 8888 signifies repeat with new data group

9999 signifies termination

notes. If code 8888 or 9999 is missing and Nj < 1 and next SNO < 7000 then prog will attempt to produce SNO copies of final printout.

* Optional Parameter

Appendix C

The Crystallite Distribution Function

Because two planes of one crystal type bear a constant relationship to each other, defined by the crystal itself, then two pole figures obtained from each of the planes will also bear a certain relationship to each other, though such a relationship may not be precisely defined (Baker, Wenk and Christie, 1969). Meieran (1962) introduced the following description of the relationship between the various pole figures.

One can draw a series of spheres around a crystal, one for each crystal form that is to be plotted. If the radius of each sphere is $1/d_{hkil}$, the reciprocal of the interplanar spacing, the poles to planes plotted on the corresponding spheres will form the reciprocal lattice.

When the crystal is rotated into another orientation with respect to a fixed coordinate system, the lattice of points rotates with the crystal. The fabric may be generated by rotating the crystal into a large number of orientations and at each orientation plotting the poles to the various planes on the appropriate spheres. The points on each sphere may be contoured and projected to produce pole figures. The pole figures are related to each other since they were produced by the same set of crystal orientations.

It is possible to describe in detail how these pole figures are related.

If rectangular cartesian axes are defined x,y,z in the sample and X,Y,Z in the crystal itself then these two sets of axes are connected by a transformation $T(\psi,\chi,\phi)$ where ψ,χ,ϕ are the Euler angles for the rotation and are as defined in Roe (1965). The density of the crystals having a particular orientation will be a function of that orientation and the crystallite distribution function of Roe (1965)

may be written as $\omega(\xi, \psi, \phi)$
where $\xi = \cos(\chi)$ and such that

$$\int_0^{2\pi}\int_0^{2\pi}\int_{-1}^{1} \omega \, d\xi \, d\psi \, d\phi = 1 \qquad \text{Eq 1.}$$

Since this function involves three angles it may not be represented on the surface of a sphere, however an axis distribution chart (Jetter et al, 1965) may be obtained by integrating with respect to ψ and then projecting the result on to the surface of a sphere.

In the special case of the sample having axial symmetry about x then ω is independent of ψ and the function may then be plotted on a sphere. The resulting diagram, which shows the frequency density of the specimen symmetry axis with respect to crystal axes, is known as an inverse pole figure (Barrett and Massalski, 1966).

In order to derive the crystallite distribution function from pole figure data the i^{th} reciprocal lattice vector r_i is considered. The orientation of r_i is given by Θ_i and Φ_i in the X,Y,Z system of the crystal, and by α_i and β_i in the x,y,z system of the sample and these angles are related by the expression

$$\begin{bmatrix} \sin\alpha_i \cos\beta_i \\ \sin\alpha_i \sin\beta_i \\ \cos\alpha_i \end{bmatrix} = T^{-1}(\theta_1, \theta_2, \theta_3) \begin{bmatrix} \sin\Theta_i \cos\Phi_i \\ \sin\Theta_i \sin\Phi_i \\ \cos\Theta_i \end{bmatrix} \qquad \text{Eq 2.}$$

where T is the transformation matrix previously defined and expanded by Roe (1965).

Let $I(\xi_i, \beta_i)$ be the intensity distribution obtained from a goniometer suitably corrected for errors. Then the normalized pole distribution is obtained from

$$q_i(\xi_i, \beta_i) = I(\xi_i, \beta_i) \Big/ \int_0^{2\pi}\int_{-1}^{1} I(\xi_i, \beta_i) \, d\xi_i \, d\beta_i \qquad \text{Eq 3}$$

where $\xi = \cos\alpha_i$

Now, $q_i(\xi_i, \beta_i)$ and $\omega(\xi, \psi, \phi)$ may be expanded in terms of spherical harmonics and generalised spherical harmonics respectively, (the symmetry properties of these functions have been dealt with by Meyer, 1954) giving

$$q_i(\xi_i, \beta_i) = \sum_{l=0}^{\infty} \sum_{m=-l}^{l} Q_{lm}^i P_l^m(\xi_i) e^{im\beta_i} \qquad \text{Eq 4.}$$

and

$$\omega(\xi, \psi, \phi) = \sum_{l=0}^{\infty} \sum_{m=-l}^{l} \sum_{n=-l}^{l} W_{lmn} Z_{lmn}(\xi)\, e^{-(im\psi + in\phi)} \qquad \text{Eq 5.}$$

where $P_l^m(\xi)$ is a normalised associated Legendre function and $Z_{lmn}(\xi)$ defined by Roe, is a generalisation of this.

Using the orthogonality properties of the functions 4 and 5 gives

$$Q_{lm}^i = \tfrac{1}{2\pi} \int_0^{2\pi} \int_{-1}^{1} q_i(\xi_i, \beta_i) P_l^m(\xi_i) e^{im\beta_i}\, d\xi_i d\beta_i \qquad \text{Eq 6}$$

and

$$W_{lmn} = \frac{1}{4\pi^2} \int_0^{2\pi} \int_0^{2\pi} \int_{-1}^{1} \omega(\xi, \psi, \phi) Z_{lmn}(\xi) e^{-(im\psi + in\phi)}\, d\xi\, d\psi\, d\phi \qquad \text{Eq 7}$$

The next step, that of relating Q_{lm}^i and W_{lmn} has been tackled differently by Roe and Baker, Wenk and Christie and, because of differences in the normalisation used, the answers differ in the multiplicative constants. Their formulae are otherwise essentially the same.

Roe's method is simpler and will be presented here.

The transformation of coordinates represented by 2 may be applied to $P_l^m(\xi_i) e^{im\beta_i}$ to produce

$$P_l^m(\xi_i) e^{im\beta_i} = \left(\frac{2}{2l+1}\right)^{\frac{1}{2}} \sum_{n=-l}^{l} Z_{lmn}(\xi) e^{im\psi} e^{in\phi} P_l^n(\Xi_i) e^{in\Phi_i} \qquad \text{Eq 8}$$

where $\Xi_i = \cos\Theta_i$

By multiplying both sides of 8 by $\omega(\xi, \psi, \phi) q_i(\xi_i, \beta_i)$ and integrating over the whole ranges of ξ, ψ, ϕ, ξ_i and β_i the required relation is obtained:

$$Q_{lm}^i = 2\pi \left(\frac{2}{2l+1}\right)^{\frac{1}{2}} \sum_{n=-l}^{l} W_{lmn} P_l^n(\Xi_i) e^{in\Phi_i} \qquad \text{Eq 9.}$$

The Q_{lm}^i may all be obtained from experimental data and the

W_{lmn} may then be found from the set of linear equations 9 , or conversely, given W_{lmn} from a previous calculation an unknown $q_i(\zeta_i, \beta_i)$ may be found.

Since 9 has $(2l+1)$ unknowns, $n = (-l \ldots 0 \ldots l)$, then, in general, $(2l+1)$ pole figures need to be determined for its solution. However, since the sample often possesses some sort of symmetry, many of the W_{lmn} cease to be independent and the number of pole figures needed is less than $(2l+1)$.

In working with a pole density distribution it is convenient, numerically, to have it in the form of a functional expression rather than a tabular plot since this simplifies the programming problems associated with interpolation.

The required expression is given by equation 4; however the function is complex and fails to take into account the interrelationships of coefficients.

If Q^i_{lm} is written as $a^i_{lm} + i\,b^i_{lm}$ then equation 4 becomes

$$q_i(\zeta_i, \beta_i) = \sum_{l=0}^{\infty} \sum_{m=-l}^{l} a^i_{lm} P_l^m(\zeta_i) \cos m\beta_i + i\, b^i_{lm} P_l^m(\zeta_i) \sin m\beta_i \qquad \text{Eq 10}$$

From Friedel's law the pole figure must always be centrosymmetric, that is

$$q(\zeta_i, \beta_i) = q(-\zeta_i, \beta_i + \pi) \qquad \text{Eq 11}$$

which, in conjunction with the property of Legendre functions

$$P_l^m(-\zeta) = (-1)^{l+m} P_l^m(\zeta) \qquad \text{Eq 12}$$

leads to

$$Q_{lm} = (-1)^l Q_{lm} \qquad \text{Eq 13}$$

Thus Q_{lm} must be identically zero when l is odd, or

$$a_{lm} = b_{lm} = 0 \qquad \text{for } l \text{ odd} \qquad \text{Eq 14}$$

By taking Roe's definition of $P_l^m(\zeta)$ which has

$$P_l^m(\zeta) = (-1)^m P_l^{\bar{m}}(\zeta) \qquad \text{where } \bar{m} = -m \qquad \text{Eq 15}$$

and applying this to equation 6 the simplifying relations

$$a_{lm} = (-1)^m a_{l\bar{m}}$$
$$b_{lm} = (-1)^{m+1} b_{l\bar{m}} \qquad \text{Eq 16}$$

are found.

Using the symmetry properties of sine and cosine and equations 15 and 16 enables $q(\zeta,\beta)$ to be written as

$$q(\zeta,\beta) = \sum_{l=0}^{\infty} \sum_{m=0}^{l} \left(A_{lm} P_l^m(\zeta) \cos m\beta - B_{lm} P_l^m(\zeta) \sin m\beta\right) \qquad \text{Eq 17}$$

where $A_{l0} = a_{l0}$, $B_{l0} = 0$

$A_{lm} = 2a_{lm}$, $B_{lm} = 2b_{lm}$

This form takes into account the possible simplifications due to the properties of the functions used without assuming anything about the symmetry of the measured texture. Since textures in rocks are not always sufficiently well defined and since it may be convenient to have the symmetry axis not coincident with the sample axis then the form equation 17 is quite suitable for general application to any problem concerning rock texture.

REFERENCES

Attewell, P.B. 1970 Triaxial anisotropy of wave velocity and elastic moduli in slate and their axial concordance with fabric and tectonic symmetry.
Int. J. Rock Mech. Min. Sci.7 pp 193 - 207.

Attewell, P.B. Taylor, R.K.T. 1969 A Microtextural interpretation of a Welsh slate.
Int. J. Rock Mech. Min. Sci.6 pp 423 - 438.

Attewell, P.B. Woodman, J.P. 1971 Stability of discontinuous rock masses under polyaxial stress systems.
"Stability of Rock Slopes", 13th.Symp.on Rock Mechanics. University of Illinois.pp 665 - 68

Baker, D.W. Wenk, H.R. and Christie, J.M. 1969 X-ray analysis of preferred orientation in fined-grained quartz aggregates.
J. of Geol. 77 pp 144 - 172.

Barrett, C.S. and Massalski, T.B. 1966 Structure of Metals. 3rd edition
McGraw Hill, N.Y., 654p.

Barron, K. 1971 Brittle fracture initiation in, and ultimate failure of, rocks. Parts 1 and 2.
Int. J. Rock Mech. Min. Sci.8 pp 541 - 575.

Berg, C.A. 1965 Deformation of fine cracks under high pressure and shear.
J. Geophys. Res. 70 pp 3447 - 3452.

Bernaix, J. 1969 New laboratory methods of studying the mechanical properties of rock.
Int. J. Rock Mech. Min. Sci.6 pp 43 - 90.

Bieniawski, Z.T. 1967 Mechanism of brittle fracture of rock. Part 1 Theory of the fracture process.
CSIR report MEG520, Pretoria, South Africa 24

Bordia, S.K. 1971 Effects of size and stress concentration on the dilatancy and fracture of rock.
Int. J. Rock Mech. Min. Sci.8 pp 629 - 640.

Brace, W.F. 1969 Micromechanics in rock systems.
Proc. Civ. Eng. Mat. Conf., Southampton,
ed. M. Te'eni, pp 187 - 204.

Brace, W.F. 1965 Relation of elastic properties of rocks to fabric.
J. Geophys. Res. 70 pp 5657 - 5667.

Brace, W.F. 1964 Brittle fracture of rocks.
in: State of Stress in the Earths Crust.
ed. W. R. Judd.
Elsevier, N.Y., pp 110 - 178

Brace, W.F. and Bombolakis, E.G. 1963 A note on brittle crack growth in compression.
J.Geophys. Res. 68 pp 3709 - 3713.

Brace, W.F. and Orange, A.S. 1968 Electrical resistivity changes in saturated rocks during fracture and frictional sliding.
J. Geophys. Res. 73 pp 1433 - 1445.

Brace, W.F. Orange, A.S. and Madden, T.M. 1965 The effect of pressure on the electrical resistivity of water-saturated crystalline rocks.
J. Geophys. Res. 70 pp 5669 - 5678.

Brace, W.F. Paulding, B.W. and Scholz, C.H. 1966 Dilatancy in the fracture of crystalline rocks.
J. Geophys. Res. 71 pp 3939 - 3953.

Brady, B.T. 1969 A statistical theory of brittle fracture for rock. Parts 1 & 2.
Int. J. Rock Mech. Min. Sci. 6 pp 21 - 42 and pp 285 - 300.

Brown, E.T. 1971 Strength-size effects in rock material.
Symp.Soc. Int. Mecanique des Roches, Nancy.
paper II - 11.

Brown, E.T. and Trollope, D.H. 1967 The failure of linear brittle materials under effective tensile stress.
Rock. Mech. Eng. Geol. 5 pp 229 - 241.

Casagrand, A. and Carrillo, N. 1944 Shear failure of anisotropic materials. J. Boston Soc. Civ. Eng. 31 pp 122 - 135.

Chernock, W.P. and Beck, P.A. 1952 An analysis of certain errors in the X-ray reflection method for the quantitative determination of preferred orientation. J. Appl. Phys. 23 pp 341 - 345.

Cook, N.G.W. and Hodgson, K. 1965 Some detailed stress-strain curves for rock. J. Geophys. Res. 70 pp 2883 - 2888.

Donath, F.A. 1961 Experimental study of shear failure in anisotropic rocks. Geol. Soc. Am. Bull. 72 pp 985 - 990.

Dunn, C.G. and Walter, J.L. 1959 Synthesis of a (110) 001 type torque curve in silicon iron. J. Appl. Phys. 30 pp 1067 - 1072.

Fayed, L.A. 1967 An X-ray diffractometry technique for preferred orientation studies in rocks. Int. J. Rock Mech. Min. Sci. 4 pp 101 - 114.

Franklin, J.A. 1968 A strength criterion for rock. Imp. Coll Rock Mech. Research Report No. 6 March 1968 36p.

Gardner, R.D. and Pincus, H.J. 1968 Flourescent dye penetrants applied to rock fractures. Int. J. Rock Mech. Min. Sci. 5 pp 155 - 158.

Gehlen, K. von 1960 Die "rontgenographische und optische Gefüge"analyse von Erzen. Beitr. Mineralog. Petrog. 7 pp 340 - 388.

Griffith, A.A. 1921 The phenomena of rupture and flow in solids. Phil. Trans. Roy. Soc. Lon. A221 pp 163 - 198

Hoek, E. 1964 Fracture of anisotropic rock. J. S. Africa Inst. Min. Met. 64 pp 501 - 518.

Hoek, E. and Bieniawski, Z.T. 1965 Brittle fracture propagation in rock under compression. Int. J. Fract. Mech. 1 pp 137 - 155.

Hsio, C.C. and Moghe, S.R. 1969 Characterisation of random microstructural systems. Proc. Civ. Eng. Mat. Conf., Southampton, ed. M. Te'eni, pp - .

Irwin, G.R. 1958 Fracture. in: Handbuch der Physik. 6 pp 551 - 590. ed. S. Flügge. Springer-Verlag.

Jaeger, J.C. 1960 Shear failure of anisotropic rocks. Geol. Mag. 97 pp 65 - 72.

Jaeger, J.C. 1959 Frictional properties of joints in rocks. Geofis. pura appl. 43 pp 148 - 158.

Jetter, L.K. McHargue, C.J. and Williams, R.C. 1956 Method of representing preferred orientation data. J. Appl. Phys. 27 pp 368 - 374

Knill, J.L. Franklin, J.A. and Malone, A.W. 1968 A study of acoustic emission from stressed rock. Int. J. Rock Mech. Min. Sci. 5 pp 87 - 121.

Ko, K.C. and Haas, C.J. 1971 The effective bulk modulus of rock as a composite material. Int. J. Rock Mech. Min. Sci. 9 pp 531 - 541.

Linney, L.F. 1969 The effects of planar anisotropy on the mechanical properties of Penrhyn Slate. Dissertation for M.Sc. Advanced Course in Engineering Geology, Univ. Durham, U.K.

McClintock, F.A. and Walsh, J. B. 1962 Friction on Griffith cracks under pressure. Proc. 4th. U.S. Nat. Cong. Appl. Mech., Berkely, pp 1015 - 1021.

Mack, C. 1953 The effect of overlapping in bacterial counts of incubated colonies. Biometrika 40 pp 220 - 222.

Mack, C. 1949 The expected number of aggregates in a random distribution of points. Proc. Camb. Phil. Soc. 46 pp 285 - 292.

Meieran, E.S. 1962 Use of the reciprocal lattice for the development of a new pole figure technique. Rev. Sci. Instr. 33 pp 319 - 322.

Meyer, B. 1954 On the symmetries of spherical harmonics. Canadian J. Mathematics 6 pp 135 - 157.

Mogi, K. 1971 Effect of the triaxial stress system on the failure of dolomite and linestone. Tectonophys, 11 pp 111 - 127.

Mogi, K. 1967 The effect of the intermediate principle stre in rock failure. J. Geophys. Res. 72 pp 5117 - 5131.

Morgenstern, N.R. and Tamuly Phukan, A.R. 1969 Non-linear stress-strain relations for a homogenous sandstone. Int. J. Rock Mech. Min. Sci. 6 pp 127 - 142.

Morlier, P. 1971 Sur le comportement des roches fragiles avant la rupture. Symp. Soc. Int. Mecanique des Roches, Nancy paper I - 4.

Murrell, S.A.F. 1969 Micromechanical basis of the deformation and fracture of rocks. Proc. Civ. Eng. Mat. Conf., Southampton. ed. M. Te'eni. pp 239 - 248.

Murrell, S.A.F. 1965 The effect of triaxial stress systems on the strength of rocks at atmospheric temperatures. Geophys. J. 10 pp 231- 281.

Murrell, S.A.F. 1964 The theory of the propagation of elliptical Griffith cracks under various conditions of plane strain or plane stress. Parts 1, 2 & 3. Brit. J. Appl. Phys. 15 pp 1195 - 1223.

Murrell, S.A.F. and Digby, P.J. 1970 The theory of brittle fracture under triaxial stress conditions. Part 2. Roy. Astr. Soc. Geophys. J. 19 pp 499 - 512.

Nightingale, J.P. and Lewis, D. 1971 Pole figures of the orientation of apatite in bones. Nature 232 pp 334 - 335.

Nishihara, M. 1954 Deformational characteristics of rocks under low stress.
Doshisha Eng. Rev. 4 pp 151 - 155.

Nur, A. 1971 Effects of stress on velocity anisotropy in rocks with cracks.
J. Geophys. Res. 76 pp 2022 - 2034.

Pincus, H.J. and Dobrin, M.B. 1966 Geological applications of optical data processing.
J. Geophys. Res. 71 pp 4861 - 4869.

Pinto, J.L. 1970 Deformability of schistous rocks.
Proc. 2nd. Int. Cong. Rock Mech., Beograd. vol 1 pp 491 - 496.

Roe, R.J. 1965 Description of crystallite orientation in polycrystalline materials. III:General solution to pole figure inversion.
J. Apply. Phys. 36 pp 2024 - 2031.

Rodrigues, F.P. 1970 Anisotropy of rocks; most probable surfaces of the ultimate stresses and of the modulus of elasticity.
Proc. 2nd. Int. Cong. Rock Mech., Beograd. vol 1 pp 133 - 142.

Rummel, F. and Fairhurst,C. 1970 Determination of the post failure behaviour of brittle rock using a servo controlled testing machine.
Rock Mech. 2. pp 189 - 204.

Scholz, C.E. 1968a Microfracturing and the inelastic deformation of rock in compression.
J. Geophys. Res. 73 pp 1417 - 1432.

Scholz, C.E. 1968b Experimental study of the fracturing process in brittle rock.
J. Geophys. Res. 73 pp 1447 - 1454.

Schulz, L.G. 1949 A direct method of determiningpreferred orientation of a flat reflection sample using a Geiger counter X-ray spectrometer.
J. Appl. Phys. 20 pp 1030 - 1033.

Simmons, G. and Brace, W.F. 1965 Comparison between static and dynamic measurements of compressibility of rock. J. Geophys. Res. 70 pp 5649 - 5656.

Starkey, J. 1964 An X-ray method for determining orientations of selected planes in a polycrystalline aggregate. Am. J. Sci. 262 pp 735 - 752.

Te'eni, M. and Staples, G.E. 1969 Stress phase interaction models. Proc. Civ. Eng. Mat. Conf., Southampton. ed. M. Te'eni. pp 469 - 486.

Tocher, D. 1957 Anisotropy in rocks under simple compression. Trans. Am. Geophys. Union 39 pp 89 - 94.

Walsh, J. B. 1966 Seismic wave attenuation in rock due to friction. J. Geophys. Res. 71 pp 2591 - 2599.

Walsh, J.B. 1965a The effect of cracks on the compressibility of rock. J. Geophys. Res. 70 pp 381 - 389.

Walsh, J.B. 1965b The effect of cracks on the uniaxial elastic compression of rocks. J. Geophys. Res. 70 pp 399 - 411.

Walsh, J.B. 1965c The effect of cracks in rock on Poisson's ratio. J. Geophys. Res. 70 pp 5249 - 5257.

Walsh, J.B. and Brace, W.F. 1966 Elasticity of rock: a review of some recent theoretical studies. Rock Mech. Eng. Geol. 4 pp 283 - 297.

Walsh, J.B. and Brace, W.F. 1964 A fracture criterion for brittle anisotropic rock. J. Geophys. Res. 69 pp 3449 - 3456.

Wawersik, W.R. 1968 Detailed analysis of rock failure in laboratory compression tests. Ph.D. Thesis. Univ. Minnesota, U.S.A.

Wawersik, W.R. and Brace, W.F. 1971 Post failure behaviour of a granite and diabase. Rock Mech. 3 pp 61 - 85.

Weibull, W. 1939 A statistical theory of the strength of materials. Ingvetens. Akad. Handl. 15 pp 5 - 44.

Weibols, G.A. and Cook, N.G.W. 1968 An energy criterion for the strength of rock in polyaxial compression. Int. J. Rock Mech. Min. Sci. 5 pp 529 - 549.

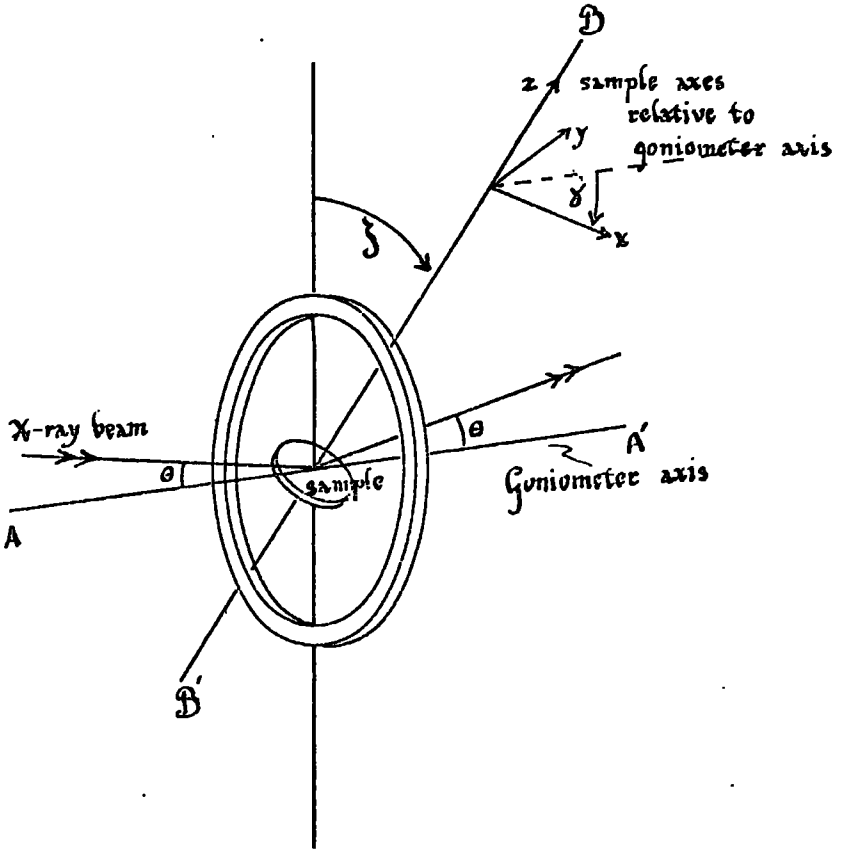

Fig. 1. Representation of sample in the goniometer, showing principal directions.

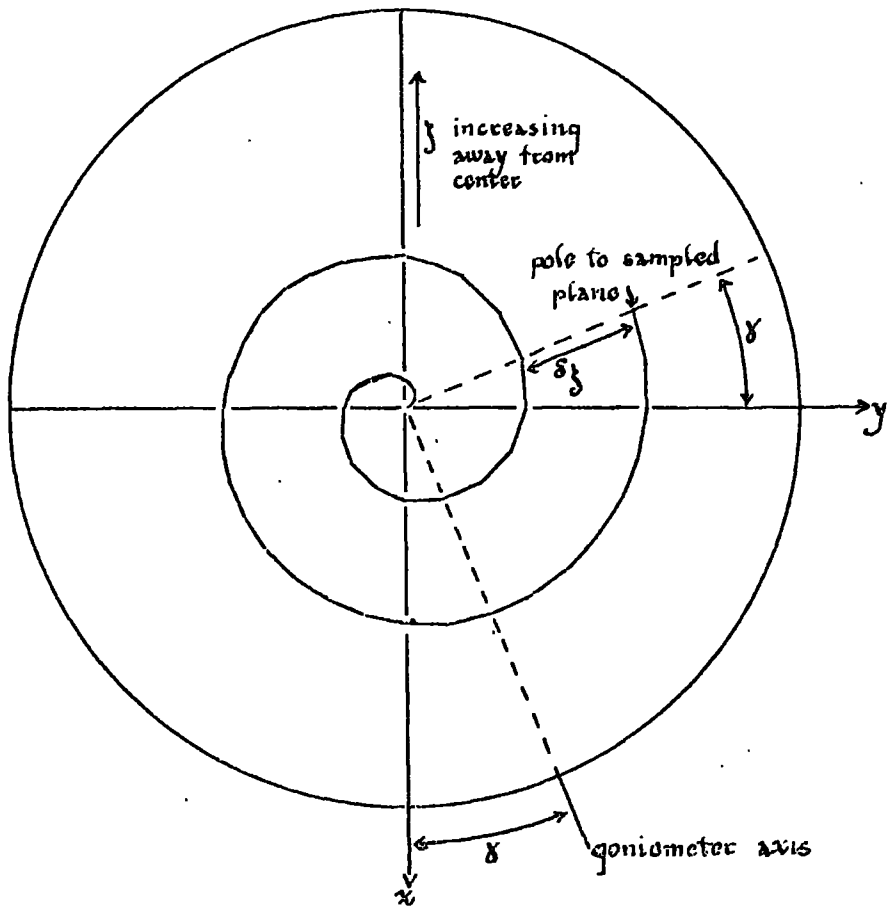

Fig. 2. Locus of projection, onto xy plane of rock specimen, of the normals to the sampled crystal planes, showing the spiral scan.

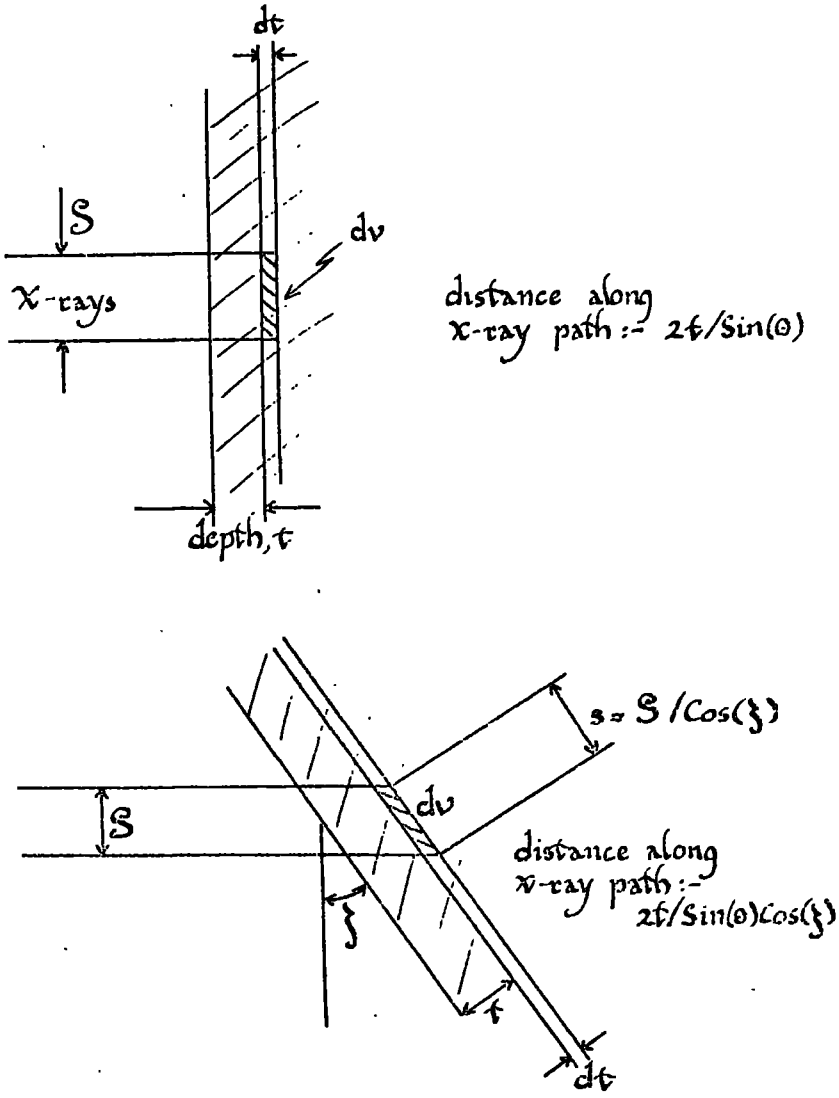

Fig 3. Diagram of X-ray reflection from a small volume in a sample. This diagram is used to show the independence of reflected intensity on the sample elevation angle, ξ.

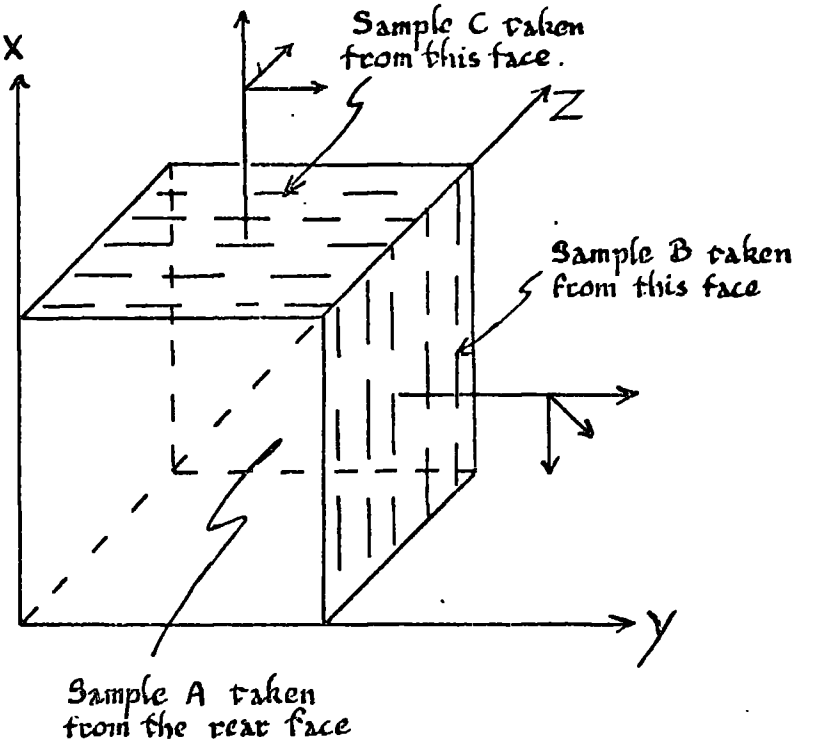

Fig. 4. Diagram showing how the 3 orthogonal samples for the X-ray texture study are related. Note that the cleavage of the rock lies parallel to the A face.

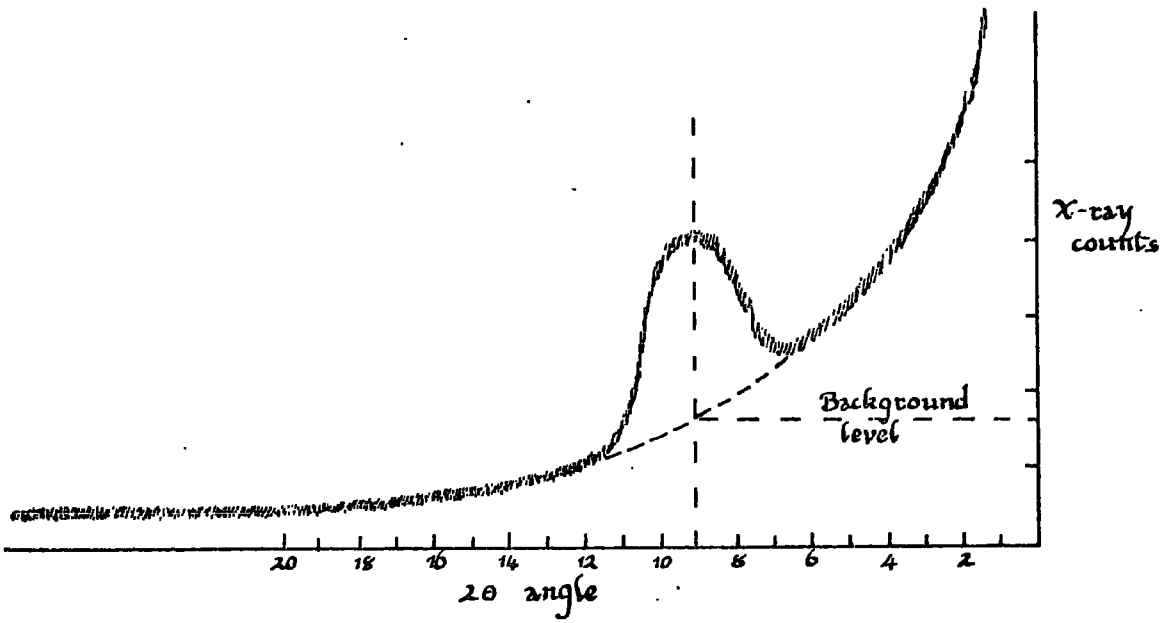

Fig. 5. Chart record with peak at $2\theta = 9^\circ$ and showing a background interpolation under the peak.

Fig. 6. Intermediate computer print out of pole figure for Penrhyn Slate, Illite (001). Sample section A.

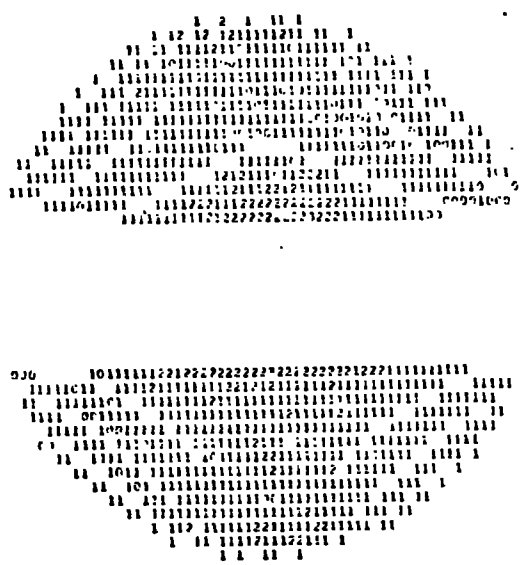

Fig. 7. Intermediate computer print out of pole figure for Penrhyn Slate, illite (001). Sample section B.

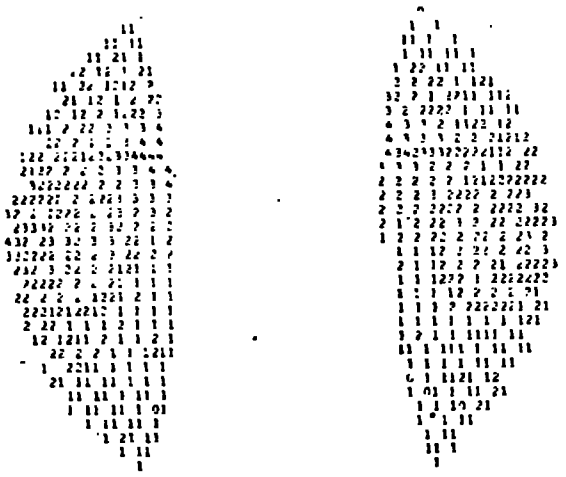

Fig. 8. Intermediate computer print out of pole figure for Penrhyn Slate, illite (001). Sample section C.

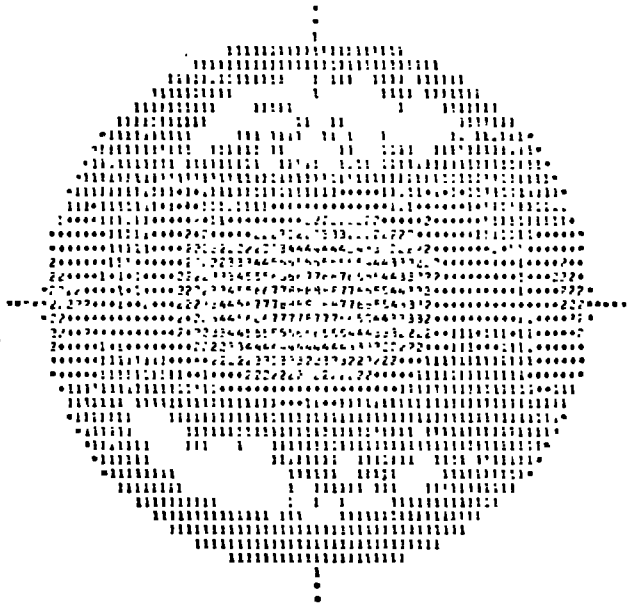

Fig. 9. Final computer print out of smoothed pole figure for Penrhyn Slate, illite (001), showing locus of average intensity, I_a

Fig. 10. Intermediate computer print out of pole figure for Penrhyn Slate, chlorite (001). Sample section A.

Fig. 11. Intermediate computer print out of pole figure for Penrhyn Slate, chlorite (001). Sample section B.

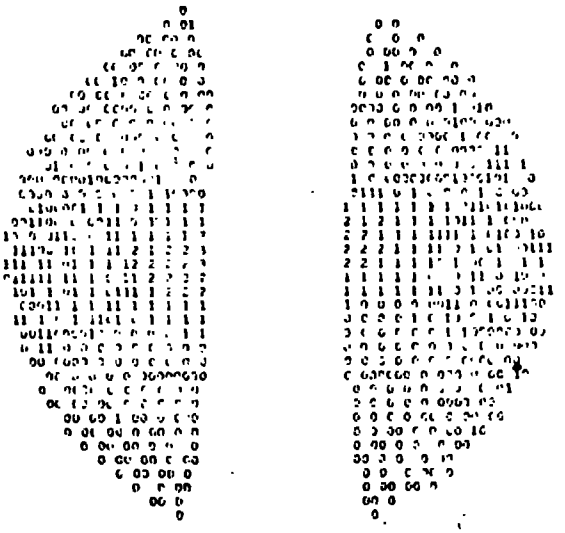

Fig. 12. Intermediate computer print out of pole figure for Penrhyn Slate, chlorite (001). Sample section C.

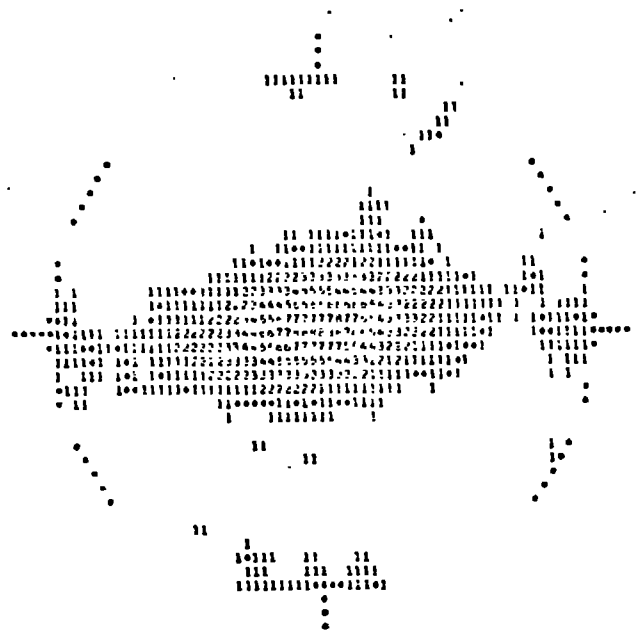

Fig. 13. Final computer print out of smoothed pole figure for Penrhyn Slate, chlorite (001), showing locus of average intensity, I_R

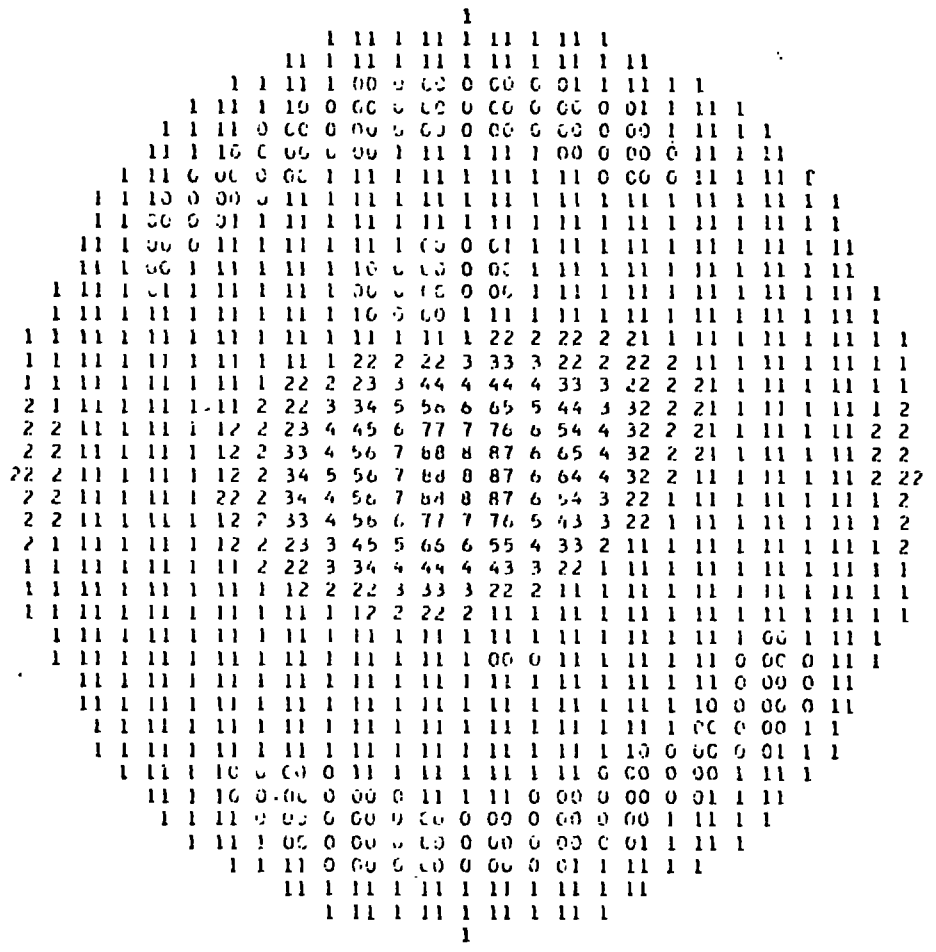

Fig. 14. Pole figure printout of Penrhyn Slate illite (001) data fitted by a series of associated Legendre polynomials.

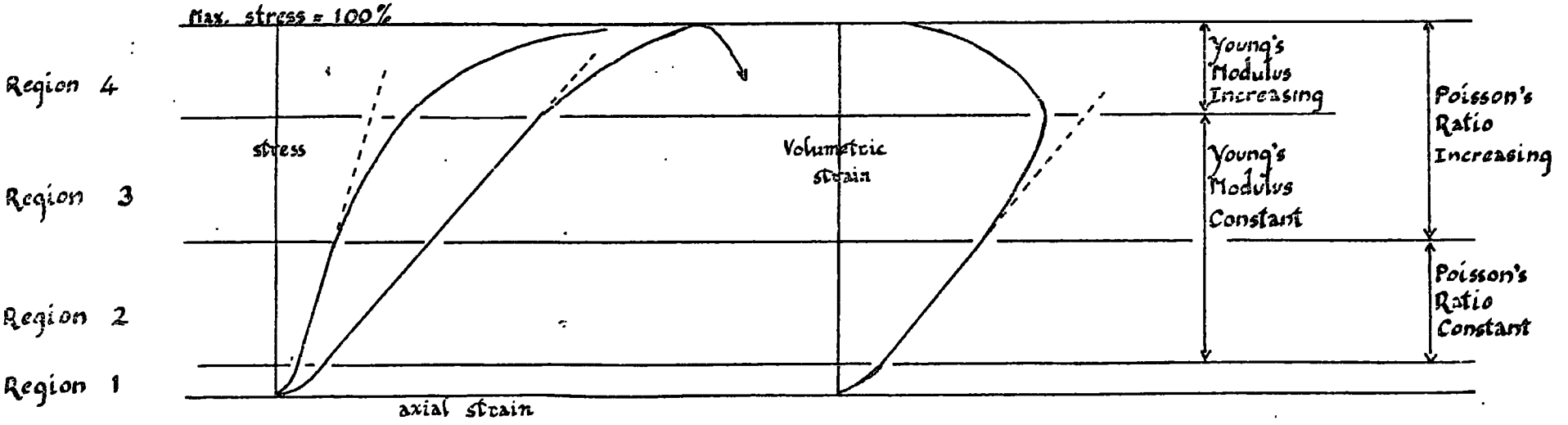

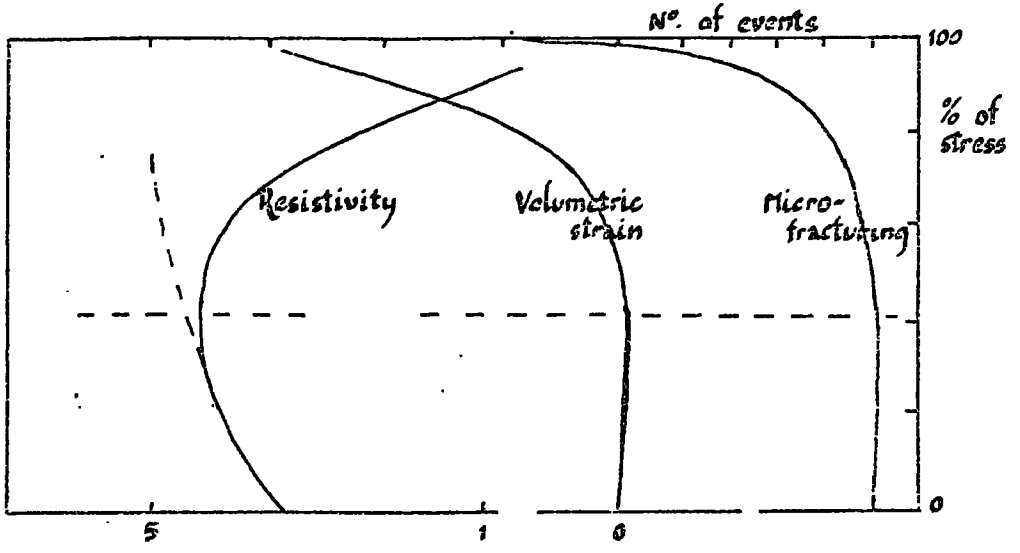

Fig 15. a) Generalized stress-strain curves for rock in compression. (after Bieniawski, 1967)

b) Generalised resistivity and microfracturing curves for rock in compression. (after Brace et al, 1968)

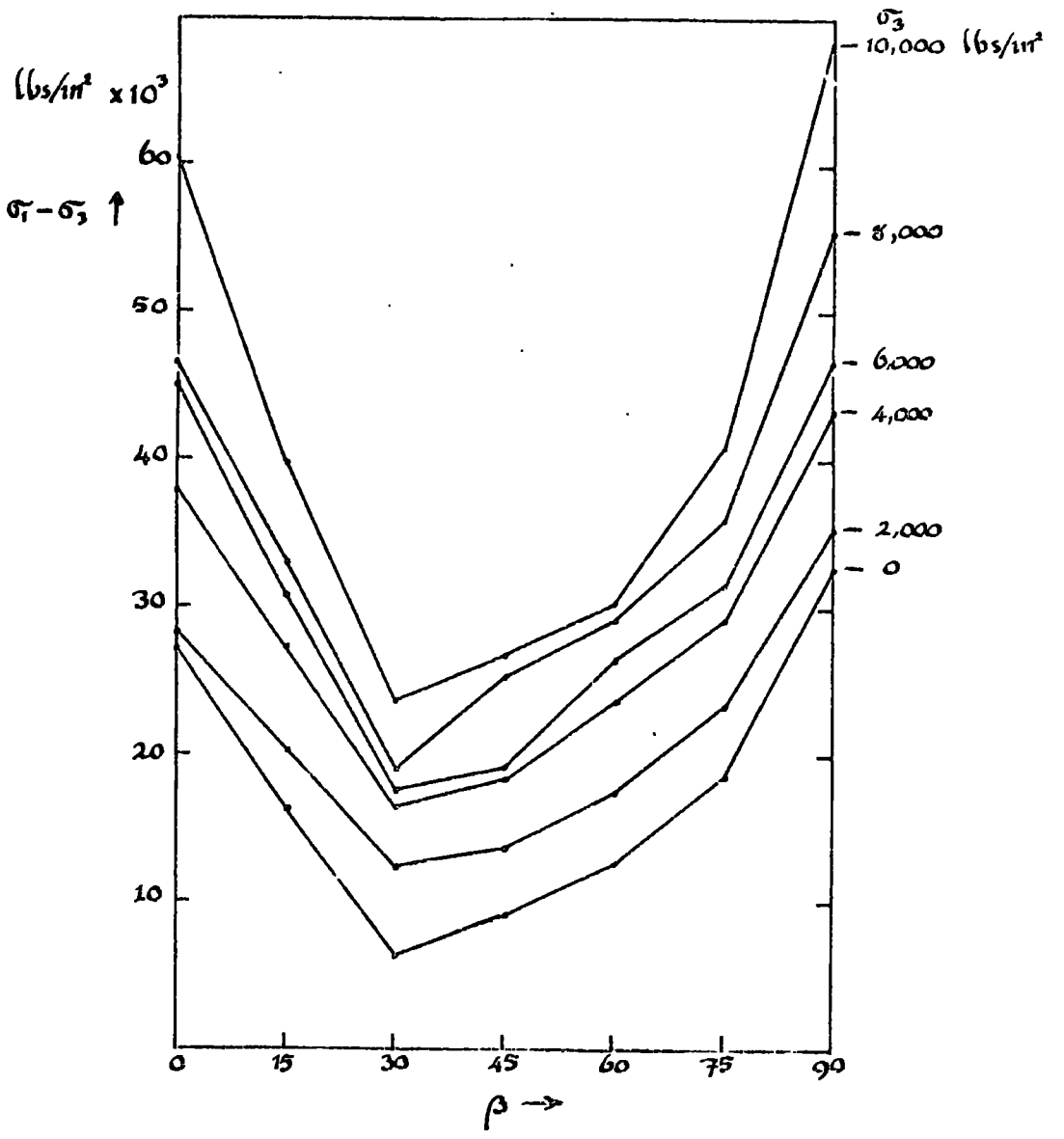

Fig. 16. Strength data for Penrhyn Slate, for various values of confining pressure, shown as a function of cleavage inclination.

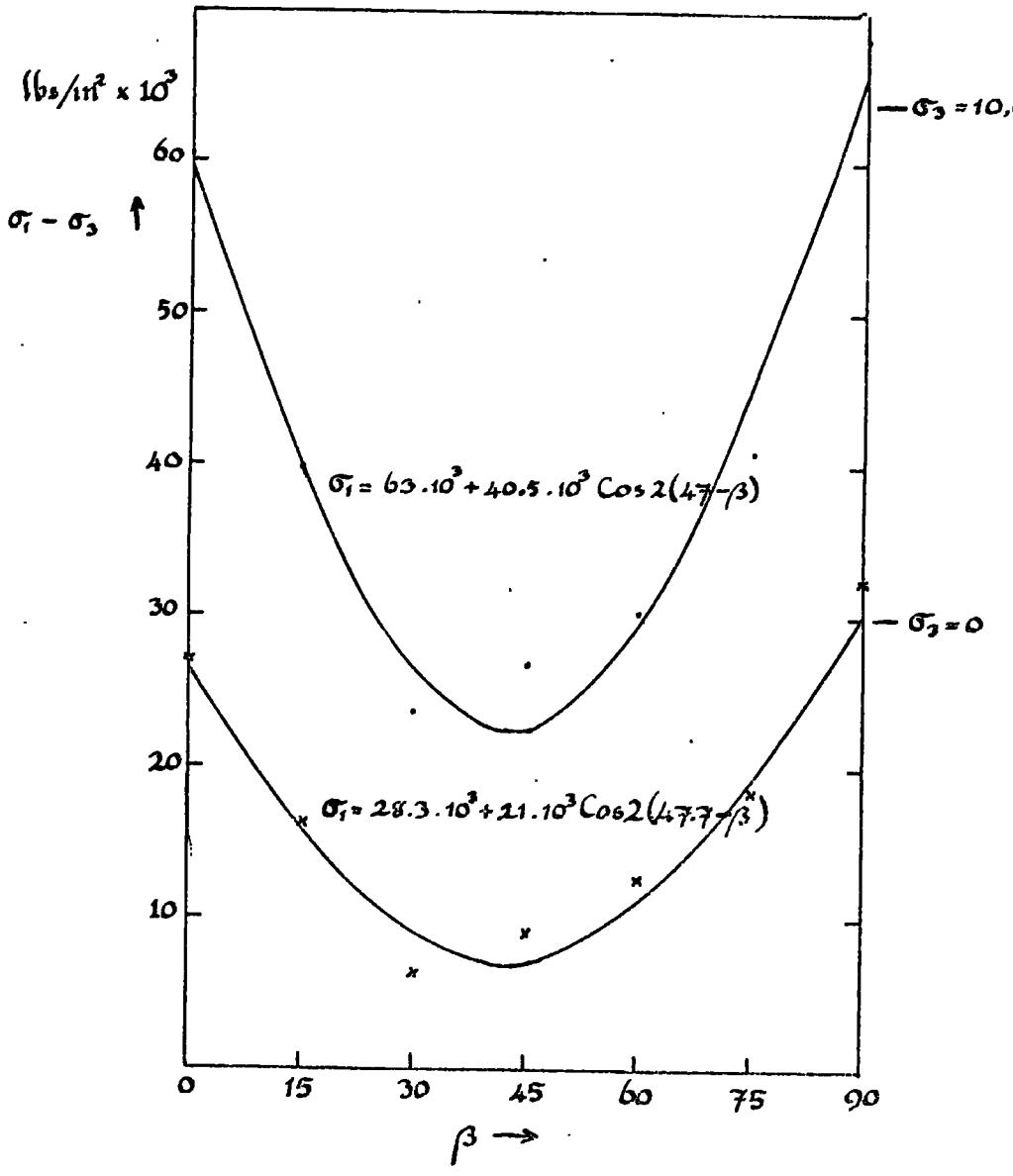

Fig. 17. Data from Penrhyn Slate compared with the modified form of Donath's equation

$$\sigma_1 = a + b \cos 2(\alpha - \beta)$$

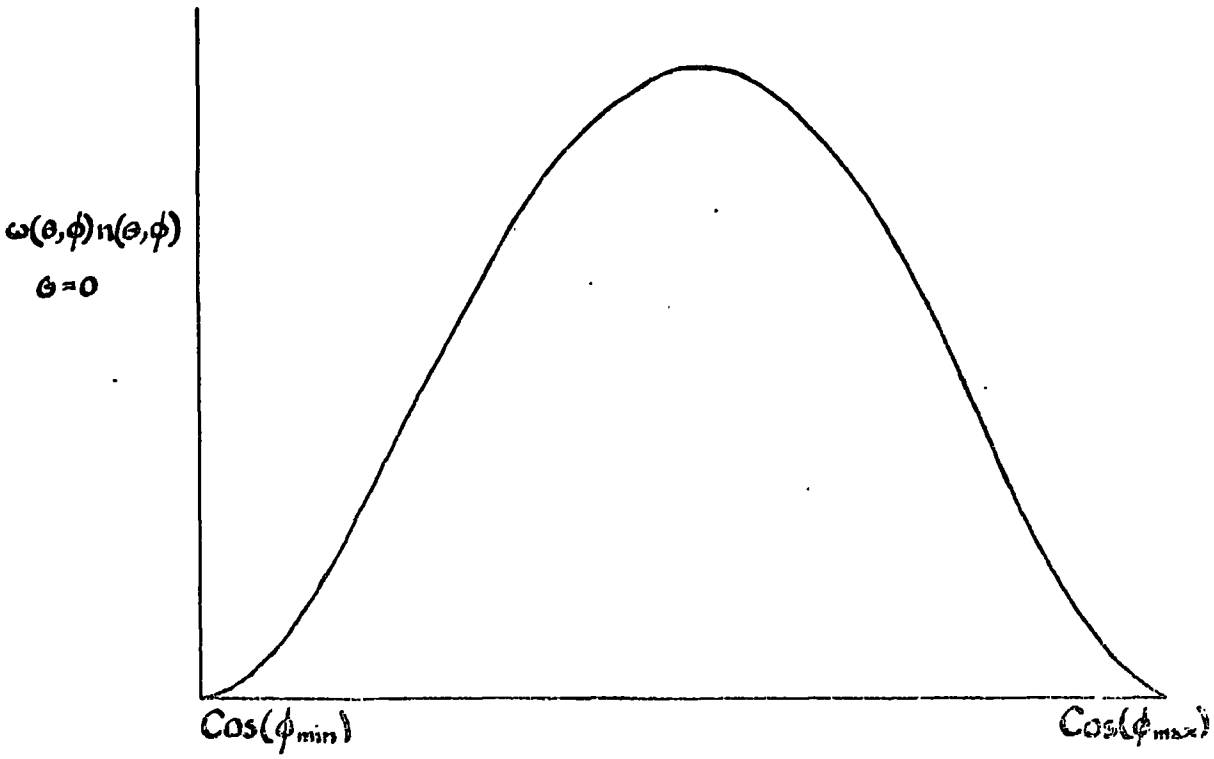

Fig. 18. Plot of the function $\omega(\zeta,\delta)\,n(\zeta,\delta)$ used in the Weibols and Cook integration showing its generally parabollic shape.

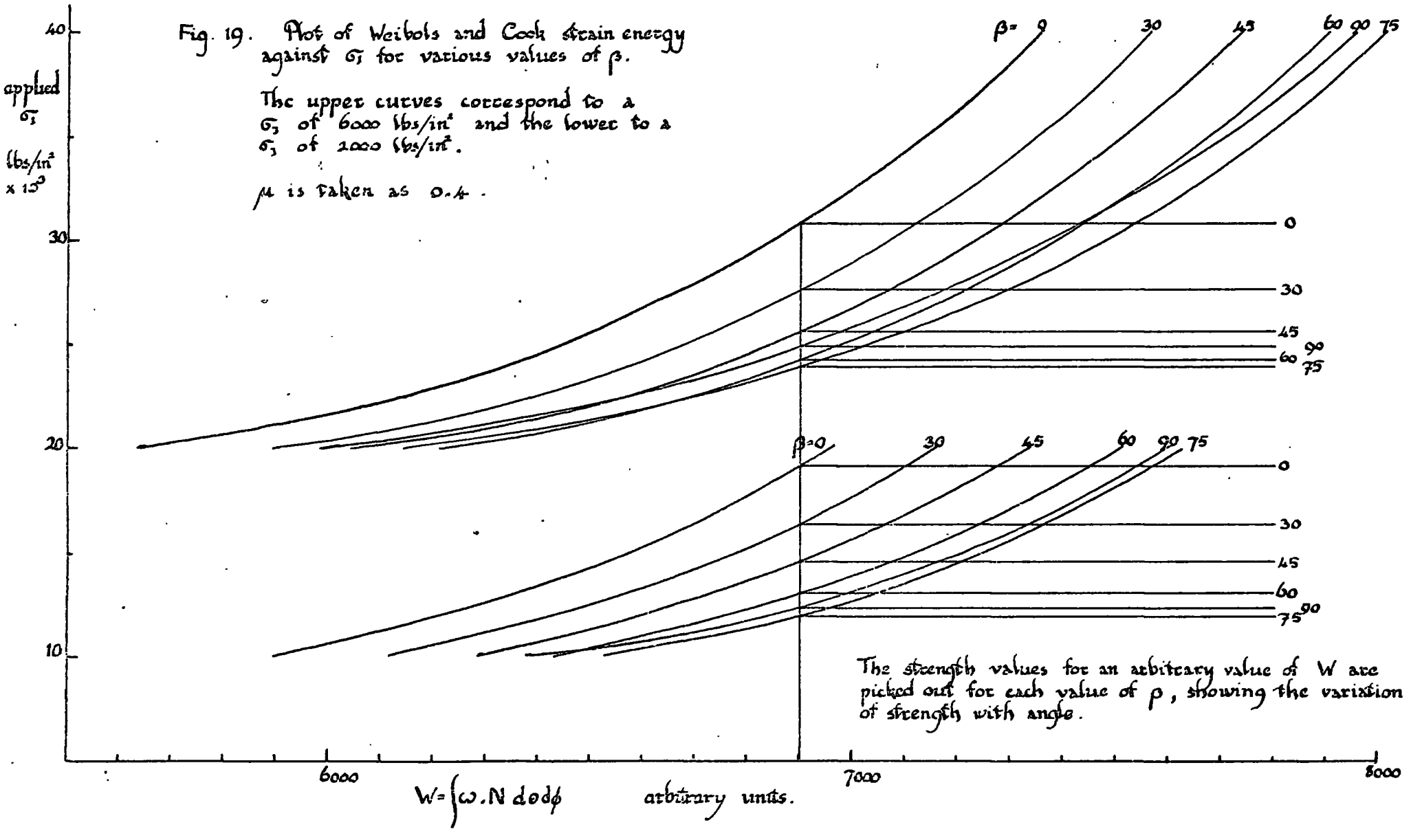
Fig. 19. Plot of Weibols and Cook strain energy against σ_1 for various values of β.
The upper curves correspond to a σ_3 of 6000 lbs/in² and the lower to a σ_3 of 2000 lbs/in².
μ is taken as 0.4.
applied σ_1
lbs/in² x 10³
40
30
20
10
β= 0
30
45
60
90
75
0
30
45
60
90
75
The strength values for an arbitrary value of W are picked out for each value of ρ, showing the variation of strength with angle.
6000
7000
8000
$W = \int \omega . N \, d\theta \, d\phi$ arbitrary units.

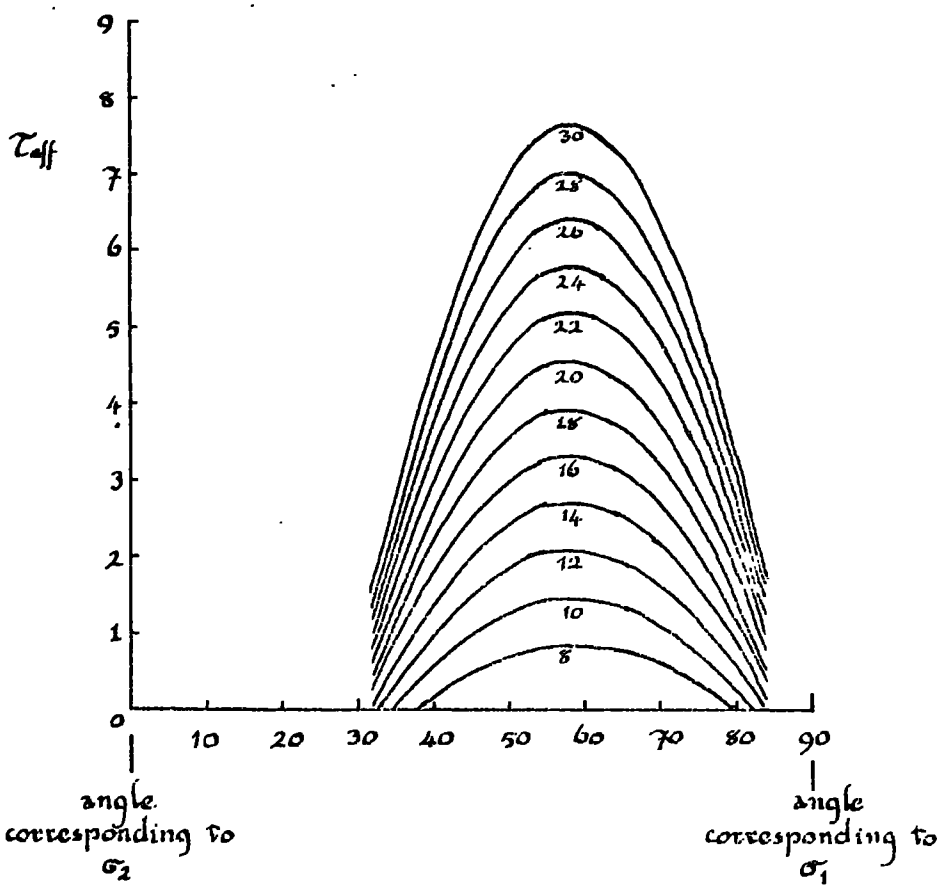

Fig. 20 Family of curves for τ_{eff}.
$\sigma_2 = 2 \cdot 10^3$ lbs/in^2 $\mu = 0.5$

values of σ_1 (10^3 lbs/in^2) are marked for each curve.

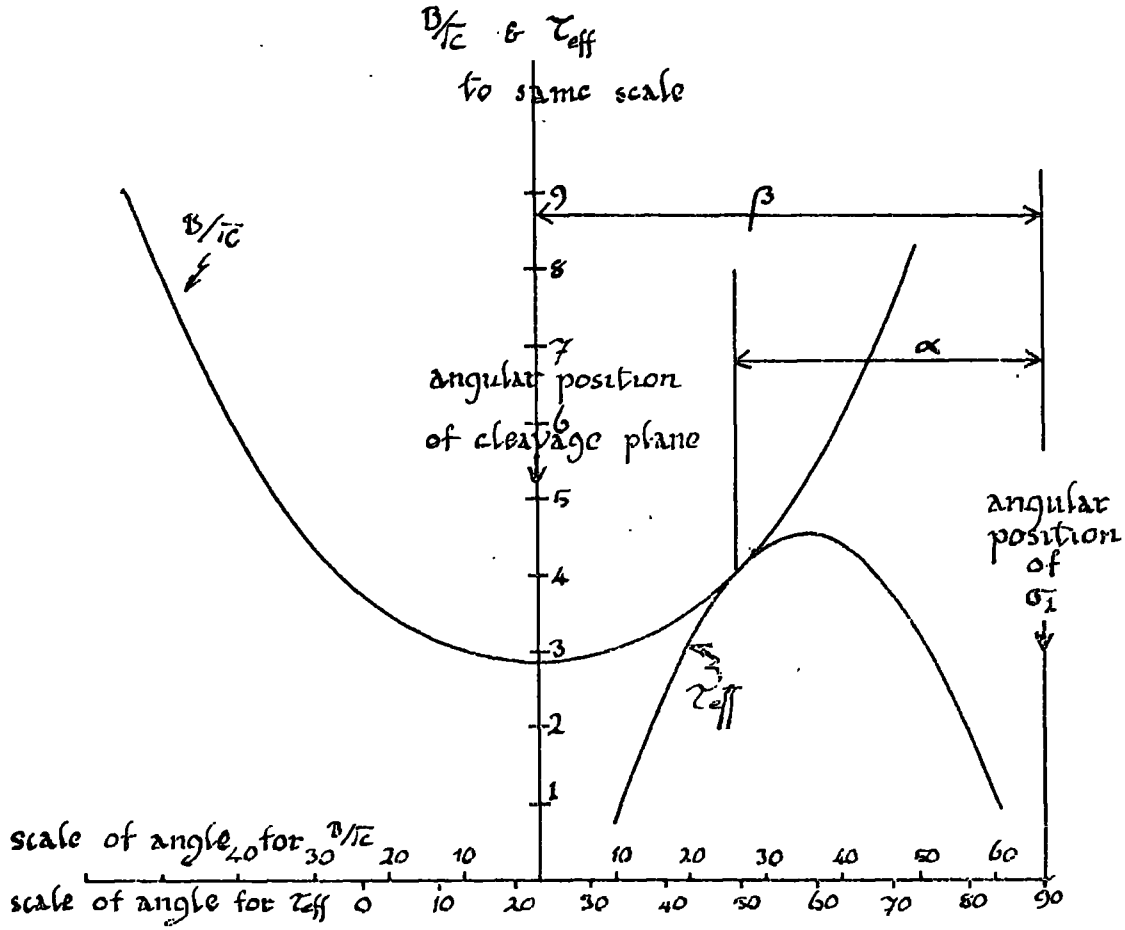

Fig. 21 showing graphical solution of

$$\tau_{eff} = B/\sqrt{c}$$

The two curves are moved relative to each other until they just touch. The displacements α & β represent the orientation of σ_1 to the failing crack and the cleavage plane respectively.

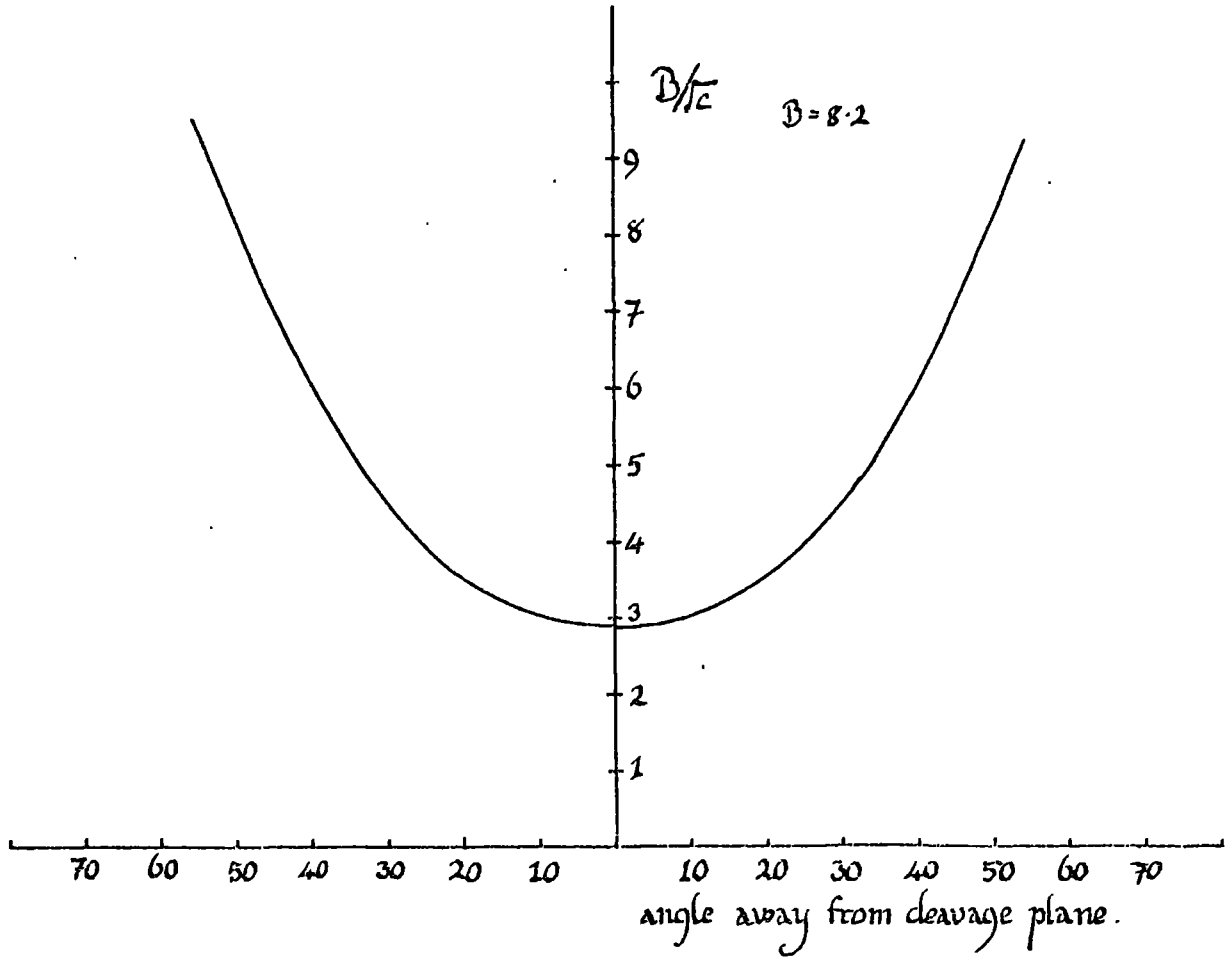

Fig. 22. Plot of $B/\sqrt{c}$, in arbitrary units, against angle of crack, length c, with respect to the cleavage plane. The crack length distribution is taken directly from X-ray data shown elsewhere.

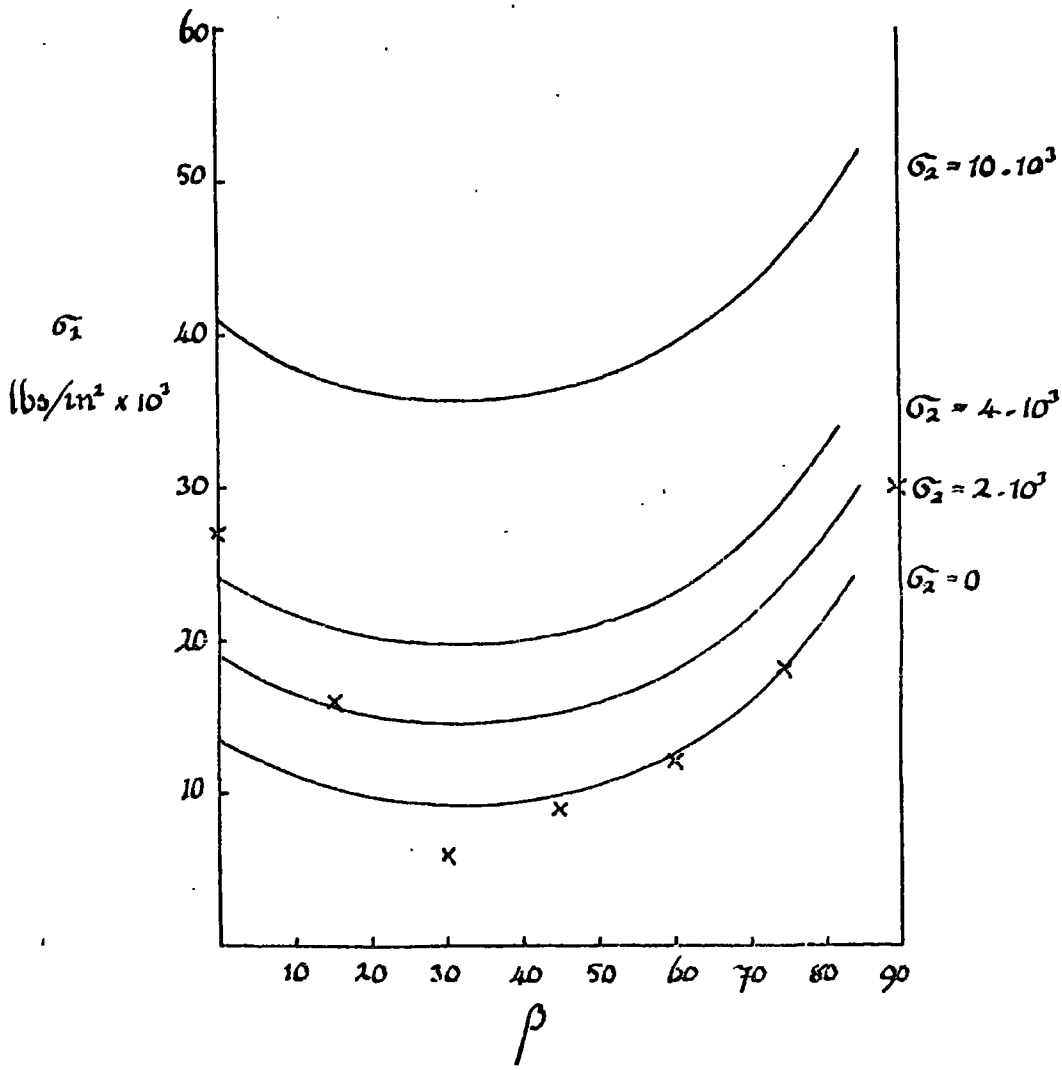

Fig.23. Theoretical curves obtained by the application of Griffith theory to X-ray derived crack distribution.
Penrhyn Slate data is shown for $\sigma_2 = 0$.

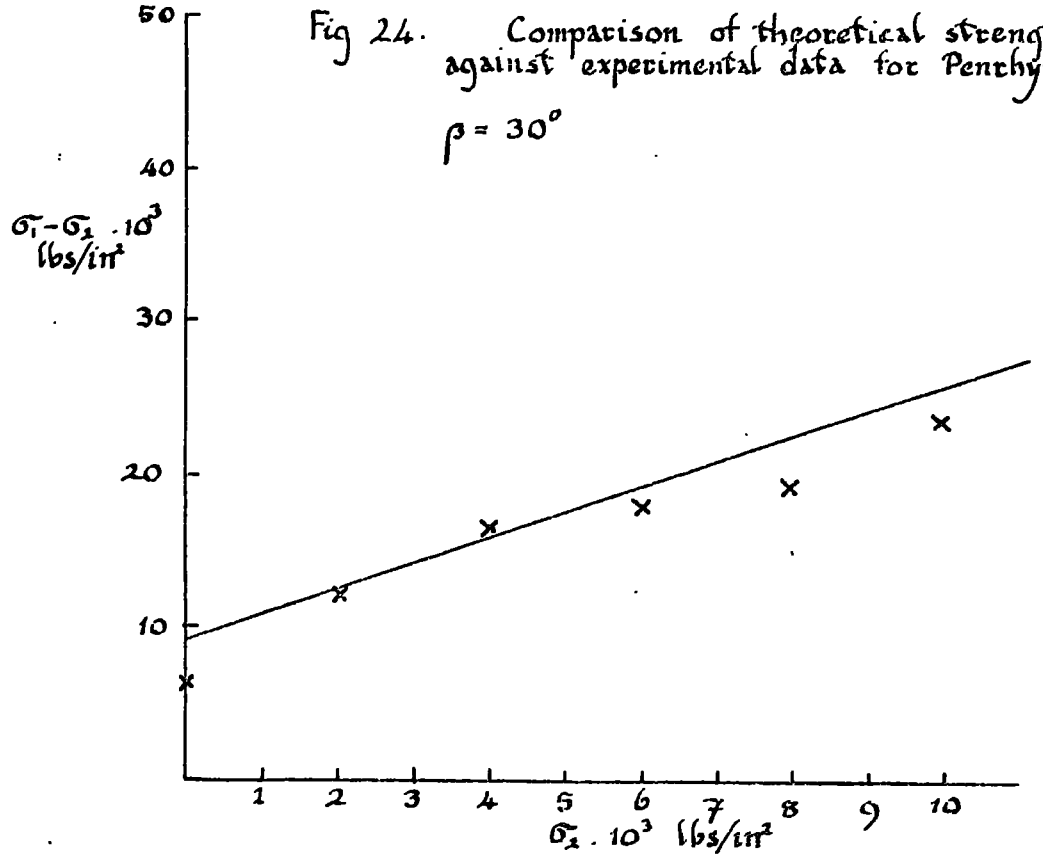

Fig 24. Comparison of theoretical strength against experimental data for Penrhyn Slate

$\beta = 30^\circ$

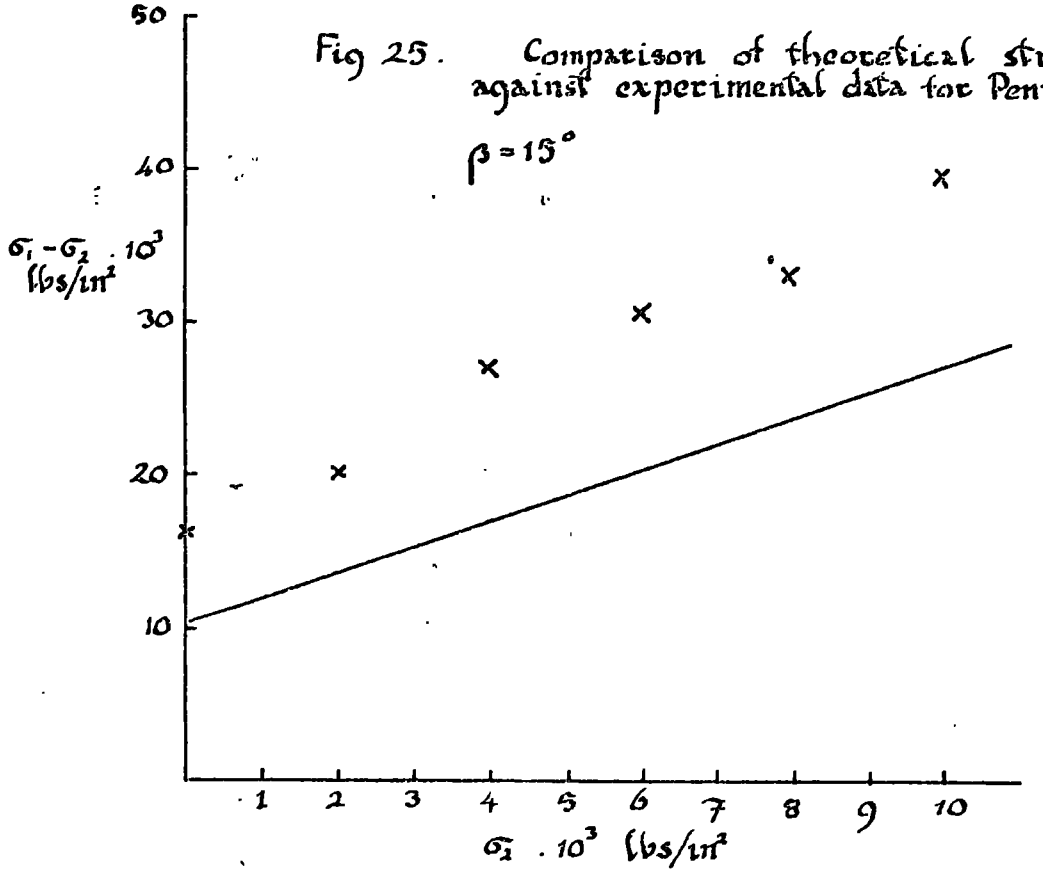

Fig 25. Comparison of theoretical strength against experimental data for Penrhyn Slate.

$\beta = 15^\circ$

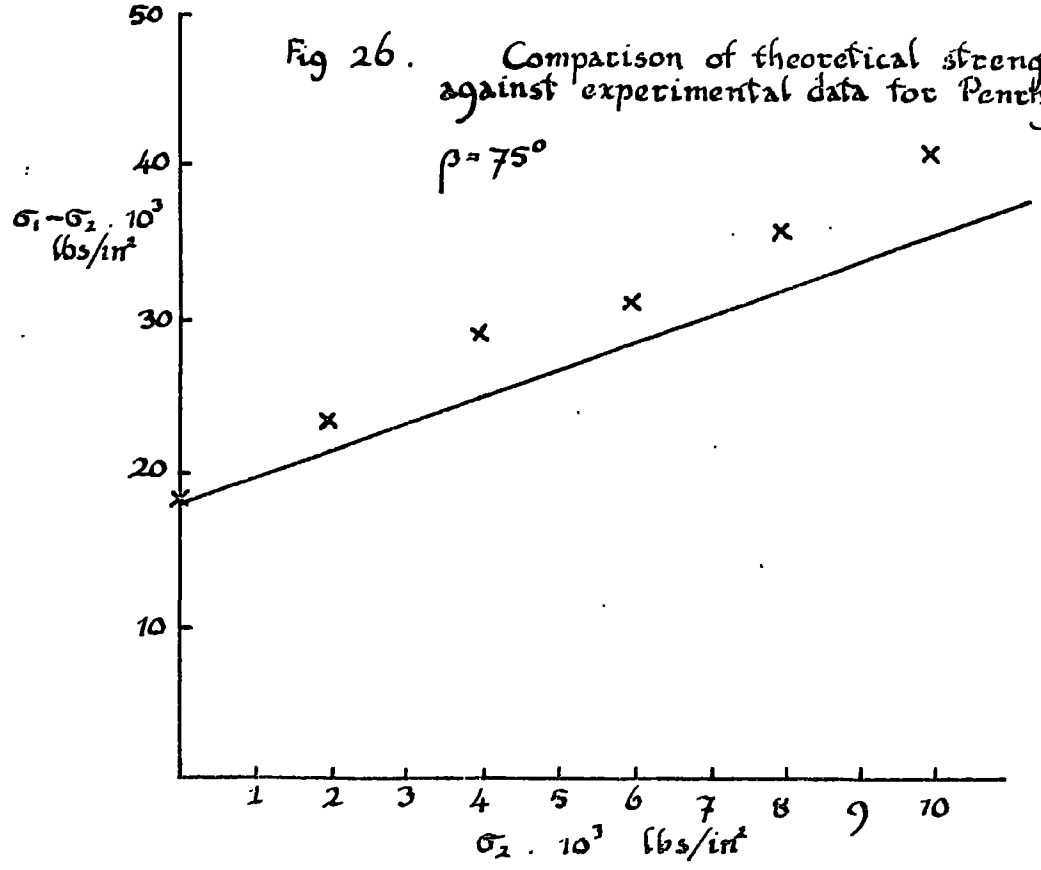

Fig 26. Comparison of theoretical strength against experimental data for Penrhyn Slate

$\beta = 75°$

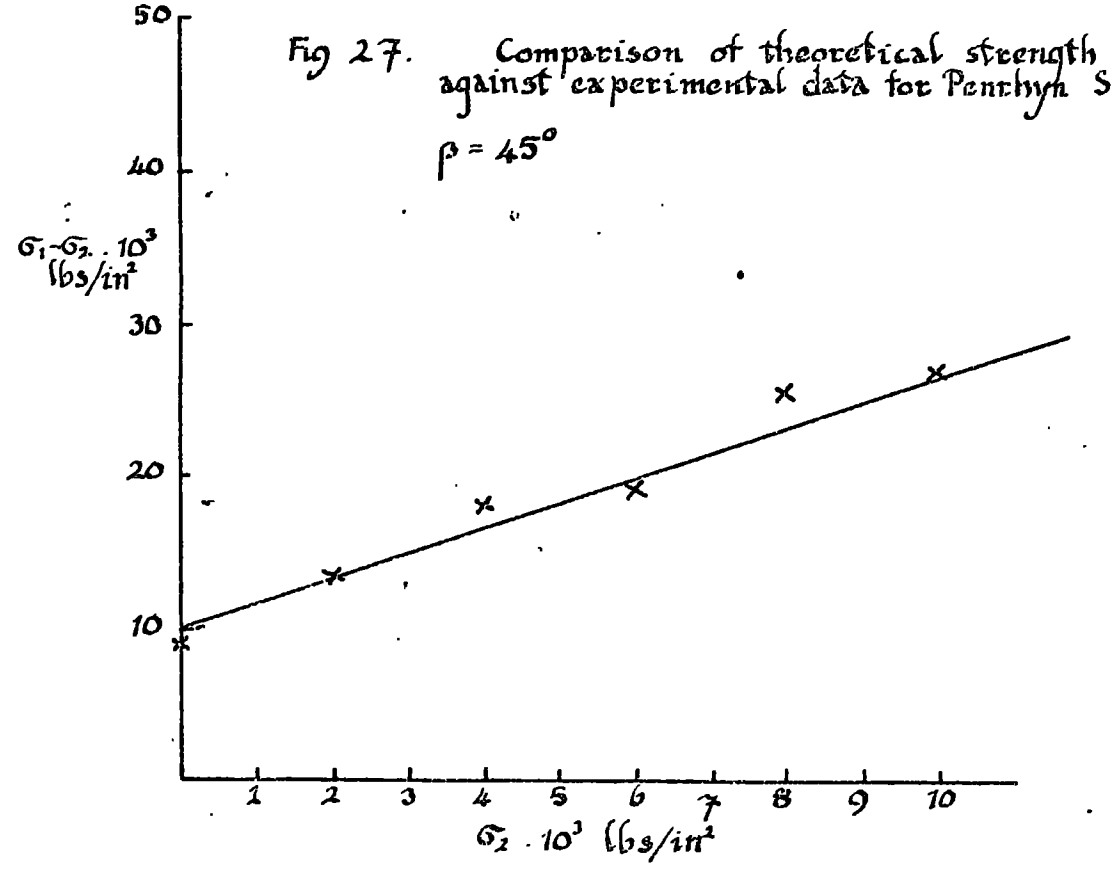

Fig 27. Comparison of theoretical strength against experimental data for Penrhyn Slate

$\beta = 45°$

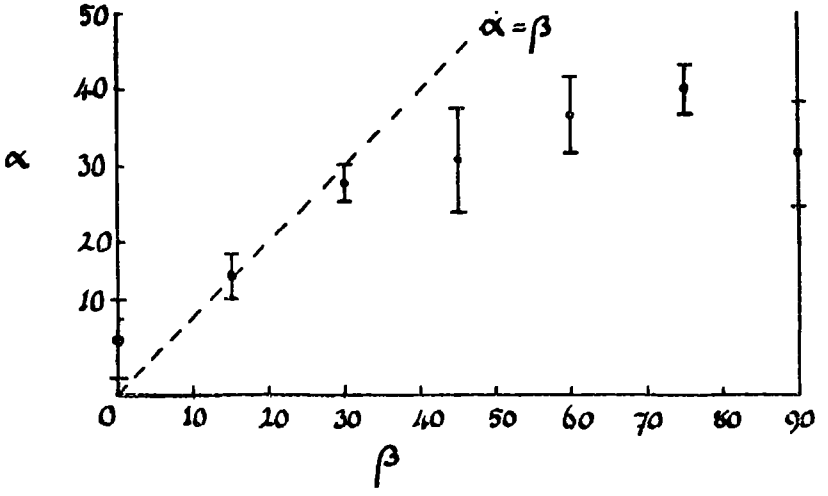

Fig 28 a. Experimental relationship between orientation of failure plane, α, and orientation of cleavage, β, for Penrhyn Slate. The bars mark one standard deviation either side of the mean.

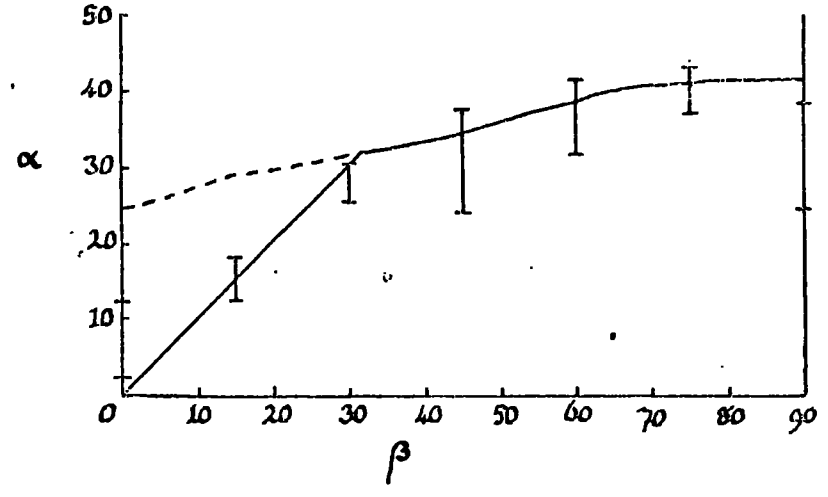

Fig 28 b. Theoretical relationship between α and β used in the final version.

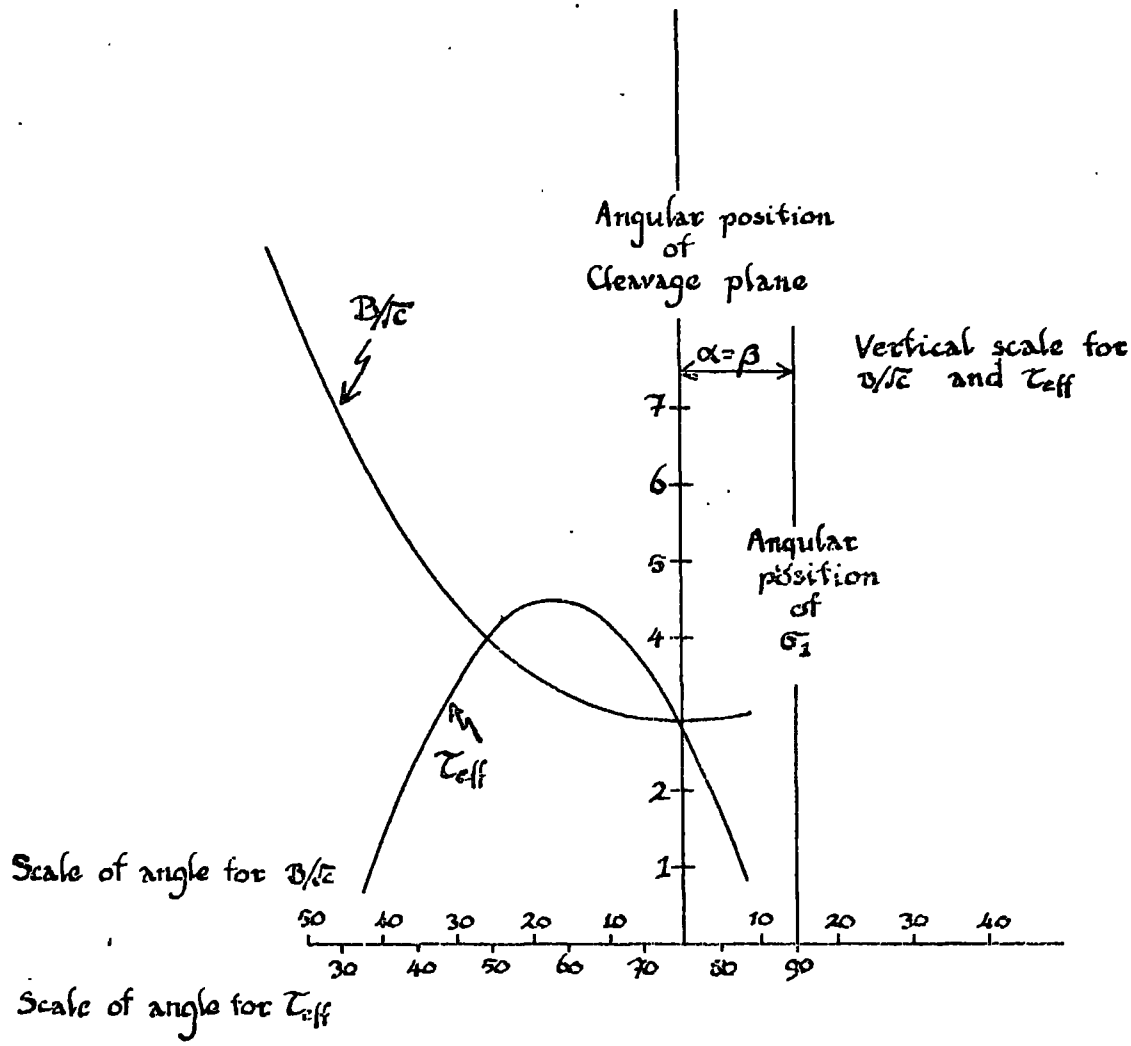

Fig. 29 Showing solution of

$\tau_{eff} = B/\sqrt{c}$

under the condition $\alpha = \beta$.

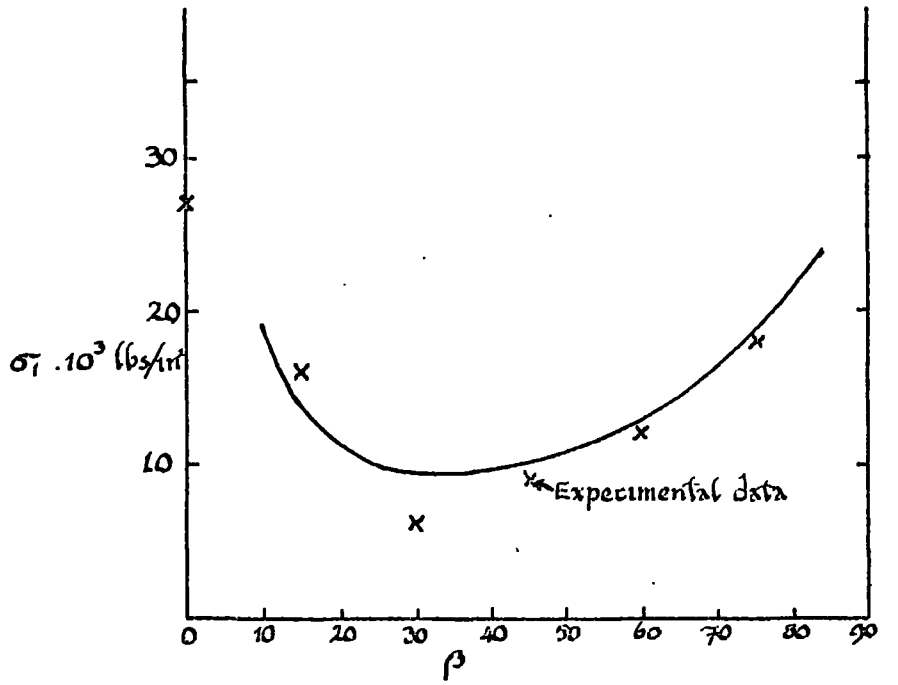

Fig 30. Plot of σ_1 vs. β for a confining pressure of zero. The full line gives the theoretical plot as modified by shear plane entrainment.

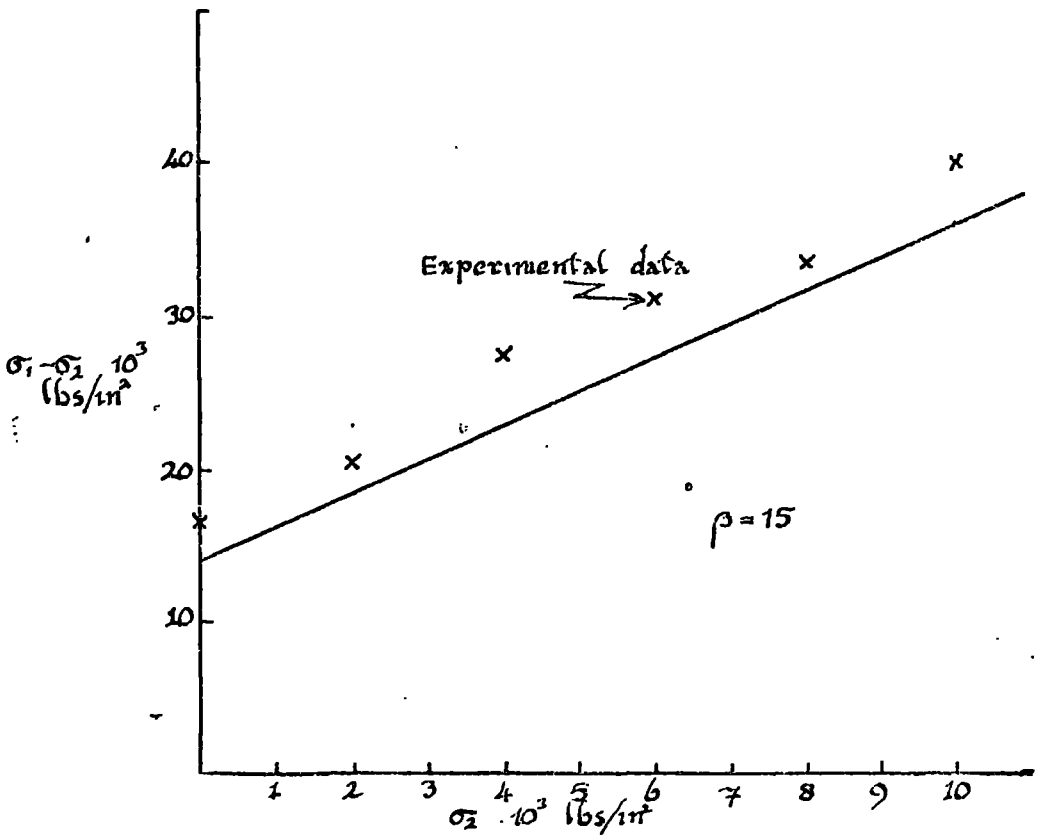

Fig 31 Plot of $\sigma_1 - \sigma_2$ vs σ_2 given by the theory modified for shear plane entrainment.

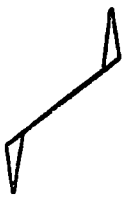

Fig 32 a. Approximate form of a failed crack.
(after Brace, Paulding and Scholz, 1966)

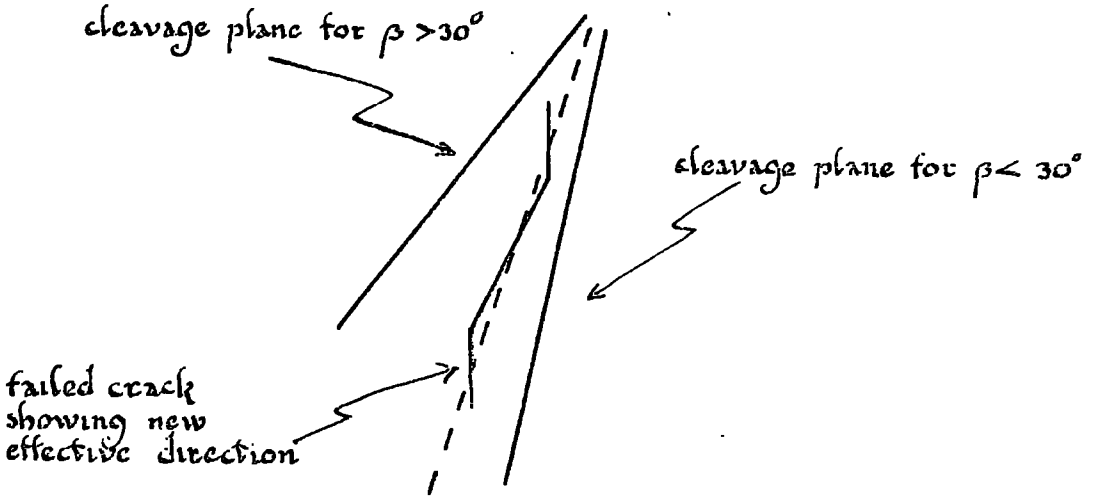

Fig 32 b. showing how a failed crack may become
entrained in the cleavage plane for angles $\beta < 30°$

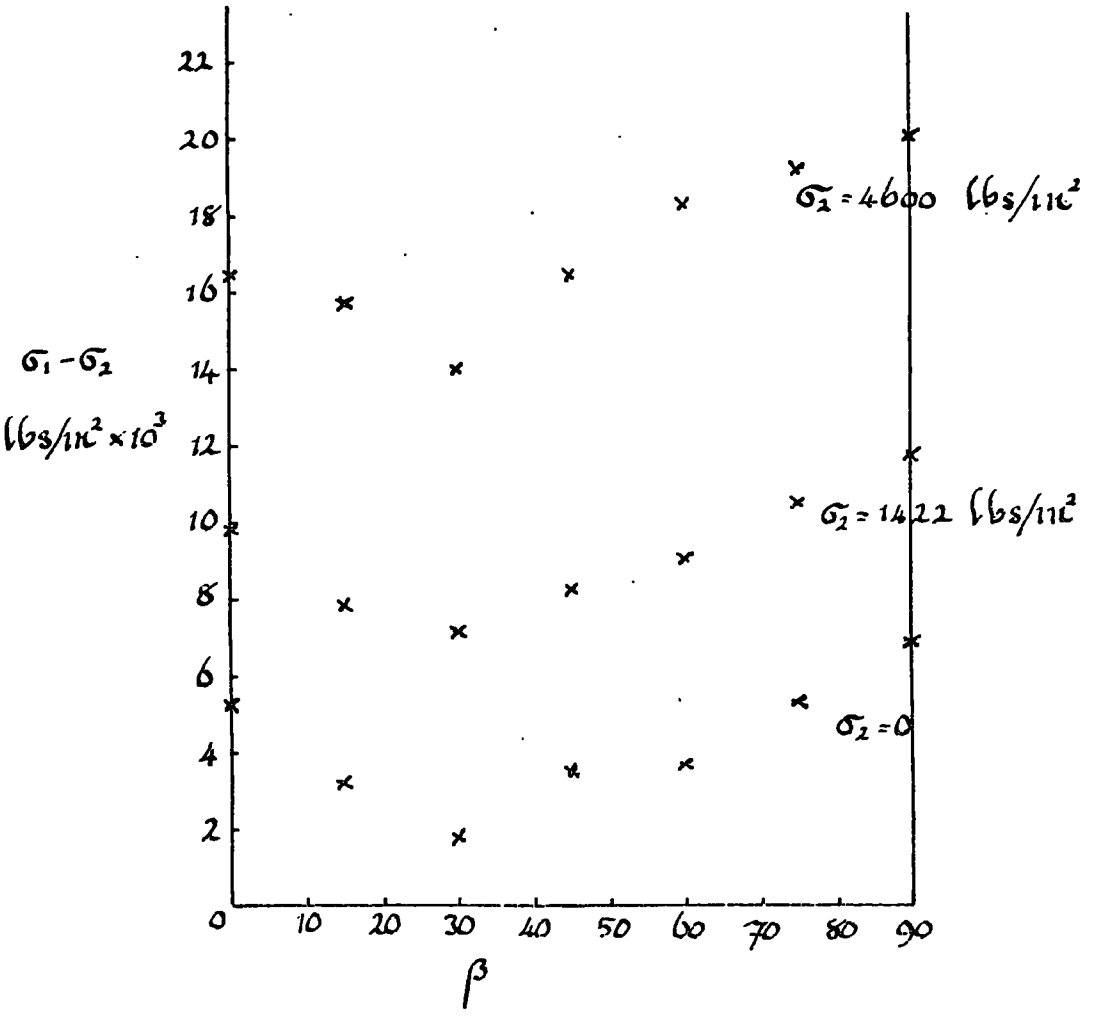

Fig 33. Experimental strength data for Lumley Mudstone.

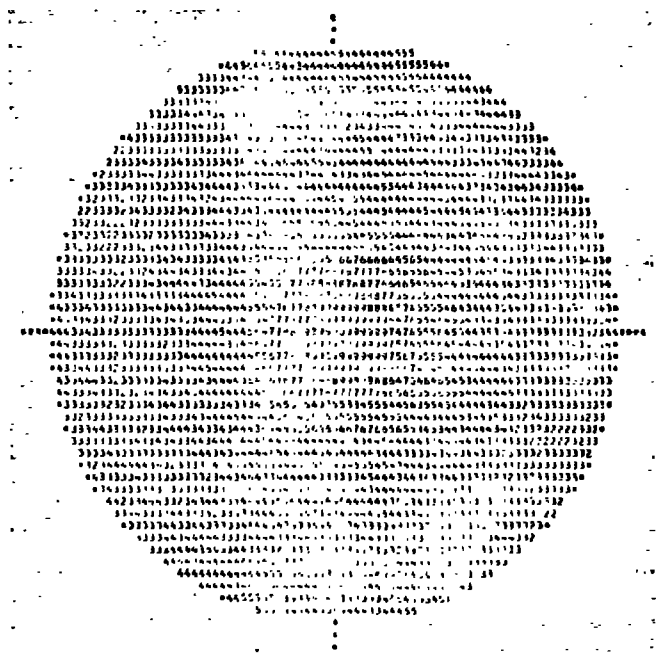

Fig. 34. X-ray texture for Lumley Mudstone used in the application of the theory.

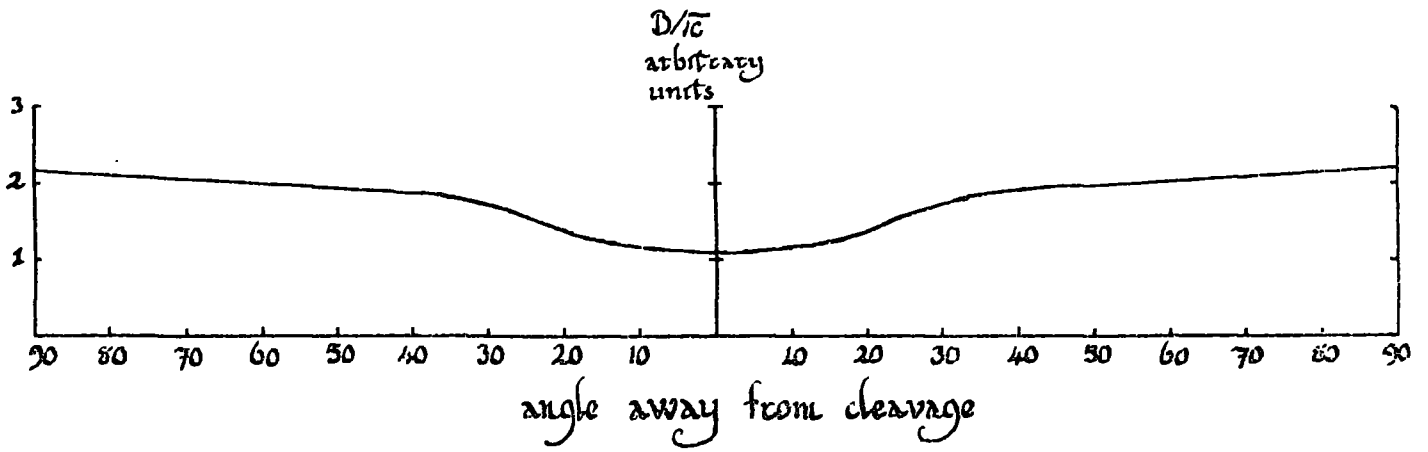

Fig 35. Plot of $B/\sqrt{C}$ as a function of orientation for Lumley Mudstone taking $B = 3$.

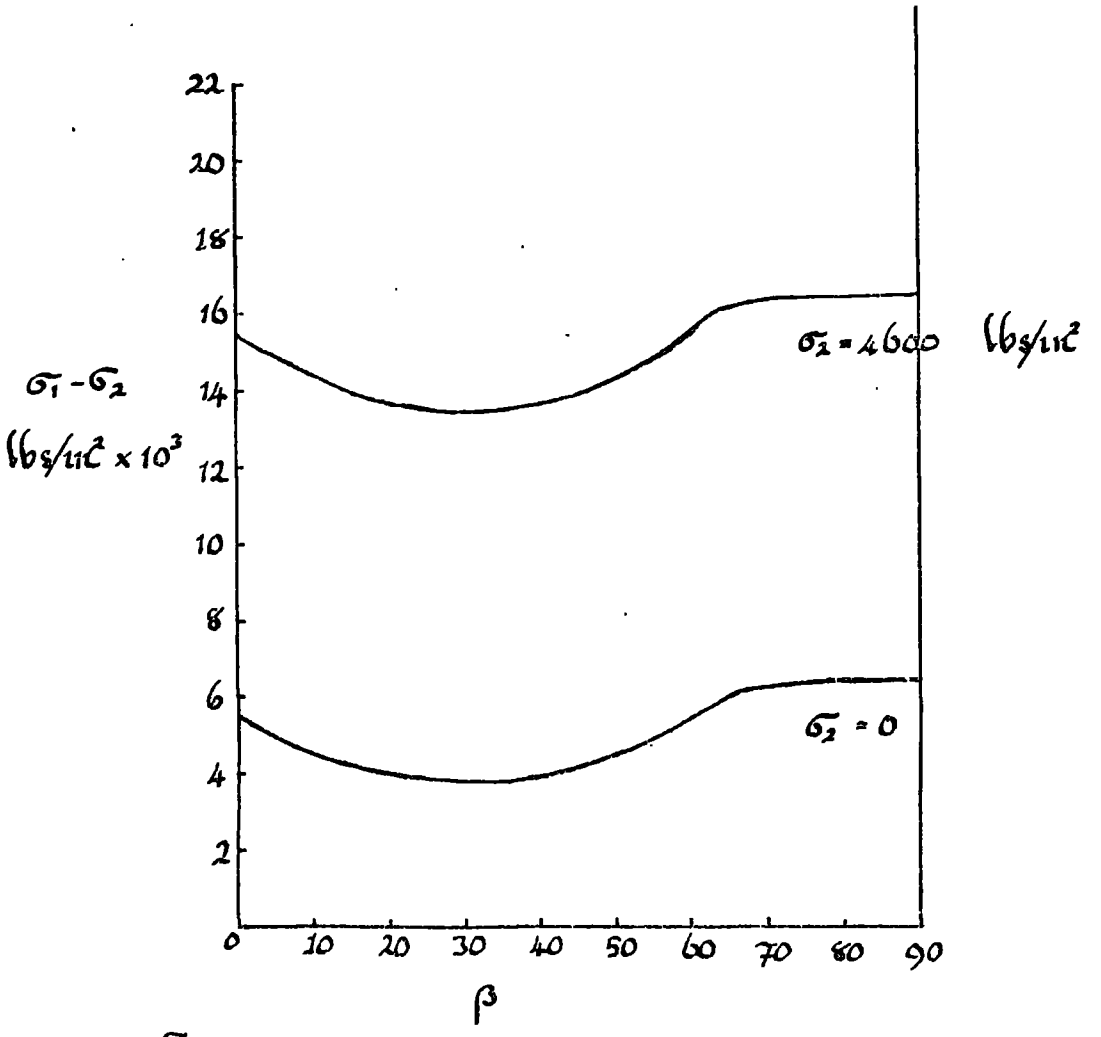

Fig 36 Strength variation with sample orientation from theory applied to a distribution for Lumley Mudstone with $B = 3$ and $\mu = 0.6$

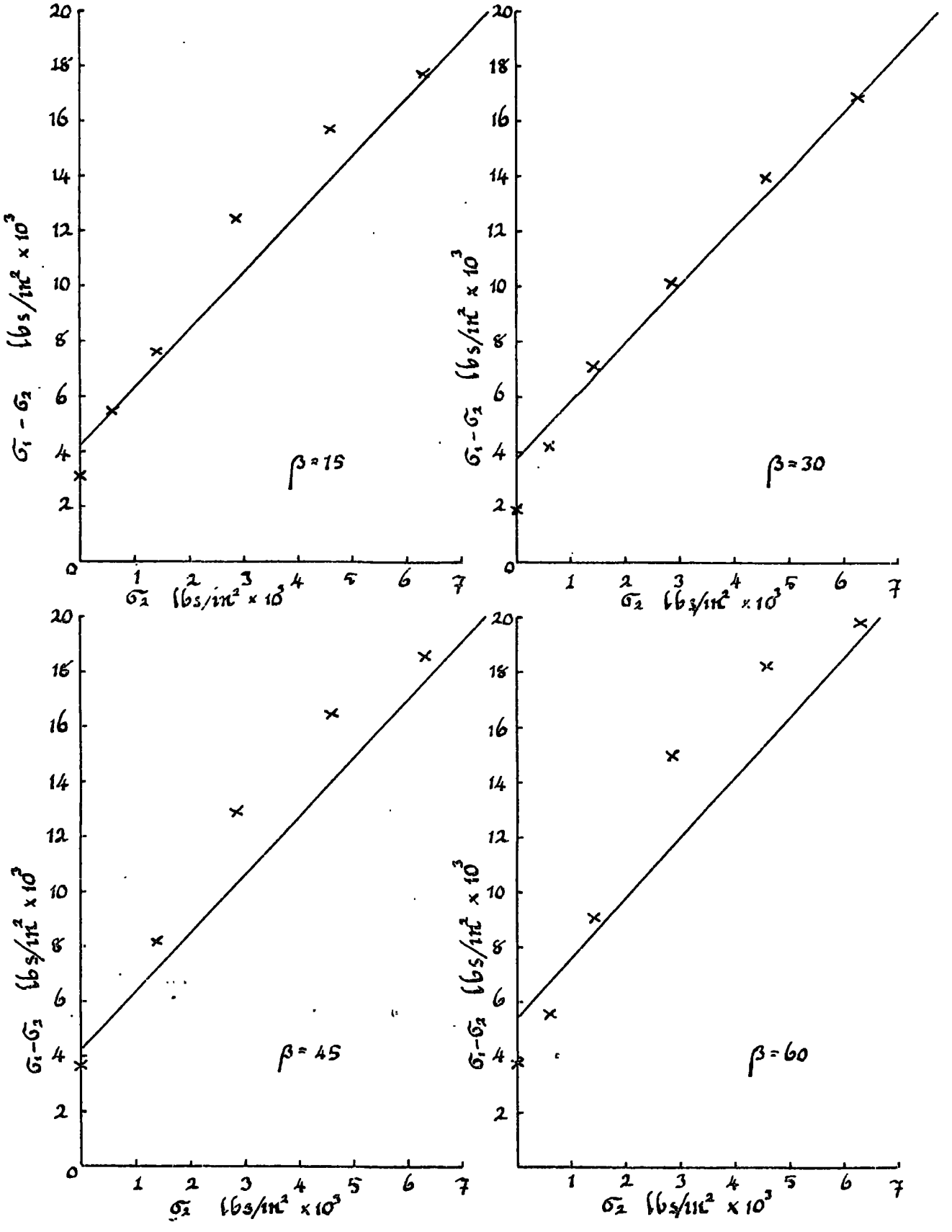

Fig 37. Comparison of theory and experiment for Lumley Mudstone for various sample orientations. $B = 3$ $\mu = 0.6$.

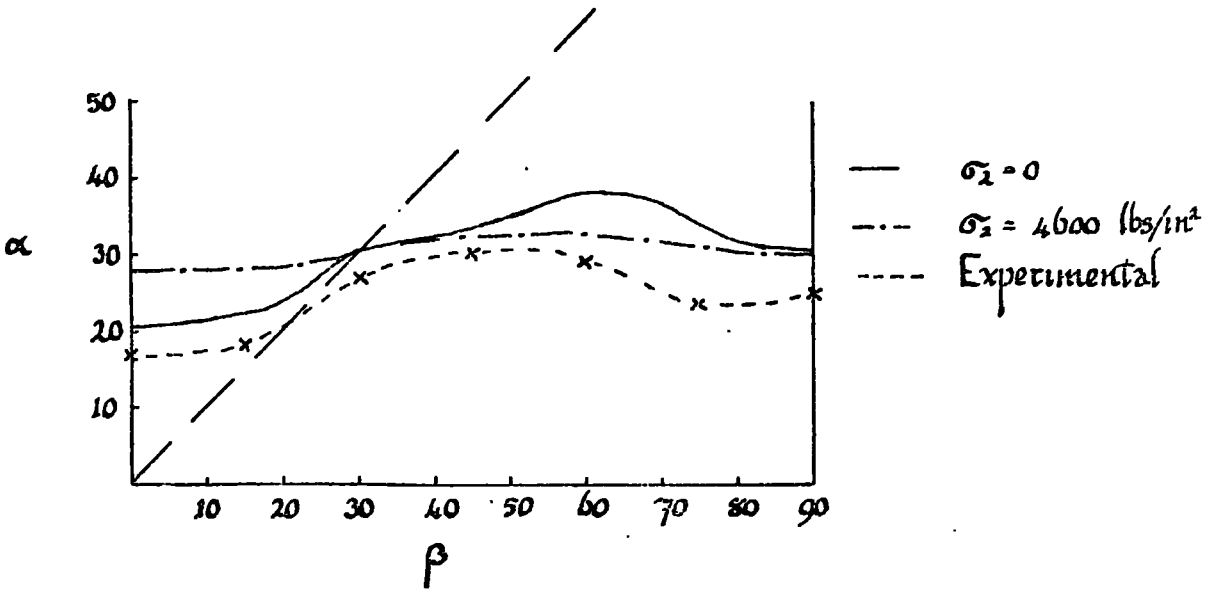

Fig 38. Theoretical and experimental relationship between failure plane angle and orientation of sample for Lumley mudstone.

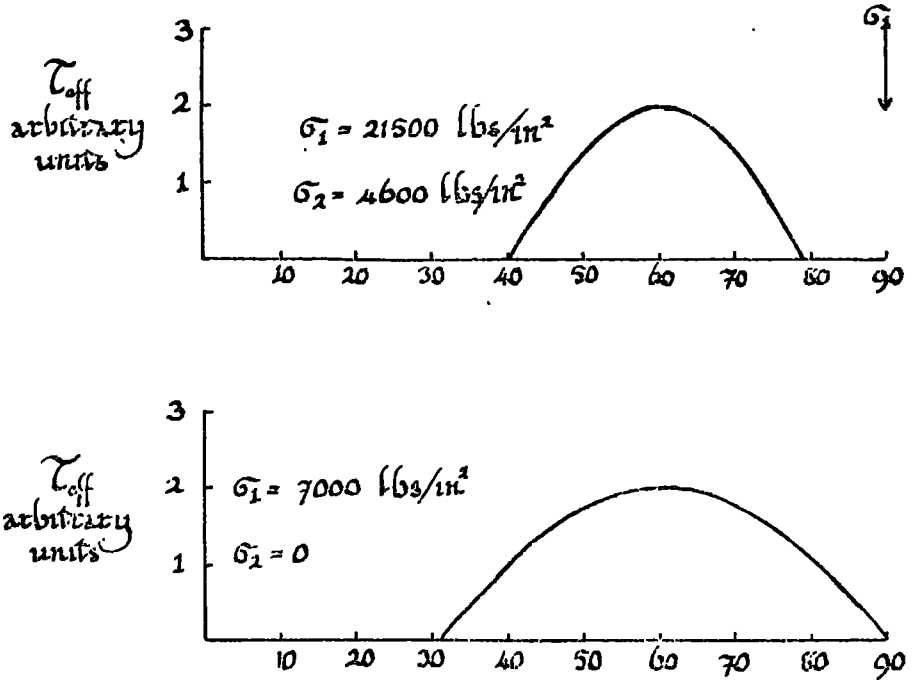

Fig 39. Comparison of two τ_{eff} curves showing effect of σ_2 on radius of curvature. $\mu = 0.6$ for both curves.